

FOR OFFICIAL USE ONLY

JPRS L/9453

18 December 1980

USSR Report

PHYSICS AND MATHEMATICS

(FOUO 10/80)



FOREIGN BROADCAST INFORMATION SERVICE

FOR OFFICIAL USE ONLY

NOTE

JPRS publications contain information primarily from foreign newspapers, periodicals and books, but also from news agency transmissions and broadcasts. Materials from foreign-language sources are translated; those from English-language sources are transcribed or reprinted, with the original phrasing and other characteristics retained.

Headlines, editorial reports, and material enclosed in brackets [] are supplied by JPRS. Processing indicators such as [Text] or [Excerpt] in the first line of each item, or following the last line of a brief, indicate how the original information was processed. Where no processing indicator is given, the information was summarized or extracted.

Unfamiliar names rendered phonetically or transliterated are enclosed in parentheses. Words or names preceded by a question mark and enclosed in parentheses were not clear in the original but have been supplied as appropriate in context. Other unattributed parenthetical notes within the body of an item originate with the source. Times within items are as given by source.

The contents of this publication in no way represent the policies, views or attitudes of the U.S. Government.

COPYRIGHT LAWS AND REGULATIONS GOVERNING OWNERSHIP OF MATERIALS REPRODUCED HEREIN REQUIRE THAT DISSEMINATION OF THIS PUBLICATION BE RESTRICTED FOR OFFICIAL USE ONLY.

FOR OFFICIAL USE ONLY

JPRS L/9453

18 December 1980

USSR REPORT
PHYSICS AND MATHEMATICS
(FOUO 10/80)

CONTENTS

CRYSTALS AND SEMICONDUCTORS

Production and Properties of Thin Films 1

LASERS AND MASERS

An Electric-Discharge Pulsed CO₂ Research Laser 4

Limiting Characteristics of a Photochemical XeO Laser 9

Development of Optical Inhomogeneities in Flashtube Photolysis
Lasers. 21

A Neodymium Pulse Laser That Produces a High-Frequency Series of
Nanosecond Pulses With Energy of ~100 J 29

Lasers Utilizing CO₂ Isotopes 33

Study of a Large-Volume Flashlamp-Initiated H₂-F₂ Chemical Laser. 41

Optical Resonators and the Problem of Laser Beam Divergence 46

MAGNETOHYDRODYNAMICS

Magnetic Plasma Compressor With Explosively-Driven Magnetic-Field
Compression Generator 63

OPTICS AND SPECTROSCOPY

Interference Phenomena When Metals Are Heated by Laser in an Oxidative
Atmosphere. 68

Time for the Origin of Plasma With the Effect of Laser Radiation of
Various Wavelengths on an Aluminum Obstacle in the Air, 78

OPTOELECTRONICS

Influence That Pumping Fluctuations Have on the Sensitivity of an
Infrared Receiver With Parametric Frequency Conversion. 85

- a - [III - USSR - 21H S&T FOUO]

FOR OFFICIAL USE ONLY

FOR OFFICIAL USE ONLY
CRYSTALS AND SEMICONDUCTORS

PRODUCTION AND PROPERTIES OF THIN FILMS

Kiev POLUCHENIYE I SVOYSTVA TONKIKH PLENOK in Russian 1979 signed to press
20 Dec 78

[Annotation and Table of Contents of collection of papers published by IPM
(Institute of Problems in Material Science) of the UkSSR Academy of Sciences,
editors A. F. Andreyeva, V. Ya. Ayvazov, et al., 295 copies, 179 pages]

[Text] The present collection of papers is the sixth volume of transactions
of the all-union seminar on "Production and Properties of Thin Films" held at
the Institute of Problems in Material Science in 1978.

The collection presents the results of research on the methods for obtaining
and the properties of thin films of oxides, nitrides and certain other compounds
which are promising in electronics and optics.

This volume is intended for the engineers, technicians and scientists of research
institutes and industrial enterprises and may also be used by graduate students
and undergraduates taking upper-level courses in micro-electronics and computer
engineering.

TABLE OF CONTENTS

1. Capabilities of the secondary ion-ion emission method for analysis of concentration profiles in thin films, M. A. Vasil'yev and S. P. Chenakin
2. Prospects for the use of REM oxide films in optics electronics, A. F. Andreyeva, I. Ya. Gil'man and M. D. Smolin
3. On evaluation of the prospects for the use of dielectrics in microelectronics, D. I. Chernobrovkin
4. Predicting metalates with specified properties, V. V. Voikova and D. I. Chernobrovkin
5. Structural studies of the initial stages of titanium film oxidation in vacuum, V. I. Khitrova and S. A. Semiletov

FOR OFFICIAL USE ONLY

6. Low-temperature oxidation of titanium in rarefied molecular and atomic oxygen, I. N. Frantsevich, V. L. Tikush, G. V. Rusakov, L. A. Gayevskaya, V. S. Dvernyakov and Ye. S. Lugovskaya
7. Porosity of copper films deposited under conditions of concurrent ion bombardment, V. Pets and A. Fleming
8. On the influence of a constant electric field on the growth of insular metallic films, V. Pets, M. Friedrich and K. G. Dang
9. Production and properties of chromium silicide resistive films, H. Helms, V. Bretschneider, G. Beddis and P. Bogdanova
10. On the question of low impurity levels in oxide films, V. A. Ogorodnik
11. Some properties of films of praseodymium oxide alloyed with aluminum, V. A. Ogorodnik
12. Use of accelerated ion source for obtaining intermetallic thin films, V. G. Grigor'yan, G. I. Kazanets, V. I. Minakov and V. A. Obukhov
13. Calculation of cathode dark space length for discharge devices with rod-type electrodes, O. Ya. Gavriluk and Yu. G. Kononenko
14. Dependence of deposition rate on the geometric dimensions of a rod-type discharge device, O. Ya. Gavriluk and Yu. G. Kononenko
15. Production of resistive thin films by cathode sputtering in a rod-type discharge device, V. G. Kobka, G. I. Kostygina, A. A. Smakovenko and O. F. Taranenko
16. Production and study of dielectric films based on REM metallate compounds for microcircuit elements, D. I. Chernobrovkin, M. N. Piganov and I. A. Korzh
17. On the structure and properties of films obtained by catalytic oxidation of titanium, N. P. Peksheva
18. Mechanical stresses in $\text{Al}_x\text{Ga}_{1-x}\text{As}$ films grown on substrates of GaAs with various dopants, N. D. Vasilenko, A. M. D'yachenko and B. P. Masenko
19. Study of gallium microinclusions in epitaxial GaAs films, G. V. Berenshtein, N. D. Vasilenko, A. M. D'yachenko and O. K. Gorodnichenko
20. Some properties of thin films of indium antimonide, O. G. Lyubutsin, I. I. Kletchenkov and A. F. Plevako
21. Temperature dependence of the brightness of $\text{GdF}_2\text{-Eu}^{3+}$ electroluminescent films, N. A. Vlasenko, Z. L. Denisova and V. S. Khomchenko
22. Electroluminescent properties of ZnS:MnF_2 films, T. P. Visheva

FOR OFFICIAL USE ONLY

23. On the effectiveness and etching characteristics of semi-insulating semiconductor crystals in a low-pressure r-f plasma discharge, N. V. Gavrilenko, A. F. Onipko and E. B. Tal'yanskiy
24. Study of the parameters of impurity centers in $\text{CdSe}_x\text{Te}_{1-x}$ films produced in their own vapors in r-f plasma, N. V. Gavrilenko, A. F. Onipko, I. I. Sava and M. G. Kolisnik
25. Phase composition and photoelectric properties of $\text{Sb}_x\text{In}_{1-x}\text{Se}$ films produced in their own vapors in r-f plasma, N. V. Gavrilenko, A. F. Onipko, I. I. Sava and I. V. Zhornovyi
26. Thermoresistive ferrite films obtained by electron beam vaporization, Yu. N. Okunevskiy, S. A. Pilipko and L. N. Tul'chinskiy
27. Study of reflection spectra of aluminum condensates in the UV part of the spectrum, V. M. Nedostup and N. N. Smirnova
28. Determination of anisotropy constant and magnetization level of thin films, A. I. Berezhnyakov, N. S. Troitskiy and V. N. Gurin
29. Production of film materials by exposure to concentrated solar radiation flux, I. N. Frantsevich, V. S. Dvernyakov, I. E. Kasich-Pilipenko, V. L. Tikush, G. V. Rusakov, L. A. Gayevskaya, L. R. Sharinyan and R. S. Biryukova
30. Plasma electron gun based on the VUP-2K universal vacuum facility, R. V. Dashtoyan, V. I. Mel'nik and R. A. Kadzhoyan
31. Study of the factors determining the chemical stability of films, N. P. Peksheva
32. Production of dielectric films on gallium arsenide by the electrochemical oxidation method, V. V. Novichkov and N. P. Novichkova
33. Properties of MDS structures with anodic GaAs oxide coating, M. K. Samokhvalov, V. V. Novichkov, A. M. Sverdlova and N. P. Novichkova
34. Growth of anodic films on GaAs in acid, alkali, and neutral electrolytes, V. V. Ovchinnikov, L. V. Kozhitov, D. U. Kamalova and V. V. Ventsov
35. Electron diffraction study of intermetallic phases in Pt and Ni films deposited on silicon, B. G. Donishev, A. Ye. Likhtman, Ye. I. Kotenko, Yu. N. Makogon and S. I. Sidorenko
36. Study of high-resistance thin-film resistors based on new cermets, N. D. Michsanin, D. I. Chernobrovkin and Ye. V. Kootryukov
37. X-ray diffraction phase analysis of films obtained by vacuum vaporization of some multicomponent copper-base alloys, V. I. Popov, V. G. Tinyayev and A. A. Popova

COPYRIGHT: Institut problem materialovedeniya AN USSR (IPM), 1978
[6-9576]

8576
CSO: 1862

FOR OFFICIAL USE ONLY
LASERS AND MASERS

UDC 621.378.3

AN ELECTRIC-DISCHARGE PULSED CO₂ RESEARCH LASER

Moscow KVANTOVAYA ELEKTRONIKA in Russia. Vol 7, No 7(97), Jul 80 pp 1456-1460
manuscript received 10 Dec 79

[Article by Z. I. Ashurly, Yu. M. Vas'kovskiy, I. A. Gordeyeva, L. V. Malyshev,
R. Ye. Rovinskiy and A. A. Kholodilov]

[Text] This paper describes a pulsed high-pressure electric-discharge CO₂ laser that provides a wide range of beam output parameters. By sectionalizing the electrode system and power supply, provisions are made for adjusting the length of the active part and for producing two or more pulses that follow one another with a predetermined delay. Stable adjustment of the duration and shape of the emission pulse is achieved by proper selection of the mixture composition. An investigation is made of the way that the weak-signal gain of the active medium depends on time and on the total pressure of the mixture for different proportions of the gas components. Treatment of the results is based on a simplified model of kinetic processes in the discharge.

In research associated with the practical application of infrared lasers for production purposes, high-pressure electric-discharge CO₂ lasers with transverse discharge have given a good account of themselves. Capabilities for controlling the parameters of output radiation of electric-discharge lasers are appreciably enhanced by sectionalizing the electrode system of the laser and the part of the power supply circuit that shapes the electric pulses. This article describes a laboratory electric-discharge laser with a sectionalized electrode system and demonstrates its research capabilities.

The electric-discharge section of the laboratory laser facility with length of about 45 cm consists of an anode in the form of a Duralumin plate with working surface measuring 42 x 15 cm, a cathode of the same material measuring 40 x 12 cm, and an auxiliary electrode for which parallel transverse grooves 2.6 mm wide and approximately as deep are milled on the working surface of the cathode. The insulated wire of the auxiliary electrode is stretched in these grooves so that half its diameter extends above the surface of the cathode.

A diagram of the power supply section is shown in Fig. 1. The electric pulse is shaped by commutating devices K₁ and K₂ that supply approximately twice the voltage U₀ of storage capacitor C₁ to the discharge gap of the laser section. Initially,

FOR OFFICIAL USE ONLY

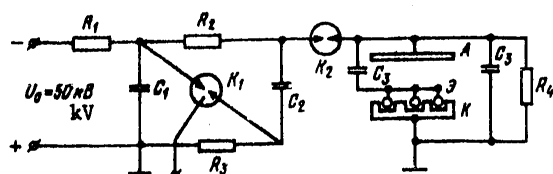


Fig. 1. Electric supply circuit of the laser section

this causes development of an auxiliary corona discharge between the wire of ionizing electrode 3 and cathode plate K, followed by a high-pressure glow discharge in the main discharge gap A-K.

Several such electric-discharge sections set up in series inside a common bulb with the mirrors of an optical cavity on the end faces make up the laboratory laser. A trigger and synchronization unit ensures simultaneous operation of the controlled commutators K_1 and all sections of the electric-discharge laser.

The sectionalized laser design enables the use of a variety of schemes for triggering the sections. For example the length of the active part of the laser can be regulated by energizing only some of the sections. Individual sections or individual groups of sections can be triggered with controllable delay relative to one another from $0.5 \mu\text{s}$ to any required value.

The controllable change of the duration and shape of the emission pulse is conducive to expansion of the research capabilities of the laboratory laser. (Pulse duration is taken as the time during which 90% of its energy is released). One way to change pulse shape and duration is to superimpose two sequential pulses produced by two groups of laser sections; however, reproducibility of the results is poor in this case since the spread in triggering delay has an effect. Research has shown that more reliable results are realized by varying the proportion of components of the gas mixture and altering electric discharge conditions.

TABLE 1

(1) Номер смеси	(2) Соотношения компонентов			(3) E, Дж	(4) E_n/E	(5) t_n , мкс
	CO ₂	N ₂	He			
1	2	0	8	60	0,66	0,75
2	4	1	3	80	0,36	1,3
3	4	1	15	200	0,25	1,8
4	1	2	3	390	0,2	2,1
5	1	4	5	430	0,15	3,6
6	1	8	8	360	0,13	4,5
7	1	15	10	160	0,1	7,8

- 1--Mixture number 4--Ratio of peak energy to total pulse energy
 2--Proportion of components 5--Pulse duration, μs
 3--E, joules

In studying this technique for regulating emission pulse shape and duration, the pulse shape was recorded by a germanium photoreceptor with photon charge enhancement, and the total energy in a pulse was measured by a TPI-2-5 graphite calorimeter. The time-resolved values of the discharge current and the voltage between electrodes were simultaneously measured by a Rogowski loop and voltage divider.

FOR OFFICIAL USE ONLY

FOR OFFICIAL USE ONLY

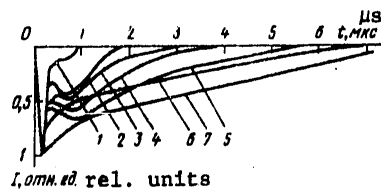


Fig. 2. Oscillograms of emission pulses in reduced form

The gas mixture compositions that were studied and resultant emission pulse durations are summarized in Table 1. Fig. 2 shows oscillograms of the corresponding pulses in reduced form. These give a graphic idea of the way that the emission pulse is deformed with a change in gas mixture composition. When nitrogen content is small or totally absent, a considerable part of the radiant energy is released in the initial peak, and the pulse has almost no "tail." The ratio of peak energy to total pulse energy reaches nearly 70%. As the percentage of nitrogen in the mixture is increased there is an increase in the proportion of the "tail" part of the pulse, which is accompanied by elongation. With the maximum relative nitrogen content (mixture 7) the initial spike is weak, containing no more than 10% of the total energy, and the pulse has the greatest duration. In all cases the total pressure of the gas mixture was 620 mm Hg.

The emission energy, and the efficiency with which the electrical energy invested in the discharge is converted to radiant energy at first increase with increasing relative content of nitrogen in the mixture, reaching a maximum in mixture 5, and then fall off. The energy input to the discharge is practically independent of the mixture composition except for the most extreme cases of nitrogen-rich or nitrogen-poor mixtures. In these cases the energy input falls off noticeably.

Since the duration and shape of the emission pulse showed good reproducibility with every predetermined mixture composition, these characteristics of the electric-discharge laser could be confidently adjusted by selecting the necessary proportion of gas components. In the optimum case (from the standpoint of maximizing output energy and efficiency) with a ratio of CO:N:He = 1:2:3 the laboratory laser produced a stable energy output of more than 30 J/l at a total efficiency of conversion of the energy stored in the capacitors to emission of about 15%. Emission pulse duration in this case was $\sim 2 \mu s$. The total range of variation of pulse duration in these experiments was from ~ 0.7 to $\sim 8 \mu s$. Pulse duration can also be varied by changing the initial voltage across the discharge gap; however, this method of adjustment is not very efficient since for a given pressure of the gas mixture and stable existence of the glow discharge the technique can be realized only over a very narrow voltage range, and involves a considerable change in the energy pattern of the emission.

Studies of the gain of the medium provide additional information on the influence that the proportion of gas mixture components has on the nature of processes in the active medium of a sectionalized laboratory electric-discharge laser. To measure the gain, plane-parallel NaCl plates were installed at the Brewster angle in place of the mirrors of the optical cavity of the laser. The bulb was illuminated along the optical axis by a thin probing beam, the source of which was a CO₂ electric-discharge laser operating in the pulse mode on a single transverse mode. The pre-ionization system for the probing laser was the same as for the main bulb. The laser operated at a relatively low pressure of the working mixture (of the order of 200 mm Hg or less), which was conducive to a fairly narrow luminescence line. The

FOR OFFICIAL USE ONLY

FOR OFFICIAL USE ONLY

laser had a short resonator and emitted close to the threshold. The energy in the emission pulse was 0.7 J at a duration of $\sim 2 \mu\text{s}$ on a level of 35% maximum.

The optical cavity of the probing laser was made up of a diffraction grating of 100 lines/mm and a flat germanium mirror. Within the cavity itself were two NaCl lenses forming a telescopic system with approximately 2x magnification, and an adjustable iris. Individual vibrational-rotational transitions, in particular the transition P(20), were isolated by rotating the diffraction grating. The probing laser was triggered with adjustable delay relative to the triggering of the discharge in the main bulb. Gain was determined from the ratio of amplitudes of the probing signal and the signal amplified after passage through the cell with an accuracy of about 15%. Absence of saturation of the amplified signal was verified by increasing the amplitude of the probing pulse by a considerable factor as compared with the level on which the gain measurements were made. The amplitude of the entering radiation pulse was regulated by using calibrated film absorbers of infrared radiation.

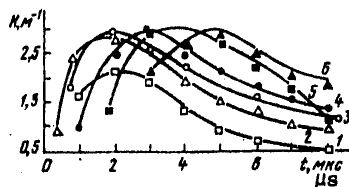


Fig. 3. Gain as a function of the delay time of the probing pulse relative to the beginning of discharge in the bulb for gas mixtures $\text{CO}_2:\text{N}_2:\text{He} = 1:1:3$ (1); $2:1:5$ (2); $1:1:2$ (3); $1:1:1$ (4); $1:2:3$ (5) and $1:2:1$ (6)

Fig. 4 shows the gain in different media as a function of total gas pressure in the pressure range where the glow discharge is stable. The maximum gain is displaced toward higher pressures as the helium content in the mixture increases. Data showing how the gain depends on the quantity E/p for four mixture compositions are summarized in Table 2.

TABLE 2

(1) Состав смеси			(2) E/p $\text{B}/(\text{cm} \cdot \text{mm}$ $\text{пт. ст.})$	K, m^{-1}
CO_2	N_2	He		
1	1	1	22 ± 0.8	2.4—3.0
1	2	1	25 ± 1.0	2.2—3.3
1	2	3	16 ± 0.5	2.0—2.5
2	1	5	14 ± 0.4	2.1—2.7

Fig. 3 shows the resultant curves for gain as a function of the delay time of the probing pulse relative to the beginning of discharge in the bulb at different gas mixture compositions. All curves were plotted at the same value of E/p (E is field strength, p is gas pressure). For the different investigated mixture compositions the position of the maximum of the curves and their initial displacement depend in a complicated way on the composition of the active medium.

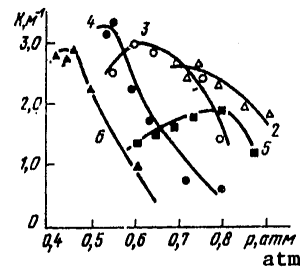


Fig. 4. Gain as a function of the total gas pressure for different gas mixture compositions. Notation is the same as on Fig. 3

KEY TO TABLE 2:

- 1--Mixture composition
2-- E/p , $\text{V}/(\text{cm} \cdot \text{mm Hg})$

FOR OFFICIAL USE ONLY

The values for the gain that are given in the table are for the range of initial voltages across the electrodes of the bulb from 94 to 100 kV. An impediment to a more detailed investigation of the way that gain depends on E/p is the fact that the region of stable existence of the glow discharge is limited to a very narrow change in field strength E or pressure p . The region of stable existence of the discharge narrows with an increase of nitrogen content in the mixture, and to an even greater extent with an increase in helium content.

The observed peculiarities in the way that gain depends on time, gas mixture composition, total pressure p , and the parameter E/p are determined by the nature of population and deactivation of the laser levels of CO_2 molecules as they interact with the electrons and molecules of the active medium. It can be shown that the following simplified model gives a satisfactory qualitative description of kinetic processes. The levels of symmetric, asymmetric and deformational vibrational modes of the CO_2 molecules are populated, and the N_2 molecules are vibrationally excited under the effect of time-variable discharge current in the volumetrically homogeneous active medium. The distribution of vibrational energy by levels is not considered. Working levels $10^0 0$ and $02^0 0$ are unified into a single "lower" level. The energy of excitation is invested directly in the upper laser level $00^0 1$ of CO_2 , ($v=1$) of N_2 , and the lower laser level. This assumption is justified by the rapid process of exchange between $00^0 1$ of CO_2 and ($v=1$) of N_2 , the strong interaction of the symmetric and deformation modes, and also rapid intermodal exchange and the low level of vibrational temperatures.

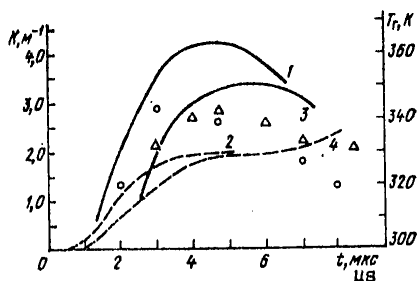


Fig. 5. Theoretical dependences of gain (1, 3) and gas temperature T_r (2, 4) as a function of the elapsed time after onset of the probing pulse for mixtures of $\text{CO}_2:\text{N}:\text{He} = 1:2:3$ (1, 2) and $1:2:1$ (3, 4); \circ --experimental values of gain for the first, and Δ --for the second mixture

The results of calculation of the gain for two mixtures of gases done by numerical methods based on the simplified kinetic model are shown in Fig. 5. The time behavior of the calculated values of gain, the presence of a maximum and its position as well as the absolute value of the gain agree satisfactorily with experiment, which favors the chosen model, at least for sections of increase and attainment of maximum gain. However, the experimental plot falls off much more rapidly than the theoretical curves. This probably due to the fact that the actual rise in vibrational temperature is more rapid than the calculation implies.

The authors thank A. A. Bakeyev for useful discussion of the materials of the paper, and also V. G. Kulikov, G. A. Bogatova and N. N. Vorob'yeva for assistance with the experiments.

COPYRIGHT: Izdatel'stvo "Sovetskoye radio", "Kvantovaya elektronika", 1980
[3-6610]

6610
CSO: 1862

FOR OFFICIAL USE ONLY

FOR OFFICIAL USE ONLY

UDC 621.378.33

LIMITING CHARACTERISTICS OF A PHOTOCHEMICAL XeO LASER

Moscow KVANTOVAYA ELEKTRONIKA in Russian Vol 7, No 7(97), Jul 80 pp 1482-1491
manuscript received 20 Dec 79

[Article by V. S. Zuyev, L. D. Mikheyev and I. V. Pogorel'skiy, Physics Institute imeni P. N. Lebedev, USSR Academy of Sciences, Moscow]

[Text] An experimental and theoretical study is done on the nature of internal losses in the active medium of a photochemical XeO laser with pumping by an open high-current electric discharge. It is shown that the specific efficiency of the XeO laser can be increased by reducing internal losses. Pumping is analyzed and the anticipated lasing energy is determined for an XeO laser with a flat resonator. The optimum composition of the mixture is found as well as the transmission of mirrors that should yield a lasing energy of ~ 40 J in a pulse with duration of ~ 10 μ s, which corresponds to a total laser efficiency of $\sim 0.1\%$. Possibilities are mentioned for further improving the efficiency of the given laser to 0.2% when isotopically pure xenon is used.

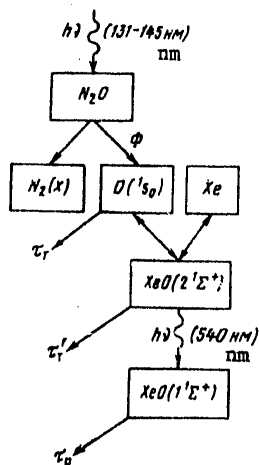


Fig. 1. Kinetic scheme of photochemical XeO laser [Ref. 1]

1. Introduction

Ref. 1 gives the results of a study of the specific characteristics of a cooled photochemical XeO laser with the kinetic scheme shown in Fig. 1. The laser was pumped by the vacuum ultraviolet radiation of a high-current pulsed electric discharge fed by a capacitor bank with stored energy of 57 kJ. Laser operation was studied in an arrangement in which the volume of active medium taking part in lasing was restricted by the small diameter of the laser chamber (5 cm). The maximum lasing energy in a pulse with half-amplitude duration of 8 μ s equal to 2.2 J was attained by using a planar-spherical cavity and a working mixture of N₂O:Xe:He = 1:75:170 at a total concentration of 3 amagat units and temperature of 160 K.

FOR OFFICIAL USE ONLY

FOR OFFICIAL USE ONLY

The experimentally measured weak-signal gain reached $K_{YC} = 3.5 \cdot 10^{-3} \text{ cm}^{-1}$. In the absence of a lasing field, the concentrations of molecules of XeO ($2^1\Sigma^+$) and oxygen atoms (1S_0) corresponding to such a value of K_{YC} are equal to $2 \cdot 10^{14}$ and $1.5 \cdot 10^{15} \text{ cm}^{-3}$ respectively. The time for quenching of oxygen atoms (1S_0) by nitrous oxide N_2O and photolysis products is known, and under the conditions of the experiment is $\tau_T \approx 200\text{--}400 \text{ ns}$. Thus at the instant when maximum lasing power is reached, the rate of formation of atoms of O (1S_0) averaged over the cross section of the active medium (the pumping rate) is $\phi = [O(^1S_0)]/\tau_T = (6 \pm 2) \cdot 10^{21} \text{ cm}^{-3} \cdot \text{s}^{-1}$. Comparing this quantity with the specific peak lasing power $W_{YD} = 300 \text{ kW/l} = 0.75 \cdot 10^{21} \text{ photons per cm}^3 \cdot \text{s}$, we find that the efficiency of converting the pumping per unit volume of active medium to stimulated emission is $\eta = 15 \pm 5\%$.

If we consider that the coefficient of internal losses in the active medium under the conditions of the experiment is $\gamma_{II} = 10^{-3} \text{ cm}^{-1}$, and the distribution of losses in transmission of the mirrors is $\gamma_C = 3.5 \cdot 10^{-4} \text{ cm}^{-1}$ [Ref. 1], it can be readily shown that the experimental value of η is due chiefly to internal losses. Thus a further reduction in γ_{II} should improve the efficiency of the XeO laser.

In this paper we examine the nature of internal losses in the active medium of an XeO laser and the feasibility of reducing them. An examination is also made of the possibility of a further considerable increase in the lasing energy of the XeO laser by increasing the volume of the active medium while using the same pumping source as was used in previous experiments. It is shown on the basis of calculations that an energy of 40 J can be attained in the laser pulse, which corresponds to a total laser efficiency of $\sim 0.1\%$. Mention is also made of the possibility for further increasing the efficiency of the given laser to 0.2% by using isotopically pure xenon in the working mixture.

2. Internal Losses in the Active Medium

Static gradient of the index of refraction. It was noted above that the efficiency with which pumping in a unit volume of active medium of a photochemical XeO laser is converted to lasing is limited by losses within the resonator. The greatest level of losses is associated mainly with the optical inhomogeneity of the working medium that arises as it is cooled in the laser chamber. This inhomogeneity shows up in particular when the chamber is exposed to the probing beam of a helium-neon laser. Deflection of such a beam was used to measure the gradient of the index of refraction ($\text{grad } n$) in the medium.

An investigation was made of the change in $\text{grad } n$ heightwise of the chamber in gas mixtures of various compositions. Fig. 2 shows graphs of the change in $\text{grad } n$ in Xe and Ar with displacement from the center of the chamber upward ($l > 0$) and downward ($l < 0$). $\text{Grad } n$ is directed downward at all points, which corresponds to an increase in the density of the medium in this direction.

$\text{Grad } n$ averaged over the cross section of the laser chamber was on a level of 10^{-5} cm^{-1} for the optimum mixture indicated above. The value of γ_{II} for a flat resonator can be estimated by the formula [Ref. 2]

$$\gamma_{II} = \sqrt{\text{grad } n L_p / (2DL_a)} \quad (1)$$

where L_p and L_a are the lengths of the resonator and the active medium respectively, D is the transverse dimension of the active zone. Under the conditions of our

FOR OFFICIAL USE ONLY

FOR OFFICIAL USE ONLY

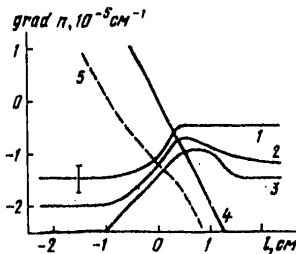


Fig. 2. Change in static grad n heightwise of the laser chamber: 1--Ar, 1.7 amagat units; 2--Ar, 3.8 amagat units; 3--Xe, 1.7 amagat units; 4--equivalent grad n for a concave spherical mirror with radius of curvature of 5 m; 5--sum of curves 2 and 4

in thermal conductivity; c) influx of heat through electric leads. (The design of the laser and the cooling technique are described in detail in Ref. 3).

To eliminate temperature inhomogeneities, plans for future experiments call for a change to steady-state cooling, use of a metal laser chamber and a considerable reduction of heat influx through electrical leads.

The problem of the chamber material must be considered in more detail. The use of a dielectric chamber in previous experiments was dictated by the inadequate electrical strength of the inert gases making up the working mixture under conditions where the initial voltage drop across the discharge gap reaches 45 kV. To convert to a metal chamber, a gas must be added to the working mixture that has high electrical strength, and simultaneously possesses the following properties: it is not frozen out when cooled to 160 K, it does not absorb radiation in the pumping band of N_2O (145-131 nm) and it does not quench atoms of $O(^1S_0)$. These requirements are satisfied by nitrogen for which the rate constant of quenching of $O(^1S_0)$ is extremely small ($5 \cdot 10^{-17} \text{ cm}^3/\text{s}$) [Ref. 4].

Experiments were done to check out the operability of the XeO laser with nitrogen. When 1 amagat unit of nitrogen was added to the working mixture, the breakdown distance for 50 kV was less than 10 cm. There was almost no reduction in the efficiency with which pumping was converted to induced emission inside the resonator. These experiments show the feasibility of using a metal laser chamber with diameter of ~20 cm.

Dynamic gradient of the index of refraction. If static temperature inhomogeneities are eliminated, losses in the active medium will be determined to a great extent by the dynamic gradient of the index of refraction that arises in photolysis of N_2O due to nonuniform heating and change in the refraction R of the active medium. Let us consider the losses due to these two effects.

experiments, typical values of the parameters appearing in (1) were: $L_p = 1 \text{ m}$, $L_a = 0.8 \text{ m}$, $D = 2 \text{ cm}$; in this case, $\gamma_{\Pi} = 2 \cdot 10^{-3} \text{ cm}^{-1}$. The value of γ_{Π} should be somewhat lower for a planar-spherical cavity, which has been experimentally confirmed [Ref. 1].

The distribution of grad n observed in Fig. 2 was integrated with respect to the height of the chamber, and it was found that the gas concentration varies with respect to height by 7%, which corresponds to a temperature difference of 10 K between the top and bottom of the chamber. Sources of such temperature inhomogeneity are: a) the unsteady nature of chamber cooling, which is done by a short burst of liquid nitrogen into the cryostat; b) the presence of dielectric and metal parts in the laser chamber, differing considerably

FOR OFFICIAL USE ONLY

FOR OFFICIAL USE ONLY

Refraction is related to the refractive index of the medium by the expression [Ref. 5]

$$n \approx 1 + 1.5 RN/A,$$

where N is gas concentration, A is Avagadro's number. Let us use N_0 to designate the initial concentration of N_2O , and $\delta(r, t)$ to denote the percentage of N_2O molecules dissociated during photolysis. Then the change in the index of refraction during photolysis is

$$\Delta n(r, t) = 1.5 \Delta R \delta(r, t) N_0 / A,$$

where we have $\Delta R = -2.6 \text{ cm}^3$ for dissociation of N_2O into N_2 and O [Ref. 6, 7], hence

$$\text{grad} n(r, t) = -0.65 \cdot 10^{-23} N_0 \text{grad} \delta(r, t). \quad (2)$$

As noted above, the second cause of the change in n is nonuniform heating of the gas as pumping radiation is absorbed. The resultant pressure differential between regions with different temperatures should shift material from the high-temperature region near the source toward the periphery.

In calculating the displacement of material due to the action of this effect, which we will call the gasdynamic effect, we can disregard the influence of thermal diffusion. To determine the gasdynamic density gradient of the working medium and the associated gradient of the index of refraction at an arbitrary point of the active medium and at an arbitrary instant of time, we use the following system of equations that includes equations of continuity, motion and the first law of thermodynamics written with consideration of smallness of the final change in density $\Delta \rho$, rate of displacement of material u and the inequality

$$u/r \ll |\partial u / \partial r|^*,$$

that reduces the equation of continuity to a form corresponding to the plane case [Ref. 8]:

$$\begin{aligned} \frac{\partial \Delta \rho}{\partial t} &= -\rho_0 \frac{\partial u}{\partial r}; \\ \frac{\partial u}{\partial t} &= -\frac{1}{\rho_0} \frac{\partial \Delta P}{\partial r}; \\ \Delta P &= B \rho_0 \Delta T, \end{aligned} \quad (3)$$

where B is the specific gas constant that depends on the molecular weight of the gas. Heating ΔT is related to the degree of dissociation of the working substance during photolysis by the expression

$$\Delta T(r, t) = \delta(r, t) N_0 W_0 / c_v,$$

where c_v is the specific heat of 1 cm^3 of gas, $W_0 = 2.5 \cdot 10^{-19} \text{ cal}$ [Ref. 1] is the thermal energy released upon absorption of a single pumping quantum.

*) The validity of this inequality can be proved by integrating the last two equations of system (3) using data on N_2O dissociation (see below).

FOR OFFICIAL USE ONLY

Solving system (3), we can readily find an expression for grad n:

$$\text{grad } n(r, t) = \frac{BW_0 N_0 (n-1)}{c_V} \int_0^t \left(\frac{\partial^2 \delta(r, t)}{\partial r^2} \right) \partial t' \partial t. \quad (4)$$

Substituting the numerical values of parameters for the optical mixture mentioned above, and also for the same mixture with the addition of 1 amagat unit of N_2 in expression (4), we get the same results:

$$\text{grad } n(r, t) \approx 3 \cdot 10^{-3} N_0 \int_0^t \left(\frac{\partial^2 \delta(r, t)}{\partial r^2} \right) dt' dt. \quad (5)$$

To calculate the dynamic grad n from (2) and (5) we can use the results of calculation of photodissociation of N_2O done in section 3 of this paper. Calculations show that the gradients of the refractive index that arise due to the given effects are oppositely directed and partially compensate one another (Fig. 3). The coefficient of internal losses $\gamma_{\Pi}^A(r, t)$ associated with the dynamic grad n can be calculated by (1). Results are shown in Fig. 4.

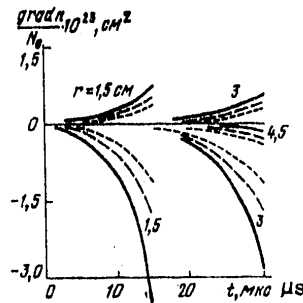


Fig. 3. Radial distribution of the dynamic grad n for the specified distances r from the axis of the source; $N_0 = 2 \cdot 10^{17}$ (---), $4 \cdot 10^{17}$ (- - -), and 10^{18} cm^{-3} (—): the upper groups of curves describe grad n due to change of refraction with photodissociation of N_2O , and the lower groups characterize the gasdynamic effect in a mixture of N_2O with Xe (1 amagat unit) and He (2 amagat units)

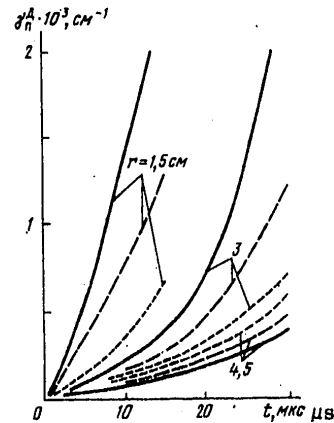


Fig. 4. Distribution of internal losses due to dynamic grad n. Notation is the same as in Fig. 3

Other sources of losses in the active medium that are independent of the initial concentration of N_2O are: a) diffuse scattering on the mirrors, taken as 0.5% on each surface; diffraction in the active layer; c) imprecise alignment of the mirrors in the cavity, taken as 5". The overall losses from these causes are estimated on a level of $\gamma_{\Pi}^{CT} = 2 \cdot 10^{-4} \text{ cm}^{-1}$.

Overall static and dynamic losses in our calculations will be taken as

$$\gamma_{\Pi} = \gamma_{\Pi}^{CT} + \gamma_{\Pi}^A(r, t).$$

FOR OFFICIAL USE ONLY

FOR OFFICIAL USE ONLY

3. Calculations of Pumping

To determine the expected energy of stimulated emission of a photochemical XeO laser with a flat resonator it is necessary to know the size of the region where threshold conditions are satisfied, and the distribution of super-threshold pumping in this region. Calculations are given below for the space-time distribution of pumping $\Phi(r, t)$ in the active medium based on the experimental time dependence of luminous flux I_0 on the surface of the source in the band of 131-145 nm [Ref. 9] (Fig. 5).

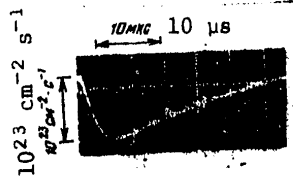


Fig. 5. Time dependence of photon flux emitted in the pumping band of N_2O from a unit of surface used in high-current electric discharge experiments

The pumping calculations were done on the assumption of a uniform directional pattern of emission on the surface of the source with consideration of such factors as the cylindrical geometry of the source, its taper, the spectral dependence of the absorption cross section of N_2O and quantum yield of $O(^1S_0)$, and the dissociation of N_2O by photolysis. The method of calculation was suggested by V. Ya. Karpov.

The rate of formation of atoms of $O(^1S_0)$ at an arbitrary instant of time t at an arbitrary distance r from the axis of the discharge is

$$\Phi(r, t) = cN(r, t) \int_{\nu_1}^{\nu_2} \kappa_{\nu} \sigma_{\nu} P_{\nu}(r, t) d\nu, \quad (6)$$

where c is the speed of light, $N(r, t)$ is the concentration of N_2O , σ_{ν} is the spectral cross section of absorption of N_2O , κ_{ν} is the spectral quantum yield of $O(^1S_0)$ and $P_{\nu}(r, t) = \int_{\Omega} f_{\nu}(r, t) d\Omega$ is the spectral density of photons.

The spectral density of photons in a unit solid angle on the surface of the source $f_{\nu}(R, t)$ is related to $I_0(t)$ by the expression

$$I_0(t) = f_{\nu}(R, t) \pi c \Delta\nu, \quad (7)$$

where $\Delta\nu$ is the spectral interval of 131-145 nm. We can readily find the relation between $f_{\nu}(r, t)$ and $f_{\nu}(R, t)$ with consideration of the absorption of photons in the active medium. As a result we get

$$\Phi(r, t) = \frac{4I_0(t)N(r, t)}{\pi\Delta\nu} \int_0^{L/2} dR \int_0^{\arccos R/r} d\varphi \frac{r \cos \varphi - R}{|AB|^3} \times \int_{\nu_1}^{\nu_2} d\nu \kappa_{\nu} \sigma_{\nu} \exp \left\{ -\sigma_{\nu} \int_A^B N(s, t) ds \right\}. \quad (8)$$

The quantity $N(s, t)$ was calculated by an analogous formula with $\kappa_{\nu} = 1$.

FOR OFFICIAL USE ONLY

FOR OFFICIAL USE ONLY

Numerical calculations were done by computer for a wide range of $N_0 = 5 \cdot 10^{16} - 10^{18} \text{ cm}^{-3}$. As an example, Fig. 6, 7 give the results of calculation of $\phi(r, t)$ and the degree of dissociation $\delta(r, t) = [N_0 - N(r, t)]/N_0$ for $N_0 = 4 \cdot 10^{17} \text{ cm}^{-3}$. This was the concentration of N_2O in the optimum mixture mentioned above.

It was shown in section 2 how the results of calculations of $\delta(r, t)$ are used in calculating the dynamic grad n in the active medium. On the basis of estimates found for γ_n and the results of calculation of pumping $\phi(r, t)$ the anticipated energy of stimulated emission of the XeO laser with plane-parallel resonator is calculated in section 4.

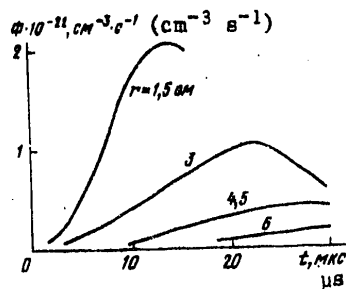


Fig. 6. Results of calculation of pumping at different distances from the discharge axis at $N_0 = 4 \cdot 10^{17} \text{ cm}^{-3}$

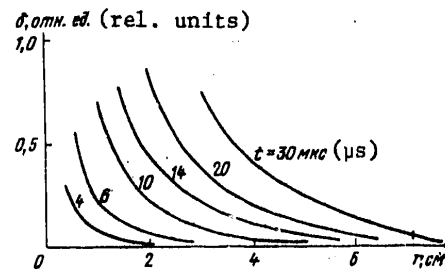


Fig. 7. Results of calculation of the degree of dissociation of N_2O at different times from the beginning of a discharge at $N_0 = 4 \cdot 10^{17} \text{ cm}^{-3}$

4. Calculations of the Energy of Stimulated Emission of the XeO Laser with Plane-Parallel Resonator

Let us estimate the size of the region taking part in lasing and the lasing energy when a plane-parallel cavity is used in a laser chamber of fairly large diameter not limited by the size of the lasing region.

To determine the lasing zone with the use of results of calculation of $\phi(r, t)$ it is necessary to assign the threshold pumping level ϕ^{th} . This quantity can be defined by the formula

$$\phi^{\text{th}} = \frac{\gamma_0 + \gamma_n}{\sigma \alpha_{v'=0} \alpha_{j'}} \left(\frac{1}{\tau_r} + \frac{1}{\tau_r K_p [\text{Xe}]} \right). \quad (9)$$

derived in Ref. 1 from analysis of the kinetics of the XeO laser. Here $\sigma = 4.5 \cdot 10^{-16} \text{ cm}^2$ [Ref. 1] is the cross section of amplification on the laser transition; $\alpha_{v'=0}$ is the fraction of molecules of $\text{XeO}(2^1\Sigma^+)$ located on the lower vibrational level; $\alpha_{j'}$ is the probability that a molecule $\text{XeO}(2^1\Sigma^+)_{v'=0}$ will be found on a rotational level of maximum population; K_p is the constant of equilibrium of processes of dissociation of $\text{XeO}(2^1\Sigma^+)$ and reverse recombination (at $T = 160 \text{ K}$, $\alpha_{v'=0} = 0.7$, $\alpha_{j'} = 0.06$, $K_p = 5 \cdot 10^{-21} \text{ cm}^3$ [Ref. 1]); τ_r and τ_T are the respective quenching times of atoms $\text{O}(^1S_0)$ and molecules $\text{XeO}(2^1\Sigma^+)$.

Let us consider the part played by different inversion quenching processes in determination of the threshold pumping level.

FOR OFFICIAL USE ONLY

The constants of quenching of molecules of $\text{XeO}(2^1\Sigma^+)$ by nitrous oxide and products of photolysis are unknown. In Ref. 10 measurements were made of the way that the luminescence quenching time of molecules of $\text{XeO}(2^1\Sigma^+)$ depends on pressure of the components of a mixture of N_2O and Xe . It was concluded on the basis of these data that the state $\text{XeO}(2^1\Sigma^+)$ is quenched by N_2O molecules with rate constant $(2.3 \pm 0.4) \times 10^{-11} \text{ cm}^3/\text{s}$, and by atoms of Xe with rate constant $(0.4 \pm 0.1) \cdot 10^{-14} \text{ cm}^3/\text{s}$. The resultant values are close to the known quenching constants of atoms $\text{O}(^1\text{S}_0)$ [Ref. 11, 12]. In stating this result it should be noted that under the conditions of experiments of Ref. 10 ($T=300 \text{ K}$, $p_{\text{Xe}} \leq 1 \text{ atm}$) less than 2% of the atoms of $\text{O}(^1\text{S}_0)$ are in the bound state. In this case, in order for the quenching of $\text{XeO}(2^1\Sigma^+)$ molecules to be noticeable against a background of quenching of atoms of $\text{O}(^1\text{S}_0)$, the quenching constants of molecules of $\text{XeO}(2^1\Sigma^+)$ must be at least two orders of magnitude greater than the corresponding quenching constants of atoms of $\text{O}(^1\text{S}_0)$. Apparently this circumstance was not taken into consideration by the authors of Ref. 10, and the observed quenching in our opinion should be attributed to oxygen atoms rather than to XeO molecules.

There are almost no data on quenching of $\text{XeO}(2^1\Sigma^+)$ molecules by inert gases either. It is true that Ref. 13 mentioned three-body quenching of $\text{XeO}(2^1\Sigma^+)$ in xenon with a rate constant of $(4 \pm 2) \cdot 10^{-33} \text{ cm}^6/\text{s}$. However, these data were not subsequently confirmed by Ref. 14. The latter paper gives only an upper estimate of the rate constant of quenching of $\text{XeO}(2^1\Sigma^+)$ by xenon: $10^{-11} \text{ cm}^3/\text{s}$.

In contrast to molecules of $\text{XeO}(2^1\Sigma^+)$, quenching of atoms of $\text{O}(^1\text{S}_0)$ has been rather thoroughly studied. The constants of quenching by nitrous oxide, products of photolysis and inert gases can be found in Ref. 11, 12, 15. In the optimum mixture with consideration of partial dissolution of N_2O by the instant of attainment of the pumping maximum, the quenching time of atoms of $\text{O}(^1\text{S}_0)$ should be $\sim 300 \text{ ns}$.

It should be noted that quenching of $\text{O}(^1\text{S}_0)$ by electrons that may be formed during photo-ionization of these atoms by pumping radiation apparently plays no appreciable role*). Actually, since the working mixture contains an electronegative gas with sticking constant of thermal electrons $k_{\text{TP}} = 10^{-10} \text{ cm}^3/\text{s}$ [Ref. 19], in a medium under the action of a flux of ionizing radiation I_{H} estimated on a level of $10^{23}-10^{24} \text{ photons}/(\text{cm}^2 \cdot \text{s})$ a quasi-steady concentration of electrons

$$N_e = \sigma_{\text{H}} I_{\text{H}} [\text{O}(^1\text{S}_0)] / (k_{\text{TP}} [\text{N}_2\text{O}])$$

should be maintained, where σ_{H} is the cross section of photoionization of atoms of $\text{O}(^1\text{S}_0)$ taken as equal to an average $3 \cdot 10^{-19} \text{ cm}^2$ [Ref. 20]. For a threshold concentration of $[\text{O}(^1\text{S}_0)] = 5 \cdot 10^{14} \text{ cm}^{-3}$ and $[\text{N}_2\text{O}] = 4 \cdot 10^{17} \text{ cm}^{-3}$, we get $N_e = 4 \cdot 10^{11} - 4 \cdot 10^{12} \text{ cm}^{-3}$. The rate constant of superelastic quenching of atoms of $\text{O}(^1\text{S}_0)$ by electrons is $5 \cdot 10^{-9} \text{ cm}^3/\text{s}$ [Ref. 21]. Thus the typical time of quenching of atoms of $\text{O}(^1\text{S}_0)$ by electrons is $0.05-0.5 \text{ ns}$, which is 2-3 orders of magnitude greater than the time of quenching by the initial substance and products of photolysis.

The resultant conclusions are confirmed by experiments [Ref. 1]. In processing the results for the optimum working mixture of the XeO laser an estimate was found for

*) Photoelectrons play a considerable role in quenching of atoms of $\text{S}(^1\text{S}_0)$ and $\text{Se}(^1\text{S}_0)$ with intense vacuum-UV photolysis of COS and COSe [Ref. 16, 17]. Electron production with photoionization of $\text{O}(^1\text{S}_0)$ was observed in Ref. 18.

FOR OFFICIAL USE ONLY

$$\tau' = [(\tau_p')^{-1} + (\tau_p K_p [\text{Xe}])^{-1}]^{-1} \approx 12-25 \text{ ns},$$

which agrees satisfactorily with the above-mentioned time of quenching of atoms of $\text{O}(^1\text{S}_0)$ by nitrous oxide and products of photolysis with consideration of heating of the mixture during photolysis.

Taking $1/\tau' \sim N_0$, at a fixed concentration of $[\text{Xe}] = 1$ amagat unit we get

$$1/\tau' = (1-2) \cdot 10^{-10} N_0, \text{ s}^{-1}. \quad (10)$$

Using the estimates of γ_{Π} found in section 2, we can estimate $\Phi^{\Pi}(r, t)$ from (9) for any initial concentration of N_2O , and by using the results of calculations of $\Phi(r, t)$ we can determine the specific lasing power $W_{\text{уд}}$ as a function of time and distance from the axis of the pumping source:

$$W_{\text{уд}}(r, t) = \frac{\gamma_0}{\gamma_0 + \gamma_{\Pi}} \frac{\Phi(r, t) - \Phi^n(r, t)}{\tau_p/\tau' + 1}, \quad (11)$$

where τ_p is the time of relaxation of the lower laser levels. Like (9), expression (11) is obtained from solution of kinetic equations [Ref. 1].

In our estimates of $W_{\text{уд}}$ from (11) and (9) we will use the maximum estimate of $1/\tau'$ from (10) and disregard the term τ_p/τ' since the results of experiments of Ref. 1 have shown that when the working mixture is sufficiently diluted with helium with a concentration of several amagat units, τ_p can be reduced to a few ns.

By integrating $W_{\text{уд}}$ with respect to time and space, we get the expected lasing energy E_r . This operation was done graphically for different values of N_0 and γ_c . The results are summarized in the table. According to calculations the maximum lasing energy of 40 J should be observed at $N_0 = 4 \cdot 10^{17} \text{ cm}^{-3}$ and $\gamma_c = 5 \cdot 10^{-4} \text{ cm}^{-1}$. In this connection, the lasing pulse duration measured at half-amplitude is $\sim 12 \text{ } \mu\text{s}$, and the diameter of the laser beam is $\sim 10 \text{ cm}$. Let us note that the optimum with respect to N_0 and γ_c corresponds approximately to the figures previously found experimentally in studies with a planar-spherical resonator.

Anticipated emission energy of a photochemical XeO laser pumped by a high-current discharge with energy input of 50 kJ

$10^{17} N_0, \text{ cm}^{-3}$	$10^{-4} \gamma_c, \text{ cm}^{-1}$	(1) $E_r, \text{ Дж}$		$10^{17} N_0, \text{ cm}^{-3}$	$10^{-4} \gamma_c, \text{ cm}^{-1}$	(1) $E_r, \text{ Дж}$	
		(2) Природ- ный Xe	(3) Изотоп Xe			(2) Природ- ный Xe	(3) Изотоп Xe
2	2,5	30	40	4	10	30	85
2	5	35	65	4	20	20	65
2	10	25	60	10	5	15	70
4	2,5	30	50	10	10	15	90
4	5	40	75	10	20	12	85

KEY: 1--Lasing energy in joules
2--Natural xenon
3--Isotopic xenon

FOR OFFICIAL USE ONLY

We noted previously [Ref. 1] that the gain of the active medium of the XeO laser can be considerably increased by using isotopically pure xenon. The fact is that natural xenon has a complicated isotopic composition, the content of the most abundant isotope ^{132}Xe being only 27%. The result is a complex lasing spectrum [Ref. 3] that is an aggregate of isotopically split components of the P-branch of the band $v' = 0 \rightarrow v'' = 4$. Fig. 8 shows the position of the maxima of the lasing lines resolved

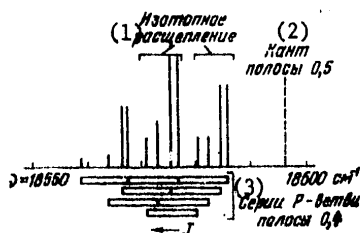


Fig 8. Identification of lines of laser emission

KEY: 1--Isotopic splitting
2--Edge of band 0,5
3--Series of the P-branch of band 0,4

on photographic film by a comparator. The distribution of intensities of the lines is given conventionally by visual observation. As we can see, the lines of the P-branch are split into several series that are displaced relative to one another by the amount of the isotopic shift. The observed approximate equidistance of lines in each series with succession interval of $9.0 \pm 0.2 \text{ cm}^{-1}$ corresponds to periodicity of lines of the P-branch of band $v' = 0 \rightarrow v'' = 4$ in the vicinity of the maximum of the quasicontinuum of the R-branch of band $v' = 0 \rightarrow v'' = 5$ [Ref. 22] where lasing occurs.

Analysis of the emission spectrum of the XeO molecule with consideration of the superposition of P- and R-branches of adjacent vibrational bands shows that the

elimination of isotopic splitting by using isotopically pure xenon can increase the cross section of amplification on the laser transition by a factor of 2-4.

Following the procedure described above, we estimated the expected energy of stimulated emission of the XeO laser with the use of isotopically pure xenon, assuming that the amplification cross section is doubled by removing isotopic splitting. The results of the calculations are summarized in the table. As we can see, the lasing energy is approximately doubled by the reduction of the threshold pumping level. Of course, isotopically pure xenon is fairly expensive, and its use is feasible only if provisions are made for chemical purification and recirculation of the xenon in the laser.

5. Conclusion

The quantum efficiency of conversion of pumping in a unit volume to radiation of a photochemical XeO laser is measured in Ref. 1, and it is shown that it is $15 \pm 5\%$ as determined by internal losses in the active medium. In this paper an experimental and theoretical investigation is made of the nature of the internal losses in the XeO laser, and they are calculated.

It is anticipated that internal losses will be appreciably reduced by improving the method of cooling the working mixture and by changing from a dielectric to a metal chamber. The latter is feasible when about 1 amagat unit of nitrogen is added to the working mixture. Preliminary experiments have been done that confirm the feasibility of effective operation of an XeO laser with nitrogen.

Numerical calculations were done on pumping, and the values of threshold pumping were found for different initial N_2O concentrations. Based on these data, the

FOR OFFICIAL USE ONLY

FOR OFFICIAL USE ONLY

anticipated output energy of an XeO laser with a flat resonator is determined in the case where the size of the laser chamber does not restrict the lasing region. In a mixture with initial concentration $[N_2O] = 4 \cdot 10^{17} \text{ cm}^{-3}$ and optimum composition of the buffer gases when the adjusted transmission of the mirrors is $\gamma_c \approx 5 \cdot 10^{-4} \text{ cm}^{-1}$ the expected lasing energy is 40 J, which corresponds to an overall electric efficiency of the laser of $\sim 0.1\%$. The lasing energy and efficiency of the XeO laser can be approximately doubled when isotopically pure xenon is used.

The working model of the photochemical XeO laser uses cryostatic cooling of the active medium. However, another cooling method that may assuredly be of interest is the cooling that occurs when the working mixture escapes from a supersonic nozzle. In this case the uniform cooling of the working mixture is combined with rapid exchange, which makes pulse-periodic operation feasible for the XeO laser.

In conclusion the authors thank B. Ya. Karpov and A. T. Matachun for assistance with the computer calculations.

REFERENCES

1. V. S. Zuyev, L. D. Mikheyev, I. V. Pogorel'skiy, KVANTOVAYA ELEKTRONIKA, Vol 6, 1979, p 1513.
2. A. L. Mikaelyan, M. L. Ter-Mikayelyan, Yu. G. Turkov, "Opticheskiye generatory na tverdom tele" [Solid-State Optical Masers], Moscow, Sovetskoye radio, 1967.
3. I. S. Datskevich, V. S. Zuyev, L. D. Mikheyev, I. V. Pogorel'skiy, KVANTOVAYA ELEKTRONIKA, Vol 5, 1978, p 1456.
4. R. Atkinson, K. H. Welge, J. CHEM. PHYS., Vol 57, 1972, p 3689.
5. B. L. Borovich, V. S. Zuyev, V. A. Katulin, V. Yu. Nosach, A. V. Startsev, Yu. Yu. Stoylov, KVANTOVAYA ELEKTRONIKA Vol 2, 1975, p 1282.
6. E. A. Melvin-Hughes, "Fizicheskaya khimiya" [Physical Chemistry], Moscow, IL, 1962.
7. "Spravochnik khimika" [Chemist's Handbook], Vol 1, Moscow, Khimiya, 1966.
8. Ya. B. Zel'dovich, Yu. P. Rayzer, "Fizika udarnykh voln i vysokotemperaturnykh gazodinamicheskikh yavleniy" [Physics of Shock Waves and High-Temperature Gas-dynamic Phenomena], Moscow, Nauka, 1966.
9. N. G. Basov, Yu. A. Babeyko, V. S. Zuyev, L. D. Mikheyev, V. K. Orlov, I. V. Pogorel'skiy, D. B. Stavrovskiy, A. V. Startsev, V. I. Yalovoy, KVANTOVAYA ELEKTRONIKA, Vol 3, 1976, p 930.
10. D. Kligler, D. Pritchard, W. K. Bishel, C. K. Rhodes, J. APPL. PHYS., Vol 49, 1978, p 2219.
11. G. Black, R. L. Sharpless, T. G. Slanger, J. CHEM. PHYS., Vol 63, 1975 p 4546.
12. R. J. Donovan, D. Husain, CHEM. REV., Vol 70, 1970, p 489.

FOR OFFICIAL USE ONLY

13. G. C. Tisone, J. CHEM. PHYS., Vol 60, 1974, p 3716.
14. K. H. Welge, R. Atkinson, J. CHEM. PHYS., Vol 64, 1976, p 531.
15. T. G. Slanger, G. Black, J. CHEM. PHYS., Vol 64, 1976, p 3763.
16. H. T. Powell, A. U. Hazi, CHEM. PHYS. LETTS, Vol 59, 1978, p 71.
17. J. K. Rice, J. R. Woodworth, J. APPL. PHYS., Vol 50, 1979, p 4415.
18. I. V. Dvornikov, L. V. Kulagina, I. V. Podmoshevskiy, A. V. Yakovleva, in:
"Tezisy dokladov IV Vsesoyuz. konf. po spektroskopii vakuumnogo ul'trafioleta
i vzaimodeystviyu izlucheniya s veshchestvom" [Abstracts of Papers of the
Fourth All-Union Conference on Vacuum-Ultraviolet Spectroscopy and Interaction
of Radiation with Matter], Uzhgorod, 1975, p 142.
19. V. A. Danilychev, Ye. P. Glotov, V. D. Zvorykin, et al., KVANTOVAYA ELEKTRONIKA,
Vol 7, 1980, p 630.
20. E. J. McGuire, PHYS. REV., Vol A19, 1979, p 1978.
21. L. D. Thomas, R. K. Nesbet, PHYS. REV., Vol A11, 1975, p 170.
22. C. D. Cooper, G. C. Cobb, E. L. Tolnas, J. MOLEC. SPECTR., Vol 7, 1961, p 223.

COPYRIGHT: Izdatel'stvo "Sovetskoye radio", "Kvantovaya elektronika", 1980
[3-6610]

6610
CSO: 1862

FOR OFFICIAL USE ONLY

UDC 621.378.33

DEVELOPMENT OF OPTICAL INHOMOGENEITIES IN FLASHTUBE PHOTOLYSIS LASERS

Moscow KVANTOVAYA ELEKTRONIKA in Russian Vol 7, No 7(97), Jul 80 pp 1516-1522
manuscript received 7 Jan 80

[Article by B. V. Alekhin, V. V. Borovkov, A. Ya. Brodskiy, B. V. Lazhintsev,
V. A. Nor-Arekyan and L. V. Sukhanov].

[Text] An experimental and theoretical study is done on the dynamics of development of optical inhomogeneities of the active medium of a photolysis laser with high-power flashtube pumping under conditions of accumulation of inverse population, rapid depopulation and free lasing. The chemical component of the index of refraction is registered for the first time in photolysis of C_3F_7I . An anomalous increase is observed in the index of refraction of the gas in the free lasing mode, and an interpretation is offered.

This paper is a continuation of Ref. 1, and is devoted to a study of regular optical inhomogeneities in photolysis lasers with excitation by the light of high-power xenon flashtubes. A change in the index of refraction of the active medium is determined by three factors [Ref. 2-4]: change in polarizability of molecules as a result of photochemical processes, gasdynamic shifting of the medium due to non-uniform heating in the pumping process, and also shock waves that arise at the walls of the cell and propagate with transonic velocity. In this paper a theoretical and experimental study is done on gasdynamic inhomogeneities for an excitation time of $\sim 10 \mu s$. Particular attention is given to optical inhomogeneities in the mode of inverse population storage, and to determination of the chemical component of the index of refraction Δn_{chem} in photolysis of perfluoroalkyl iodides since there have been no reliable data up to now on the magnitude and sign of the change in polarizability of molecules. To describe gasdynamic optical inhomogeneities during the above-mentioned photolysis laser operating time, when changes in density are small ($\Delta \rho \ll \rho_0$), gas velocities are much less than sonic ($v \ll v_{son}$), we can disregard heat conduction, viscosity, and the influence of $\Delta \rho$ on the change in pressure p , considering the gas incompressible, and by analogy with Ref. 5 we can utilize linearized hydrodynamic equations in the cylindrical symmetry approximation:

$$\begin{aligned} \frac{\partial v}{\partial t} &= -\frac{1}{\rho_0} \frac{\partial p}{\partial r}, \\ \frac{\partial \delta N}{\partial t} + \frac{N_0}{r} \frac{\partial}{\partial r} r v &= 0, \end{aligned} \quad (1)$$

FOR OFFICIAL USE ONLY

FOR OFFICIAL USE ONLY

where v is radial velocity, δN is change of concentration, r is the instantaneous radius.

Considering that heating takes place isochorically, we can readily get an expression for the pressure in the gas from the Mendeleyev-Clapeyron equation:

$$p(r, t) = (\gamma - 1) Q(r, t) + p_0, \quad (2)$$

where p_0 is the pressure of the undisturbed gas, γ is the adiabatic exponent, and $Q(r, t)$ is the heat introduced per unit volume at a given point by a given time. Without consideration of transillumination of the medium, we can write

$$Q(r, t) = f(r) q(t), \quad (3)$$

where $f(r)$ is a dimensionless function that characterizes the distribution of pumping over the cross section of the cell, $q(t)$ is the heat release close to the wall of the cell due to photodecomposition and secondary chemical reactions.

The solution of system (1)-(3) is

$$\delta N = \frac{N_0(\gamma - 1)}{p_0} \left(\frac{1}{r} \frac{df}{dr} + \frac{d^2 f}{dr^2} \right) \int_0^t dt' \int_0^{t'} q dt''. \quad (4)$$

Then the change in the index of refraction $\Delta n = (n_0 - 1) \delta N / N$ takes the form

$$\Delta n = \frac{(n_0 - 1)(\gamma - 1)}{p_0} \left(\frac{1}{r} \frac{df}{dr} + \frac{d^2 f}{dr^2} \right) \int_0^t dt' \int_0^{t'} q dt''. \quad (5)$$

It was shown in Ref. 6 that this conclusion is valid for $t \ll R_0 / v_{\text{son}}$, where R_0 is the size of the region of perturbation (the inside radius of the cell).

Experimental studies of optical inhomogeneities were done in a photolysis laser with pumping by four xenon flashtubes placed around a quartz cell 4 cm in diameter and 62 cm long. The inner surface of the cell was frosted and a cylindrical diffuse illuminator was used. For a stored electrical energy of 16 kJ, the power supply provided a pumping light pulse in the UV region with duration of 10 μ s on a level of $1/e$. At a C_3F_7I pressure of 16 mm Hg, which is optimum with respect to power output and uniformity of pumping, the stored laser energy averaged over the cross section was 20 mJ/cm³, and for 21 mm Hg of CF_3I -- 16 mJ/cm³. The buffer gases were Xe, Ar, He and SF_6 . Optical inhomogeneities were measured by a Michelson interferometer on a wavelength of $\lambda = 633$ nm in modes of inverse population storage, depopulation by a magnetic field, and free lasing. The interference pattern was recorded by a high-speed camera operating in the mode of continuous scanning with time resolution of 0.75 μ s. Part of the flashtube emission was fixed on the film of this camera, providing a time "tie-in" of the excitation pulse. The slit of the camera was oriented along the diameter of the cell between the pumping flashtubes; control experiments were also done with rotation of the slit through 45° or displacement by 1 cm from the center. Photometric measurements of the interference patterns were made on a microdensitometer with subsequent computer processing, enabling registration of band displacement by 1/40 of the natural width of the

FOR OFFICIAL USE ONLY

band in regions with small perturbations of the medium (the error of measurement of Δn was $\pm 1.3 \cdot 10^{-8}$) and no worse than $1/20$ in regions of large perturbations ($\Delta n \geq 5 \cdot 10^{-7}$).

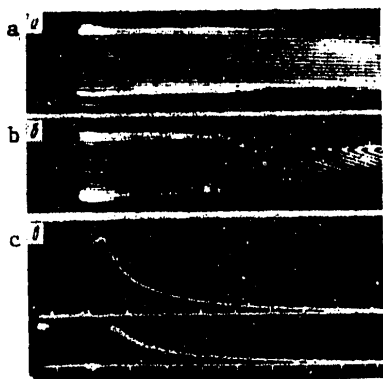


Fig. 1. Interference patterns of optical inhomogeneities in the mode of storage for 16 mm Hg of C_3F_7I (a) and a mixture of $C_3F_7I:Xe = 16:300$ mm Hg (b), and also an oscillogram of pumping pulses (top) and lasing pulses (bottom) (c); time marks show $5 \mu s/div$

Fig. 1 shows typical interference patterns of optical inhomogeneities, and oscillograms of the pumping pulse in the UV region and of the lasing pulse. In choosing the pressure of the working gas, we were guided by the results of calculation of pumping distribution over the cross section of the cell [Ref. 7], where it was shown that when $\sigma_0 N_p R_0 = 1$, where σ_0 is the cross section of absorption at the band maximum (this corresponds to the chosen optimum pressures), the radial distribution of pumping is satisfactorily described by the formula

$$f(r) = 0.3 (r/R_0)^2 + 0.7. \quad (6)$$

As implied by (5), in this case the index of refraction of the active medium should increase, and should not depend on t . Fig. 2 shows the profile of Δn over the cross section of the cell at different times, and $\Delta n(t)$ in the central part of

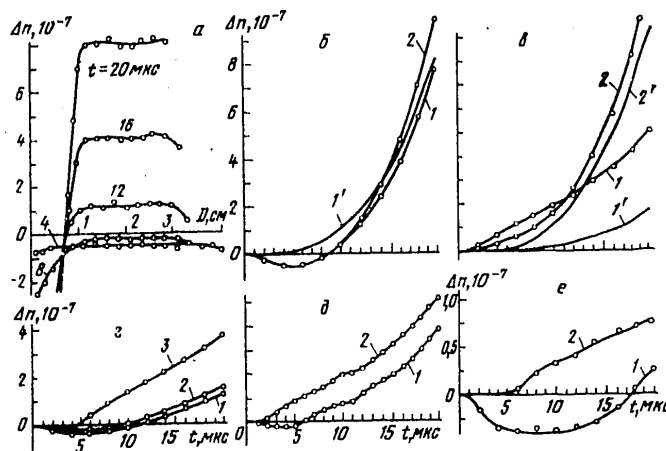


Fig. 2. Distribution of Δn over the cross section of the cell in the storage mode for a mixture of $C_3F_7I:Xe = 16:300$ (a) and curves for $\Delta n(t)$ for different mixtures: δ — $C_3F_7I:Xe = 16:300$ (1, 1'), $C_3F_7I:Ar(Xe) = 16:300$ (2); ϵ — $CF_3I:SF_6 = 21:50$ (1, 1'), $CF_3I:Xe = 21:300$ (2, 2'); α — $C_3F_7I = 16$ (1, 3), $C_3F_7I:SF_6 = 16:50$ (2, 3); ∂ — $C_3F_7I:SF_6 = 16:50$ (1), $CF_3I:SF_6 = 16:50$ (2); e — $C_3F_7I:Xe = 4:300$ (1), $C_3F_7I = 4$ (2); partial pressures are given in millimeters of mercury; MKC = μs

FOR OFFICIAL USE ONLY

FOR OFFICIAL USE ONLY

the cell for the investigated mixtures and modes of operation of the photolysis laser. The curves for $\Delta n(t)$ in Fig. 2b were obtained in the mode of rapid depopulation, in Fig. 2c(3) and Fig. 2c(2) -- in the free lasing mode, and the others -- for storage of inverse population. At a pressure of $C_3F_7I = 4$ mm Hg the average stored energy is 10 mJ/cm^3 . The theoretical curves are denoted by the numbers with a prime. It is clear from Fig. 2a that there is a central region of the cell where the gradient of the index of refraction is near zero, which is confirmed by conclusions from (5) and (6). However, the size of this region is somewhat smaller than that not covered by the shock wave, which is probably due to a lack of complete axial symmetry of pumping. The proposed model implies that the influence of buffer gases on optical inhomogeneities can be evaluated by calculating the parameter

$$F = (n_0 - 1)(\gamma - 1)/\rho_0, \quad (7)$$

since the other terms in (5) are determined only by the design particulars of the specific laser. The results of calculation of F for binary mixtures (at optimum pressures of the working gases and a pressure of 300 mm Hg for the buffer gases) are summarized in Table 1.

TABLE 1

Working gas	$F, 10^{-2} \text{ cm}^3/\text{g}$				
	Without buffer	Xe	Ar	He	SF ₆
CF ₃ I	1.6	6.1	8.0	8.8	1.1
C ₃ F ₇ I	0.65	4.8	6.2	6.5	1.0

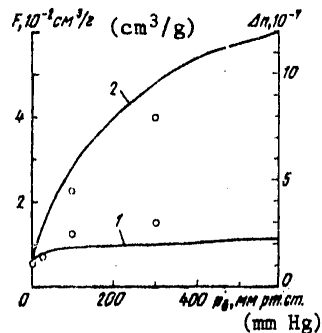


Fig. 3. Dependences of F (solid lines) and Δn (points) on the pressure of the buffer gas in mixtures with C_3F_7I

Consideration was taken in the calculations of the influence of the temperature of the medium on the specific heat of polyatomic gases. Fig. 3 shows the way that F depends on the pressure of the buffer gas for mixtures of 16 mm Hg of C_3F_7I with SF₆ (1) and Xe (2); the points show the values of Δn measured in the storage mode at $t = 20 \mu\text{s}$. It can be seen that for mixtures with Xe the values of Δn are to each other as their parameters F with an error of no more than 10%, and in the case of SF₆ the experiment gives a value of Δn that is overstated by a factor of ~ 1.4 at SF₆ pressures of 100 and 300 mm Hg.

From an analysis of the behavior of $\Delta n(t)$ we can conclude that gasdynamics begins to have an appreciable effect on optical inhomogeneities within approximately $10 \mu\text{s}$ after the onset of pumping, leading only to an increase of n in the central region of the cell. However, in experiments with C_3F_7I in the storage mode at all orientations of the high-speed camera slit it was observed that the index of refraction of the medium decreases over the entire cross section of the cell simultaneously with the onset of excitation, and reaches a minimum value at $t = 4-5 \mu\text{s}$, which should be interpreted

FOR OFFICIAL USE ONLY

FOR OFFICIAL USE ONLY

as evidence of a chemical component of the index of refraction Δn_{chem} . However, even a qualitative comparison of the experimental results with calculation shows that the behavior of $\Delta n(t)$ cannot be attributed in all experiments to merely two processes: change of polarizability of molecules in photolysis of $\text{C}_3\text{F}_7\text{I}$ and the presence of the gasdynamic component Δn_{gd} . Actually, in this case the lower the Δn_{gd} , the more strongly should the Δn_{chem} show up in the experiment. However, the most negative value of $\Delta n = 5 \cdot 10^{-8}$ is observed for mixtures with noble gases for which the gasdynamics (parameter F) is 5-6 times as great as in other mixtures. When the cell was filled with buffer gases alone, we did not observe any changes of n during operation of the pumping flashtubes. A relatively rapid increase of n in the free lasing mode is noteworthy (see Fig. 22, curve 3). In mixtures with noble gases it was not possible to determine the regular displacement of interference bands at the given pumping levels in the lasing mode due to the arising of localized inhomogeneities [Ref. 1], while in experiments with a quencher (a mixture of $\text{C}_3\text{F}_7\text{I}:\text{Xe}:\text{O} = 16:300:5$ mm Hg) the value of Δn by the 20th microsecond reached $1.1 \cdot 10^{-6}$, which is 40% greater than in the case of storage. To elucidate the nature of heat release in the medium and evaluate the change of polarizability of molecules for a given pumping duration, it is sufficient to consider fast photochemical processes [Ref. 1]:



Where the R are CF_3 or C_3F_7 radicals, and the subscripts H and L stand for "pumping" and "lasing" respectively.

Only processes (8) and (11) need be accounted for in the storage mode. Machine calculation was done for the kinetics of the reactions of the photolysis laser in the modes of storage and free lasing with consideration of the actual pumping pulse. The excitation pulse shape was approximated by the function

$$a(t) = \frac{J_{\text{H}}(t)}{\int_0^t J_{\text{H}}(t) dt} = \begin{cases} 0.0279 t^{1.25} e^{1.25(1-t/3)}, & 0 \leq t \leq 3, \\ 0.33/t, & 3 \leq t \leq 20, \end{cases} \quad (12)$$

where time t is in microseconds.

The rate constants [Ref. 8] and heats of reactions [Ref. 9, 10] used in the calculations are summarized in Table 2.

TABLE 2

Working gas	$K_1 \cdot 10^{12}$, cm ³ /s	$K_2 \cdot 10^{12}$, cm ³ /s	Q_1 , eV	Q_2 , eV	Q_3 , eV
CF_3I	16	5.5	1.24	2.5	4.15
$\text{C}_3\text{F}_7\text{I}$	8	3	1.5	2.3	4.1

FOR OFFICIAL USE ONLY

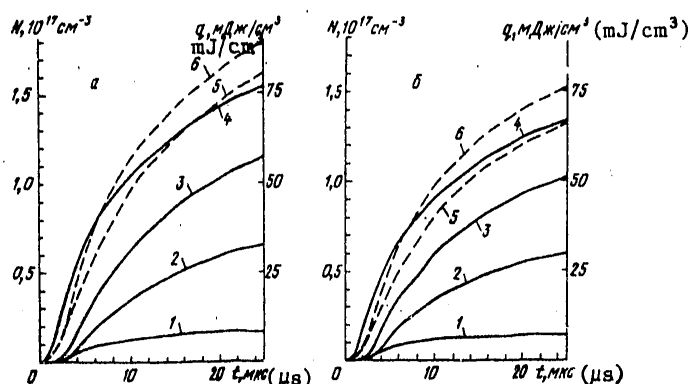


Fig. 4. Results of numerical calculation of the kinetics of reactions (8)-(11) for C_3F_7I (a) and CF_3I (b): concentrations R_2 in lasing (1) and in the storage mode (2), $R+J$ in lasing (3) and J^* in the storage mode (4); heat release in the storage mode (5) and in lasing (6)

Fig. 4 shows the results of calculation of the kinetics for optimum pressures of C_3F_7I (a) and CF_3I (b). On the basis of these results, we were able to calculate

and with consideration of (5) we were able to calculate the dependence

$\Delta n_{gd}(t)$ (denoted by the numbers with primes on Fig. 2).

Let us note that the heat releases in the storage and lasing modes differ by no more than 20%. For rougher estimates of gasdynamic perturbations, we can use an expression derived from (5) in explicit form:

$$\Delta n_{gd} = \frac{1}{6} \frac{(n_0 - 1)(\gamma - 1)}{p_0} \left(\frac{d^2 f}{dr^2} + \frac{1}{r} \frac{df}{dr} \right) St^3. \quad (13)$$

Here we have used $q(t) = St$, where $S = 5 \cdot 10^{10}$ ergs/(cm³·s) is the rate of specific heat release for the given level of excitation.

A comparison of the experimental and theoretical curves in Fig. 2 shows that in mixtures with noble gases $\Delta n(t)$ is satisfactorily described by the gasdynamic and chemical components of the index of refraction. The behavior of $\Delta n(t)$ with buffer gas SF_6 is apparently more complicated since it has been noted that the addition of SF_6 leads to an increase in n even in the very first instants. Development of optical inhomogeneities in the free lasing mode is also difficult to explain by an increase in gasdynamic perturbations; for instance in order for Δn_{gd} to reach a value of $1.3 \cdot 10^{-7}$ by the 10th microsecond (see Fig. 2a, curve 3), the gradient of heat release must increase by a factor of 10 as compared with the storage mode. Furthermore, while $\Delta n(t) \sim t^3$ in storage, the dependence $\Delta n(t)$ is closer to linear in free lasing.

Probably the anomalous increase in the index of refraction in lasing is due to the increase in polarizability of molecules in the reaction of reverse recombination

FOR OFFICIAL USE ONLY

FOR OFFICIAL USE ONLY

(10). Actually as a result of this reaction the binding energy (~ 2.5 eV) is converted to heat, starting with excitation of individual vibrational levels, after which with a certain relaxation time the energy is redistributed with respect to other degrees of freedom. The problem of the change in polarizability of some gases with induced Raman scattering of light was theoretically and experimentally studied in Ref. 5, 11, 12; however, the authors have not come across any data on the change of polarizability of molecules in vibrational excitations of perfluoro-alkyl iodides in the literature. The suggested hypothesis also gives a qualitative explanation of the anomalous influence of SF_6 on optical inhomogeneities, caused by a possible resonant excitation of vibrations of the molecules. This hypothesis does not contradict results for mixtures with noble gases which should be more effective in converting the vibrational energy of the mixture to translational energy as their partial pressure increases.

It should be noted that heat (~ 4 eV) is also released in the reaction of dipolymerization of C_3F_7 (11); however, in the storage mode, where it plays an appreciable part, without a buffer gas and with small additions of SF_6 (~ 50 mm Hg) the increase in polarizability is weaker than in reaction (10). Besides, when inversion is suddenly flipped by a magnetic field in $0.5 \mu\text{s}$, we observe a jump of $\Delta n \sim -10^{-8}$, which is apparently due to a change of polarizability of iodine atoms with transition from the excited to the ground state. Fig. 2 shows $\Delta n(t)$ with discharge of inversion in 5 and $10 \mu\text{s}$ (curve 1) and for $10 \mu\text{s}$ (curve 2). Thus to evaluate the change in polarizability of $\text{C}_3\text{F}_7\text{I}$ molecules as a result of photodecomposition, use was made of relations $\Delta n(t)$ in mixtures with noble gases and for $\text{C}_3\text{F}_7\text{I}$ a value of $\Delta\alpha_0 \sim -2 \cdot 10^{-25} \text{ cm}^3$ was obtained. Similar estimates for CF_3I are difficult because the part played by the change in polarizability of CF_3 radicals has not been finally explained in optical inhomogeneities with photolysis and reaction (11), although it is clear that vibrational excitation of CF_3 should be stronger than for C_3F_7 . Apparently this question needs further study both in photolysis lasers and in other types of gas lasers. For example in chemical lasers at excitation times of the order of a few microseconds the gasdynamic perturbations are small and the changes of polarizability of molecules due both to chemical reactions and to the excitation of vibrations may play the major role in optical inhomogeneities.

It should be noted in conclusion that the high uniformity of the active medium with short-pulse flashtube excitation in the given laser with unstable resonator produced divergence with intensity distribution close to the diffraction limit without any loss of energy as compared with a flat cavity. Transverse coherence reached 90%, and 60% of the lasing energy was in the central spot ($7 \cdot 10^{-5}$ radian) of the diffraction pattern. The active medium was $\text{C}_3\text{F}_7\text{I}$ (16 mm Hg), and specific power output was 10 mJ/cm^3 .

REFERENCES

1. B. V. Alekhin, V. V. Borovkov, V. A. Lazhintsev, V. A. Nor-Arevyan, L. V. Sukhanov, V. A. Ustinenko, KVANTOVAYA ELEKTRONIKA, Vol 6, 1979, p 1948.
2. L. Ye. Golubev, V. S. Zuyev, V. A. Katulin, V. Yu. Nosach, O. Yu. Nosach, KVANTOVAYA ELEKTRONIKA, No 6(18), 1973, p 23.
3. L. I. Zykov, G. A. Kirillov, S. B. Kormer, S. M. Kulikov, V. A. Komarevskiy, S. A. Sukharev, KVANTOVAYA ELEKTRONIKA, Vol 2, 1975, p 123.

FOR OFFICIAL USE ONLY

FOR OFFICIAL USE ONLY

4. B. L. Borovich, V. S. Zuyev, V. A. Katulin, V. Yu. Nosach, O. Yu. Nosach, A. V. Startsev, Yu. Yu. Stoylov, KVANTOVAYA ELEKTRONIKA, Vol 2, 1975, p 1282.
5. M. I. Baklushina, B. Ya. Zel'dovich, N. A. Mel'nikov, N. F. Pilipetskiy, Yu. P. Rayzer, A. N. Sudarkin, V. V. Shkunov, ZHURNAL EKSPERIMENTAL'NOY I TEORETICHESKOY FIZIKI, Vol 73, 1973, p 831.
6. Yu. P. Rayzer, ZHURNAL EKSPERIMENTAL'NOY I TEORETICHESKOY FIZIKI, Vol 52, 1967, p 470.
7. F. K. Rutkovskiy, ZHURNAL PRIKLADNOY SPEKTROSKOPII, Vol 13, 1970, p 781.
8. L. S. Yershov, V. Yu. Zalesskiy, V. N. Sokolov, KVANTOVAYA ELEKTRONIKA, Vol 5, 1978, p 863.
9. Ye. V. Arkhipova, B. L. Borovich, A. K. Zapol'skiy, KVANTOVAYA ELEKTRONIKA, Vol 3, 1976, p 1276.
10. K. I. Witte, Report PLF-2, Max Planck Gesellschaft, West Germany, 1977.
11. G. A. Askar'yan, PIS'MA V ZHURNAL EKSPERIMENTAL'NOY I TEORETICHESKOY FIZIKI, Vol 4, 1966, p 400.
12. B. Vil'gel'mi, E. Goyman, ZHURNAL PRIKLADNOY SPEKTROSKOPII, Vol 19, 1973, p 550.

COPYRIGHT: Izdatel'stvo "Sovetskoye radio", "Kvantovaya elektronika", 1980
[3-6610]

6610
CSO: 1862

FOR OFFICIAL USE ONLY

UDC 621.378.325

A NEODYMIUM PULSE LASER THAT PRODUCES A HIGH-FREQUENCY SERIES OF NANOSECOND PULSES WITH ENERGY OF ~100 J

Moscow KVANTOVAYA ELEKTRONIKA in Russian Vol 7, No 7(97), Jul 80 pp 1575-1577
manuscript received 15 Dec 79

[Article by B. N. Borisov, S. V. Datsykov, Yu. I. Kruzhilin and V. K. Orollov]

[Text] The limiting energy output per unit of area is estimated for a solid-state pulsed laser operating in the mode of shaping a series of giant pulses. A description is given of the design and test results of a pulsed neodymium laser that emits a series of nanosecond pulses with recurrence rate up to 20 kHz and output energy of ~100 J. Information is given on preliminary experiments on conversion of a powerful pulse burst to the second harmonic.

The solution of many problems in quantum electronics requires a source of laser radiation that shapes a high-frequency train of short powerful pulses both in the infrared and on visible wavelengths. Such series are produced by solid-state lasers with periodic Q-switching during the pumping pulse [Ref. 1-4]. Since such lasers have high pulse power, their radiation can be converted with relatively high efficiency to emission in the visible and infrared wave bands by methods of nonlinear optics.

It is shown in Ref. 3 that at switching frequencies $F_{\text{rec}} \geq \tau^{-1}$ (τ is lifetime on the metastable level) the energy characteristics of a Q-switched laser approach the free lasing mode. The limiting energy output from a unit area of the active element is determined by the radiation strength of the optical elements of the laser, which depends on the duration and shape of the lasing pulse. If laser power is high enough so that the laser can produce a series of equidistant pulses in which the energy density of each pulse is close to the radiation strength $\epsilon_{\text{II}}(\tau_0)$ (τ_0 is the duration of a monopulse), then the limiting energy density $\epsilon_{\text{II}}(T)$ and the number of pulses N in a series of duration T can be approximately estimated from the ratio of radiation strengths of the optical elements for pulses of duration τ_0 and T [Ref. 5]:

$$\epsilon_{\text{II}}(T)/\epsilon_{\text{II}}(\tau_0) = (T/\tau_0)^{1/2}; N = \epsilon_{\text{II}}(T)/\epsilon_{\text{II}}(\tau_0). \quad (1)$$

The pulse recurrence rate in such a series is determined from (1):

$$f = (T/\tau_0)^{-1/2}. \quad (2)$$

FOR OFFICIAL USE ONLY

FOR OFFICIAL USE ONLY

When a monopulse of duration τ_0 with energy density close to $\epsilon_H(\tau_0)$ and the given pulse train are converted to the second harmonic in the approximation of low drift of the angle of synchronism of the crystal under the action of pulse heating by radiation and under condition of identical spatial characteristics, the conversion efficiencies will be the same. Consequently the ratio of energy densities in the pulse train and in the monopulse on the second harmonic will also be determined by formula (1).

For characteristic values of $T \approx 1$ ms and $\tau_0 \approx 50$ ns this ratio is ~ 100 . Thus under certain conditions a laser that produces a pulse train can attain a much greater energy output from a unit area not only on the fundamental frequency, but also on the frequency of the converted radiation.

To carry out experiments, a neodymium glass laser was produced as diagrammed in Fig. 1. It consists of a master laser with Q-switched cavity and an amplifier.

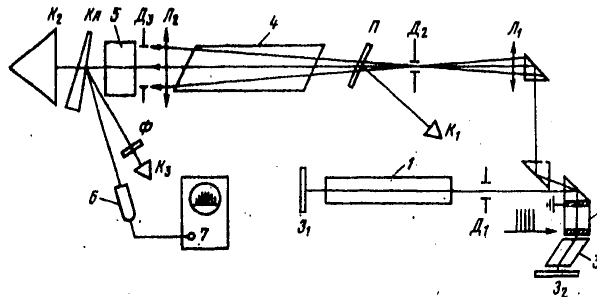


Fig. 1. Diagram of laser that generates a train of giant pulses: 1--active element of the master laser $\phi 10 \times 300$ mm; 2--electro-optical shutter; 3--Fresnel rhomb; 4--active element of the amplifier; 5--KDP crystal; 6--FEK-09 photocell; 7--S8-9A oscilloscope; 81, 82--mirrors, $R=100\%$; A1-A3--diaphragms; L1, L2--lenses; K1-K3--calorimeters; K4--wedge; P--plane-parallel plate; Φ --SZS-22 filter

A monoblock electro-optical shutter of DKDP crystal was used as the Q-switch. To reduce the controlling voltage on the shutter, an optical system was used that enabled modulation of the reflectivity of the output mirror, so that the amplitude of the controlling pulses could be reduced by a factor of about three as compared with quarter-wave shutters based on the longitudinal electro-optical effect. The way that the output energy of the master laser depends on recurrence rate is shown in Fig. 2.

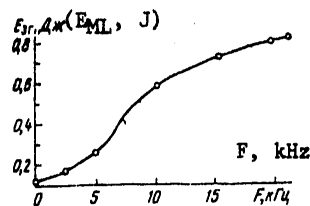


Fig. 2. Output energy of the master laser as a function of pulse recurrence rate

FOR OFFICIAL USE ONLY

The amplifier was a single-pass stage with phosphate glass active element measuring 20 mm in diameter and 680 mm long, based on a GOS-1001 laser. The pumping pulse duration of the amplifier was ~1.5 ms, and maximum pumping energy was 40 kJ.

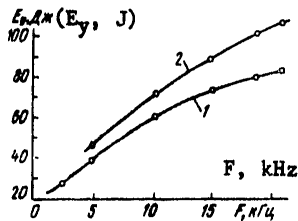


Fig. 3. Energy in the pulse train at the amplifier output as a function of pulse recurrence rate: amplifier pumping energy 30 kJ (1) and 38 kJ (2)

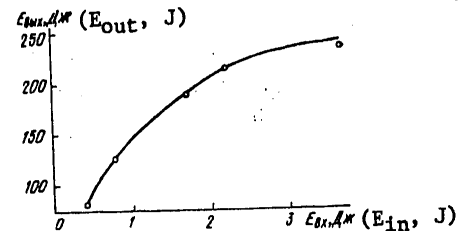


Fig. 4. Output energy of the amplifier as a function of the energy of the amplified free lasing pulse from the master laser

The way that the energy in the pulse train at the output depends on recurrence rate is shown in Fig. 3. The maximum energy at a recurrence rate of 18 kHz was ~100 J. The envelope of the pulse train basically reproduced the pumping pulse shape. The energy from the amplifier head in the lasing mode was measured to determine the relative energy output from the active element of the amplifier. At pumping of ~40 kJ, the lasing energy was ~700 J. The way that output energy depends on input energy with amplification of a free lasing pulse from the master laser was also determined (Fig. 4). A comparison of the curves shown in Fig. 2-4 shows that the output energy with amplification of a free lasing pulse is 20% greater than with amplification of a nanosecond pulse train for the same input signal amplitudes. The lower value of the energy output in amplification of a pulse train can be attributed to the fact that for recurrence rates up to 20 kHz the losses due to luminescence and finite lifetime of the lower working level are greater than in amplification of microsecond spikes of free lasing with higher duty factor. The maximum energy density at $f \approx 18$ kHz reached ~50 J/cm².

Detailed experiments were done with the described laser on doubling the frequency of emission by a KDP crystal. The energy efficiency in doubling of a pulse train with $f = 5$ kHz was ~20%, and at $f = 10$ kHz was 12%. The maximum energy of the second harmonic was ~5 J, and showed little variation at recurrence rates in the range from 5 to 10 kHz. This can be attributed to the compensation of increasing energy as F_{rec} rises by a reduction in the effectiveness of doubling due to a fall in the peak power density. Let us note that the reduction in peak power density with increasing F_{rec} may be compensated by compression of the emission beam in the plane with maximum width of the angle of synchronism of the crystal. In this case there may be an increase in the energy of the second harmonic with increasing F_{rec} .

Our experiments showed that in generation of a train of nanosecond pulses with high peak power density, due to the greater energy radiation resistance of the optical

FOR OFFICIAL USE ONLY

FOR OFFICIAL USE ONLY

elements to the action of a train of monopulses, there may be an increase in the energy output from a unit of area of the active element on both the fundamental and the doubled emission frequency. In the concluding experiments an energy output of $\sim 20 \text{ J/cm}^2$ was obtained on the second harmonic.

REFERENCES

1. M. P. Vanyukov, S. V. Yevdokimov, Ye. V. Nilov, A. A. Chertkov, KVANTOVAYA ELEKTRONIKA, No 3, 1971, p 108.
2. G. A. Aver'yanov, S. V. Yevdokimov, Ye. V. Nilov, B. M. Savichev, A. A. Chertkov, KVANTOVAYA ELEKTRONIKA, No 6, 1971, p 133.
3. T. A. Kuzovkova, Ye. V. Nilov, V. A. Rusov, I. N. Semënov, A. A. Chertkov, ZHURNAL TEKHNIЧЕСКОY FIZIKI, Vol 44, 1974, p 797.
4. Ye. V. Nilov, V. A. Rusov, PIS'MA V ZHURNAL TEKHNIЧЕСКОY FIZIKI, Vol 4, 1978, p 138.
5. I. M. Buzhinskiy, A. Ye. Pozdnyakov, KVANTOVAYA ELEKTRONIKA, Vol 2, 1975, p 1550.

COPYRIGHT: Izdatel'stvo "Sovetskoye radio", "Kvantovaya elektronika", 1980
[3-6610]

6610
CSO: 1862

FOR OFFICIAL USE ONLY

UDC 621.378.33

LASERS UTILIZING CO₂ ISOTOPES

Moscow KVANTOVAYA ELEKTRONIKA in Russian Vol 7, No 8, 1980 pp 1803-1807
manuscript received 11 Feb 80

[Article by Yu.V. Pechenin and M.S. Domanov]

[Text] A study is made of the lasing spectra and energy characteristics of lasers utilizing the isotopes C¹²O₂¹⁶, C¹³O₂¹⁶, C¹²O₂¹⁸ and C¹²O₂¹⁶O¹⁸. It is demonstrated that the level of the output power of a laser operating on CO₂ isotopes is determined by the content of this isotope in the carbon dioxide gas. With equal enrichment for all the isotopes studied, except C¹²O₂¹⁶O¹⁸, output power levels are comparable. The unsaturated gain in the most intense transitions of symmetric molecules is identical and it is twofold lower in asymmetric. The gain increases linearly with an increase in enrichment. The maximum power output, determined by the product of the saturation power density and the gain, practically does not depend on the enrichment.

Although the employment of oxygen O¹⁸ and carbon C¹³ isotopes in lasers utilizing carbon dioxide gas makes it possible to extend considerably the range of lasing wavelengths [1-3], the energy characteristics of these lasers have still practically not been studied. The purpose of this study is to compare the energy characteristics of continuous CO₂ lasers with various isotope compositions of the carbon dioxide gas and to determine the relationship between the key parameters of the active medium and this composition.

1. Experimental Apparatus

A diagram of the experimental apparatus is given in fig 1. A laser with a convolute cavity design and internal reflectors had a discharge section length of 3.2 m. Four water-cooled gas discharge tubes, 1, 20 mm in diameter, were excited by source 2 by means of a direct-current discharge through ballast resistors R_b and high-voltage contactors 3, making it possible to switch the discharge on independently in all tubes. The laser's cavity consisted of an opaque spherical reflector, 4, with a radius of curvature of 7 m, rotating flat reflectors, 5, and a diffraction grating,

FOR OFFICIAL USE ONLY

FOR OFFICIAL USE ONLY

6, with a spacing of 10μ and a blaze angle of $19^{\circ}10'$ (first-order reflectivity of 58 percent), serving the purpose of simultaneously selecting wavelengths and as an outlet for radiation from the cavity. The mechanism for positioning the diffraction grating made it possible, by varying its slant, to tune the cavity's operating wavelength from 9 to 12μ . Single-mode lasing was made possible by a diaphragm 16 mm in diameter installed at the cavity's spherical reflector. The lasing power was measured by means of an IMO-2 meter, 7, the laser was tuned to the central frequency of the working transition with respect to maximum power by means of a pyrometer, 8, and the emission wavelength was monitored by means of an IKS-21 spectrometer, 9. Employed in all measurements were a constant gas mixture composition of $\text{CO}_2:\text{N}_2:\text{He} = 1:1.5:7.5$ at a pressure of 13 mm Hg and a constant discharge current of 20 mA, close to the optimal values with enrichments greater than 50 percent. The isotopic composition of the carbon dioxide gas used was monitored by means of mass spectrometer analysis and was varied by diluting the isotope-enriched CO_2 with carbon dioxide gas with a natural isotope content ($\text{C}^{12}\text{O}_2^{16} > 98$ percent).

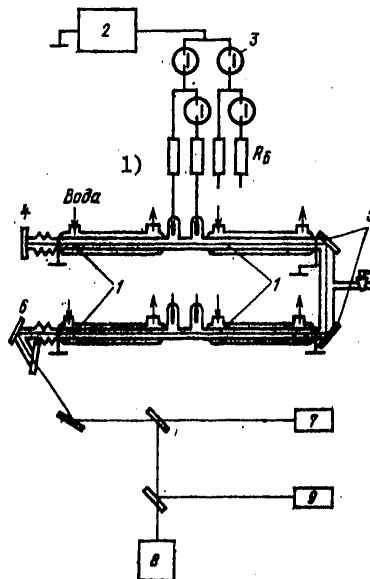


Figure 1. Diagram of Experimental Apparatus
[Key on following page]

FOR OFFICIAL USE ONLY

FOR OFFICIAL USE ONLY

Key:

1. Water

In analyzing the measurement results it was taken into account that in working with isotope O^{18} , because of intense CO_2 dissociation reactions in the gas discharge, $CO_2 \rightarrow CO + O$, a random redistribution of isotopic atoms takes place over three kinds of molecules, $C^{12}O_2^{16}$, $C^{12}O_2^{18}$, and $C^{12}O^{16}O^{18}$; it was furthermore assumed that the chemical reaction rates are identical for all isotopic molecules. In this case, in enriching oxygen with isotope O^{18} to a value of m the carbon dioxide gas in the laser's active medium should consist of

$$\frac{m^2}{C^{12}O^{16}O^{18}} \%, \frac{C^{12}O_2^{18}}{(100 - m)^2/100 \%}, \frac{C^{12}O_2^{16}}{2m(100 - m)/100 \%}$$

The instrument operated under sealed conditions. Measurements were made after the cessation of the buildup processes which take place after the discharge is switched on and are caused by dissociation of the gas mixture.

2. Lasing Spectra

The laser's emission spectra are shown in fig 2. The values of the emission's output power are plotted along the Y axis and wavelengths along the X axis. The data were obtained when working with natural $C^{12}O_2^{16}$ (a), with carbon dioxide gas enriched with isotope C^{13} to 59 percent (b), and with carbon dioxide gas enriched with isotope O^{18} to 80 (c) and 60 percent (d). In the latter case the composition of the carbon dioxide gas was as follows: 36 percent $C^{12}O_2^{18}$, 16 percent $C^{12}O_2^{16}$ and 48 percent $C^{12}O^{16}O^{18}$. For the purpose of increasing the output power and the number of lasing lines, the pressure and discharge current for this composition were optimized individually and equaled 10 mm Hg and 10 mA. The lasing wavelengths in spectra (a), (b) and (c) correspond to the wavelengths of the working transitions of lasers operating with isotopes $C^{12}O_2^{16}$, $C^{13}O_2^{16}$ and $C^{12}O_2^{18}$ [1, 2]. In spectrum (d), in its shortwave section, are observed lasing lines of the three molecules $C^{12}O_2^{16}$, $C^{12}O_2^{18}$ and $C^{12}O^{16}O^{18}$, and in its longwave section, just of $C^{12}O_2^{16}$.

Attention is drawn by the distinctly pronounced segregation of lasing intensity at line P(6) of the 00^01-10^00 $C^{12}O_2^{16}$ transition in the longwave section of spectrum (d), caused by the practically complete agreement of the gain contour of this line with the gain contour of line P(13) of the $001-100$ $C^{12}O^{16}O^{18}$ transition. According to [2] the distance between the central frequencies of these transitions equals 3.6 MHz, which is considerably less than the width of the gain contour of a CO_2 laser, equal to 100 MHz. The relatively weak lasing intensity in $C^{12}O^{16}O^{18}$ transitions, comparable with the lasing intensity in $C^{12}O_2^{16}$ transitions, while the $C^{12}O_2^{16}$ content in the mixture equaled a total of 16 percent and the $C^{12}O^{16}O^{18}$ 48 percent, is explained by enrichment of the spectrum of $C^{12}O^{16}O^{18}$ on account of the removal of degeneration in an asymmetric

FOR OFFICIAL USE ONLY

molecule [4], resulting in doubling of the number of lasing lines and, accordingly, in a reduction in gain in each of them.

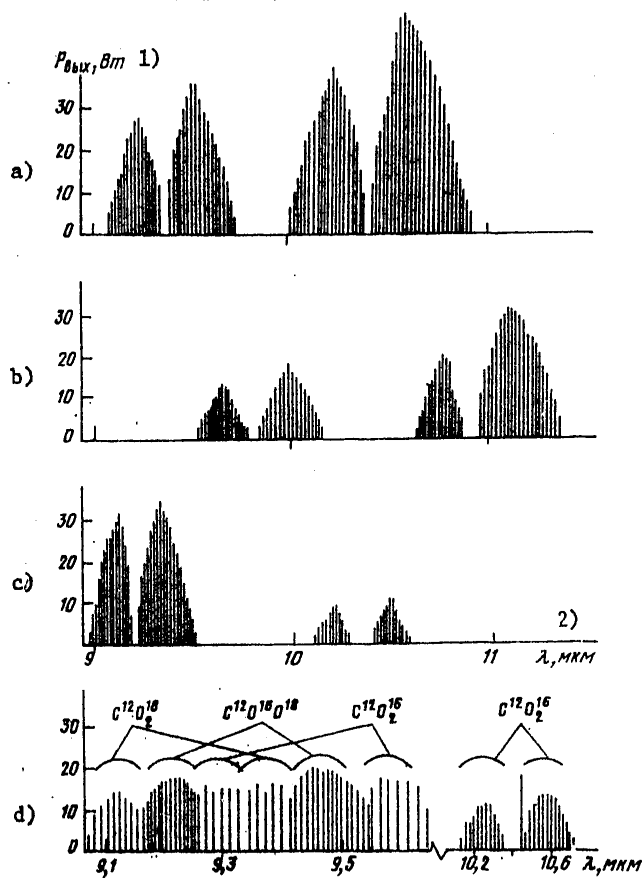


Figure 2. Lasing Spectra of Laser Studied, Using Various Isotopes of CO_2

Key:

1. P_{vykh} [output], W

2. λ , μ

FOR OFFICIAL USE ONLY

FOR OFFICIAL USE ONLY

3. Influence of Enrichment of the Working Isotope on the Laser's Output Power

In studying the characteristics of a laser operating with isotopes of carbon dioxide gas, a measurement was made of the dependence of the power in the most intense lasing lines, $P(20)$, of the $00^0_1-10^0_0$ transition of various isotopic molecules, on enrichment of the carbon dioxide gas with the working isotope. The measurement results are given in fig 3. Curves 1 and 2 show the change in lasing power in $C^{12}O_2^{16}$ and $C^{13}O_2^{16}$ transitions, respectively, in the binary mixture $C^{12}O_2^{16}-C^{13}O_2^{16}$, and curves 3 to 5 in transitions of $C^{12}O_2^{18}$, $C^{12}O_2^{16}$ and $C^{12}O_2^{16}O^{18}$ in the equilibrium ternary mixture $C^{12}O_2^{16}-C^{12}O_2^{18}-C^{12}O_2^{16}O^{18}$, formed under the influence of the discharge on the mixture $C^{12}O_2^{16}-C^{12}O_2^{18}$.

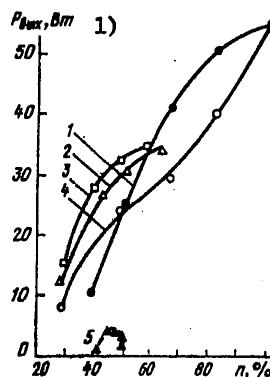


Figure 3. Dependence of Laser's Output Power on Enrichment of Working Isotope

Key:

1. P_{vykh} , W

Transitions of asymmetric molecule $C^{12}O^{16}O^{18}$ yield considerably lower values of power than in working with transitions of symmetric molecules. This is associated not only with a reduction in gain caused by doubling of the number of lasing lines on account of the removal of degeneration, but also with the principal limitation of enrichment of the carbon dioxide gas by these molecules in the discharge (the enrichment cannot be greater than 50 percent). The lasing power for all symmetric molecules of the carbon dioxide gas ($C^{12}O_2^{16}$, $C^{12}O_2^{18}$ and $C^{13}O_2^{16}$), as follows from fig 3, depends practically identically on the enrichment. The substitution of

FOR OFFICIAL USE ONLY

FOR OFFICIAL USE ONLY

one isotope with another with equal enrichment makes it possible to change the lasing wavelength of the CO₂ laser while preserving the radiated power.

4. Influence of Enrichment of the Working Isotope on Saturating Power Density, I_s , and Unsaturated Gain, α_0

For the purpose of determining I_s and α_0 we utilized the relationship between the laser's output power and the parameters of the cavity and active medium. For example, in [5] this relationship is given by the equation

$$P = \frac{I_s \sigma \tau}{1 + \rho} \left[\frac{\alpha_0 l}{\delta l + \ln(\rho \rho_0)^{-1/2}} - 1 \right],$$

where P is the laser's output power, τ is the transmission coefficient of the outlet reflector, σ is the effective cross section of the emission beam, I_s is the saturating power density, ρ is the reflection coefficient of the outlet reflector, α_0 is the unsaturated gain, l is the length of the active medium, δ is the distributed loss index and ρ_0 is the reflection coefficient of the opaque reflector.

Having determined experimentally the values of the output power for various lengths of the active medium and knowing the parameters of the cavity, it is possible by using this equation to calculate the values of I_s and α_0 . It should be mentioned that in the cavity of a laser the cross section of the radiation beam is not constant in relation to the length, which hinders the employment of this equation. In connection with this, in processing the experimental results we used the more precise method of calculating the dependence of the lasing power on parameters of the active medium and cavity described in [6].

An experimental determination was made of the values of the output power of a laser for three lengths of the active medium, $l = 1.6, 2.4$ and 3.2 m. From these values of P a determination was made of I_s and α_0 . The dependences of α_0 and of the product $\alpha_0 I_s$, characterizing the maximum power output from a unit of volume of the medium for line P(20) of the 00⁰1-10⁰ transition of isotopes C¹²O₂¹⁶, C¹²O₂¹⁸ and C¹³O₂¹⁶ and line P(20) of the 001-020 transition of C¹²O₂¹⁶¹⁸ are shown in fig 4. The designations of the points are the same as those in fig 3. In the top graph are also given points at which the gain with a change in enrichment is compared with losses in the cavity; they have been outlined by the solid line.

For isotopes C¹²O₂¹⁶, C¹²O₂¹⁸ and C¹³O₂¹⁶ the gain is practically identical and increases linearly with enrichment. This result agrees with the result of [7] in which it was obtained from calculation. For an asymmetric molecule the gain is approximately twofold less than the gain in transitions of symmetric molecules and reaches the maximum in the vicinity of enrichment equal to 50 percent, the maximum for the molecule in question.

FOR OFFICIAL USE ONLY

FOR OFFICIAL USE ONLY

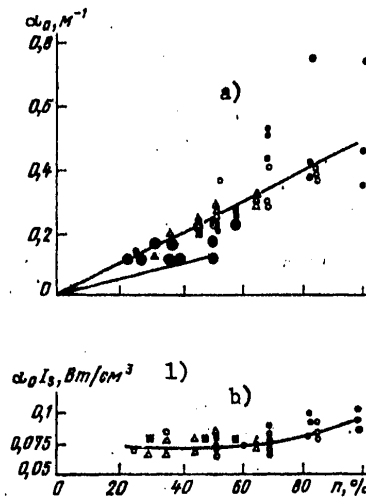


Figure 4. Dependence of Unsaturated Gain, α_0 (a), and of Maximum Power Output from a Unit of Volume of the Medium (b) on Enrichment

Key:

1. W/cm^3

Product $\alpha_0 I_s$, as follows from fig 4b, practically does not depend on the enrichment. This result testifies to the fact that the exchange of energy between molecules of all isotopes takes place sufficiently effectively; therefore, all the power expended on excitation of the working levels of all isotopes may luminesce through a single line of one isotope if we can achieve a considerable excess of the density of emission being amplified over and above the saturation density I_s for the given line.

5. Conclusions

An investigation of the characteristics of a laser employing various isotopes of CO_2 demonstrated the following. The maximum output power in transitions of asymmetric molecule $C^{12}O^{16}O^{18}$ under optimal conditions is four- to fivefold lower than in transitions of other isotopes, which is associated with doubling of the number of lasing lines in the spectrum of this molecule on account of the removal of degeneration and with the limitation in relation to enrichment caused by the dissociation of $C^{12}O^{16}O^{18}$ in the discharge and by the formation of $C^{12}O_2^{16}$ and $C^{12}O_2^{18}$ molecules.

The values of the output power in individual lines of transitions of $C^{12}O_2^{16}$, $C^{12}O_2^{18}$ and $C^{13}O_2^{16}$ are practically identical with equal enrichment; therefore, the substitution of one isotope with another with the same

FOR OFFICIAL USE ONLY

FOR OFFICIAL USE ONLY

enrichment does not change the energy characteristics of the laser; only the region of wavelengths generated is changed.

The unsaturated gain increases linearly with an increase in enrichment; for an asymmetric molecule it is twofold lower than for a symmetric with equal enrichment. The maximum power output from a unit of volume of the medium does not depend on the enrichment and equals the power output with 100-percent enrichment.

Bibliography

1. Freed, C., Ross, A.H.M. and O'Donnell, R.G. J. MOL. SPECTROSC., 49, 439 (1974).
2. Freed, C., O'Donnell, R.G. and Ross, A.H.M. IEEE TRANS. ON INSTRUM. AND MEASUREMENT, IM-25, 431 (1976).
3. Yin, P.K.L. APPL. OPTICS, 8, 997 (1969).
4. Yel'yashevich, M.A. "Spektry atomov i molekul" [Spectra of Atoms and Molecules], Moscow, Mir, 1962.
5. Ishchenko, Ye.F. and Klimov, Yu.M. "Opticheskiye kvantovyye generatory" [Lasers], Moscow, Sovetskoye Radio, 1968.
6. Samokhin, G.S., Kolosovskaya, L.A. and Pechenin, Yu.V. ELEKTRONNAYA TEKHNIKA, SER. ELEKTRONIKA SVCH, No 10, 124 (1978).
7. Doronin, V.G. and Novikov, V.I. ZHPS, 28, No 1, (1978).

COPYRIGHT: Izdatel'stvo "Sovetskoye Radio", "KVANTOVAYA ELEKTRONIKA", 1980
[4-8831]

8831

CSO: 1862

FOR OFFICIAL USE ONLY

FOR OFFICIAL USE ONLY

UDC 621.3.038.8

STUDY OF A LARGE-VOLUME FLASHLAMP-INITIATED H_2-F_2 CHEMICAL LASER

Moscow KVANTOVAYA ELEKTRONIKA in Russian Vol 7, No 8, 1980 pp 1821-1823
manuscript received 3 Mar 80

[Article by A.S. Bashkin, N.P. Vagin, O.R. Nazyrov, A.N. Orayevskiy,
V.S. Pazyuk, O.Ye. Porodinkov and N.N. Yuryshev, USSR Academy of Sciences
Physics Institute imeni P.N. Lebedev, Moscow]

[Text] A study is made of the potentialities of an H_2-F_2 laser initiated by means of IFP-20000 flashlamps and having an active volume of approximately 7.3 liters with a diameter of approximately 14 cm. For the purpose of understanding the physical features of the laser's operation was utilized the technique of measuring the initial concentration of fluorine $[F]_0$ atoms from the absorption of UV radiation by metastable FO_2 radicals. From the value of $[F]_0$ found in the experiment a determination was made of the laser's efficiency, η_f , in relation to the energy put into the working mixture. The experimental value arrived at of $\eta_f = 5500$ percent is much higher than all values of η_f presented in the published data for an H_2-F_2 laser with any method of initiation. The technical efficiency of the laser equaled 30 percent for an $H_2:F_2:O_2:He = 3:20:2:75$ mixture at atmospheric pressure. Here the specific energy output reached approximately 26 J/liter and the total radiation energy of the laser was approximately 200 J. On the basis of the experiments conducted, methods are indicated for further improving the parameters of an H_2-F_2 laser.

At the present time a number of studies are known which are devoted to an investigation of the energy characteristics of chemical lasers based on a hydrogen-fluorine chain reaction initiated by means of pulsed photolysis [1-5]. Interest in the study of these lasers is associated with the fact that they have a long laser chain length of $\nu_{ef} \gg 1$, and the sources of photoinitiation are rather simple and fully developed technologically. It is precisely the long laser chain length which determines the potential advantages of H_2-F_2 lasers over both photodissociation and HF lasers based on non-chain reactions. It is possible to understand this fact if one considers the principal kind of equations for the values of the specific energy output, ϵ_1 , and technical efficiency, η_t , in an H_2-F_2 laser with initiation by means of pulsed photolysis:

FOR OFFICIAL USE ONLY

FOR OFFICIAL USE ONLY

$$\epsilon_1 = N \tilde{\nu}_{ef} hc / \lambda_1, \quad (1)$$

$$\eta_t = \eta_f \eta_i K_p, \quad (2)$$

$$\eta_f = 2 \tilde{\epsilon} \nu_{ef} \lambda_{fd} / \lambda_1, \quad (3)$$

where λ_1 is the wavelength of the laser's radiation (approximately 3μ), λ_{fd} is the wavelength of the radiation resulting in photodissociation of the F_2 molecule, N is the initial concentration of atomic fluorine, $\tilde{\epsilon} \nu_{ef}$ is the number of laser emission quanta necessary for a single fluorine atom formed in initiation, η_f is the physical efficiency of the laser, defined as the ratio of the laser's energy to the energy put into the working mixture and expended on initiation of the chemical reaction, η_i is the efficiency of the initiation source, and K_p is the capture coefficient for the radiation of the initiation source in the F_2 photodissociation band of the laser's working medium.

Actually the existence in these expressions of factor $\tilde{\epsilon} \nu_{ef} \gg 1$ results in the fact that rather high values of ϵ_1 and η_t can be arrived at with low expenditures for initiation of the hydrogen-fluorine chain reaction. The investigation of an H_2-F_2 laser with almost instantaneous initiation ($t_i \sim 40$ ns) by means of an electron beam has demonstrated that in such a laser the value of $\tilde{\epsilon} \nu_{ef} \sim 300$ with a degree of initiation of $[F]_0/F_2 \sim 0.1$ percent for mixtures at atmospheric pressure [6]. Then from (3) it follows that with initiation by means of flash photolysis the physical efficiency of an H_2-F_2 laser can reach a value of approximately 6000 percent, which is so high that it promises the obtainment of exceedingly high values of η_t with the accomplishment of an effective capture of the radiation of the photo source ($K_p \sim 1$) and with the utilization of flashlamps with an efficiency equal to several percent.

However, the results arrived at in experiments with photoinitiated H_2-F_2 lasers differ from one another strongly ($\epsilon_1 = 10$ J/liter [1] and 80 J/liter [4] and $\eta_t = 1$ percent [1] and 30 percent [5]). The majority of these data refer to a specific experimental apparatus and it is difficult on their basis to predict the characteristics of a laser of a somewhat different design or to judge the potentialities of an H_2-F_2 laser with pulsed photoinitiation.

Actually it is not clear what the possibilities are for the effective capture of the radiation of the photoinitiation source by the laser's working medium and where the potentials lie in the job of achieving the maximum possible energy parameters for the laser. Therefore, of obvious interest is a study on determination of such parameters of an H_2-F_2 laser as the initial concentration of active centers (of atomic fluorine) created by the photo source, the effectiveness of the capture of radiation of the photo source by the working medium, and the efficiency of standard initiation sources operating under conditions corresponding to the conditions in an H_2-F_2 laser.

FOR OFFICIAL USE ONLY

FOR OFFICIAL USE ONLY

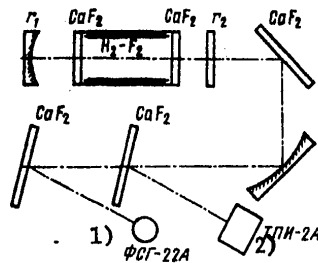


Figure 1. Basic Diagram of Experimental Apparatus

Key:

1. FSG-22A

2. TPI-2A

A basic diagram of the apparatus is shown in fig 1. The laser cell was in the form of a stainless steel cylinder 900 mm long with an inside diameter of 150 mm. The ends of the cell were closed with windows made of CaF_2 . The active volume equaled 7.3 liters when using windows 140 mm in diameter. Initiation of the chemical reaction was accomplished by means of the light of IFP-20000 flashlamps placed inside the laser cell. The number of lamps could be varied from one to four. For the purpose of increasing the effectiveness of the utilization of the radiation of the flashlamps, the inside surface of the laser cell was covered with Teflon and the capacitance and inductance of the electric circuit were selected so that the duration of the radiation of the flashlamps at half-intensity (approximately 2.5 μs) would not exceed the duration of lasing. For this purpose in the electric circuit were used low-inductance KMK-50-1 capacitors and measures were taken to reduce the inductance of the input. The laser's cavity was formed by "opaque" spherical reflector r_1 with a radius of curvature of 20 or 40 m and a flat dielectric reflector, r_2 , with a reflection coefficient of 35 percent. The shape of the lasing pulse was recorded by means of an FSG-22A photodetector employing an S8-2 double oscillograph. At the same time was also monitored the shape of the UV radiation pulse in the wavelength region of 250 to 350 nm. In fig 2 are presented typical oscillographs of the photoinitiation and lasing pulses. The laser's emission energy was measured by means of a TPI-2A calorimeter.

For the purpose of determining the initial concentration of active centers of $[F]_0$ averaged for the active volume was employed the technique suggested in [7] and based on measuring the concentration of metastable FO_2 radicals formed as the result of the reaction $F + O_2 + M \rightarrow FO_2 + M$, from the

FOR OFFICIAL USE ONLY

FOR OFFICIAL USE ONLY

absorption of UV radiation. In fig 3 are given dependences of $[F]_0$ on the pressure of molecular fluorine in the presence of a Teflon reflector and without it. From this it is possible to draw the conclusion that with transverse dimensions of the laser cell similar to those used in this study the effective capture of the radiation of the photo source by the laser's working medium takes place at rather high fluorine pressures ($p_{F_2} \geq 200$ mm Hg). For the purpose of utilizing this fact a study was conducted at atmospheric pressure of a mixture with the composition $H_2:F_2:O_2:He = 3:20:2:75$. In this mixture was achieved a technical efficiency of $\eta_t \sim 30$ percent with a specific energy output of $\varepsilon_1 \sim 26$ J/liter (the total energy of the laser emission was 194 J). The measured initial concentration of atomic fluorine equaled approximately $1.35 \times 10^{15} \text{ cm}^{-3}$.

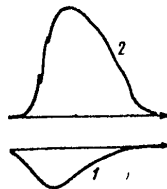


Figure 2. Oscillogram of Photoinitiation (1) and Emission (2) Pulses of an H_2-F_2 Laser

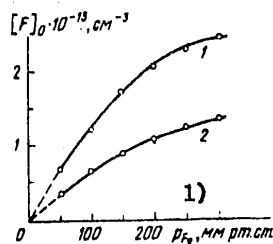


Figure 3. Dependence of Initial Concentration of $[F]_0$ on Pressure of Molecular Fluorine in the Presence of a Teflon Reflector (1) and Without It (2): $U = 30$ kV; four lamps

Key:

1. mm Hg

FOR OFFICIAL USE ONLY

FOR OFFICIAL USE ONLY

Utilizing equations (1) and (3) it is possible to obtain an expression convenient for computing η_f from experimental data:

$$\eta_f = 2 \frac{\lambda_{fd}}{\lambda_1} \frac{\epsilon_1 \lambda_1}{hc[F]_0}.$$

From this the computations give a value of $\eta_f \approx 5500$ percent. Estimates of the effectiveness of the conversion of the electric energy stored in the capacitor battery into energy expended for the dissociation of molecular fluorine, $\eta_1 K_p = \eta_1 / \eta_f \approx 0.55$ percent, demonstrate that the principal potential in the job of improving the technical efficiency of this laser consists precisely in seeking ways of increasing this conversion effectiveness. Measurements of η_1 specially made in this study, of an IFP-20000 lamp operating in the mode described above, gave a value of $\eta_1 \approx 1.5$ percent. From this we get $K_p = 0.37$.

Thus, the analysis of the results obtained indicates that in this case the value of η_f was limited by the low values of η_1 and K_p . Therefore, further improvement of the technical efficiency of the laser requires optimization of the performance of the flashlamp-reflector system.

Bibliography

1. Batovskiy, O.M. and Gur'yev, V.I. KVANTOVAYA ELEKTRONIKA, 1, 801 (1974).
2. Greiner, N.R. IEEE J., QE-8, 872 (1972).
3. Greiner, N.R. IEEE J., QE-9, 1123 (1973).
4. Chen, H.L., Taylor, R.L., Wilson, J., Levis, P. and Fyfe, W. J. CHEM. PHYS., 61, 306 (1974).
5. Nichols, D.B., Hall, R.B. and McClure, J.D. J. APPL. PHYS., 47, 4026 (1975).
6. Bashkin, A.S., Konoshenko, A.F., Orayevskiy, A.N., Tomashov, V.N. and Yuryshv, N.N. FIAN Preprint, Moscow, 1978, No 274.
7. Chegodayev, P.P. Candidate's dissertation, Moscow, Physicochemical Institute imeni L.Ya. Karpov, 1974.

COPYRIGHT: Izdatel'stvo "Sovetskoye Radio", "KVANTOVAYA ELEKTRONIKA", 1980 [4-8831]

8831

CSO: 1862

FOR OFFICIAL USE ONLY

FOR OFFICIAL USE ONLY

OPTICAL RESONATORS AND THE PROBLEM OF LASER BEAM DIVERGENCE

Moscow OPTICHESKIYE REZONATORY I PROBLEMA RASKHODIMOSTI LAZERNOGO
IZLUCHENIYA in Russian 1979 signed to press 29 Oct 79 pp 2-18

[Annotation, table of contents, foreword, and Introduction from a book
by Yu. A. Anan'yev, Moscow, "Nauka" Glavnaya redaktsiya fiziko-matematicheskoy literatury, 1979, 4000 copies, 314 pages]

[Text] The book presents the principles of the optical resonator theory, and factors that determine the divergence of the laser beam are considered. The basic attention is concentrated on the problem of obtaining a narrow beam; data is cited on various methods for reducing the angular divergence. Considered in greatest detail are the properties of lasers with so-called unstable resonators, and methods for their calculation and optimization are presented, as well as special features of circuits used in various laser devices. The book also contains some information data on the causes of the origination and nature of optical nonuniformities in an active medium, as well as on methods that make it possible to reduce these nonuniformities.

One hundred twelve figures, three tables. Bibliography contains 343 titles.

Table of Contents

Foreword	6
Introduction. Development of concepts on the optical resonator as a device for forming narrow beams	9
Chapter 1. General information	19
1.1. Laws of light beam propagation and angular beam divergence	19
Huygens-Fresnel principle (19). Far zone distribution (22). Ideal radiator (24). Arbitrary monochromatic emitter (28). Nonmonochromatic radiator (35). Certain conclusions. Measurement of divergence (36).	
1.2. Optical resonators and their classification. Initial information. Some history (38).	38

FOR OFFICIAL USE ONLY

FOR OFFICIAL USE ONLY

Passage of light beams through optical systems. Beam matrix (41). Classification of resonators according to the properties of their beam matrices (46). Equivalency conditions for resonators (52).	
1.3. Oscillation modes of an empty ideal resonator and their application for describing a laser situation	55
Classification of natural oscillations (53). Integral equation and natural oscillation of an arbitrary vacant oscillator (59). Resonator with an active layer (61). On the suitability of a standard model of an open resonator for describing actual lasers (64).	
1.4. Efficiency of excitation energy conversion in laser resonators	66
Efficiency of energy conversion in an elementary volume of medium (67). Calculation of nonuniformity of laser beam distribution along the length of the resonator (70). Total balance of excitation energy and beam generation (73). On the meaning and possibilities of applying the derived relationships (76).	
Chapter 2. Divergence of laser beams with stable and plane resonators	80
2.1. Oscillation modes of empty stable resonators	80
Natural functions and frequencies of a stable oscillator with infinite mirrors (80). Spatial structure of natural oscillations (83). Stable resonators with finite dimension mirrors (88).	
2.2. Fringe diffraction and types of oscillation of a vacant plane resonator	92
Auxiliary diffraction problem (92). Reflection from an open edge of a waveguide. Natural oscillations of a resonator made up of plane band or rectangular mirrors (97). Plane resonator made of round mirrors (102). Beam polarization of types of natural oscillation (104).	
2.3. Certain results of experimental investigations	106
Early observation of oscillation of solid-state lasers (107). Beam divergence of solid-state lasers (109).	

FOR OFFICIAL USE ONLY

2.4. Multimode oscillation in ideal resonators	112
On the mechanism of multimode oscillation (112). Methodology and some results of the calculations of multimode oscillations (116). Competition between transverse modes in lasers with plane resonators (119). On the shortcomings of the model and possibilities of its refinement (122).	
2.5. Effect of resonator deformation on the field configuration of individual modes of oscillations	124
Some general remarks. Perturbation theory (124). Plane resonators with small aberrations (128). Plane resonators with considerable size of aberrations (131).	
2.6. Methods for angular beam selection.	135
Attempts to solve the divergence problem on the basis of resonators with small diffraction losses (135). Lasers with plane resonators and angular selectors (138). Angular selection of laser beams with plane resonators by reducing the number of Fresnel zones (143). Plane resonators of large effective length (146). Multistage laser devices (149).	
Chapter 3. Elements of the unstable resonator theory	152
3.1. Some initial information	152
Brief historical reference (152). Elementary consideration of an ideal unstable resonator (154). Properties of convergent waves (159).	
3.2. Resonators with a weakly nonuniform medium	163
The simplest method for calculating a non-uniform medium (164). Aberration coefficients (166). Some remarks on the possibilities of optical-geometric approximation (169).	
3.3. Fringe effects and natural oscillations spectrum	172
Equivalency of unstable resonators and inter-relationship between solutions for their various types (172). Unstable resonators with a fully "smoothed" edge (174). Unstable resonators with a sharp edge (177). Specific nature of edge effects under actual conditions (181).	
3.4. Unstable resonators with a central beam hole	188
Initial pulses. Caustic curve oscillations of a two-dimensional resonator (188). Two-dimensional resonator with a central hole (192). Three-dimensional resonator with a beam hole. Discussion of results (195).	

FOR OFFICIAL USE ONLY

3.5. Certain properties of unstable multimirror and prism resonators	199
The problem of unidirectional lasing (199). Stabilization of beam direction in prism resonators (205).	
3.6. Unstable resonators with field rotation.	210
Operation of turning the cross section and the polarization characteristics of the beam (210). Aberration characteristics of unstable resonators with field rotation (213). Resonators with a compact output aperture (216).	
Chapter 4. Use of unstable resonators	220
4.1. Unstable resonators in pulsed lasers with free lasing	220
Selection of type and parameters of resonator (220). Experimental results with neodymium glass lasers (227). Gas pulsed lasers with unstable resonators. Problems of establishing steady state oscillations (234).	
4.2. Resonator instability in continuous lasers.	238
Review of experimental work (238). Method of calculating effectiveness of continuous flow lasers (240). Simplest model of gasdynamic laser medium. Methodology and results of gasdynamic laser power calculations with a two-mirror resonator (245). Problem of forming a uniform field distribution along the cross section of a continuous flow laser (251).	
4.3. Unstable resonators in lasers with controlled time-spectral beam characteristics	254
Simplest laser types with controlling components (254). Lasers with a three-mirror resonator (257). Lasers controlled by an external signal (260). Multi-passage amplifiers (264).	
Chapter 5. Optical nonuniformity of active media and methods for correcting wave fronts	268
5.1. Thermal deformations of solid-state lasers (269).	
Origin and value of thermal aberrations in the presence of round active rods (269). Consequences of aberrations and attempts to correct them (274). Various methods for reducing resonator deformations (278). Lasers with active components of stretched rectangular cross section (281).	

FOR OFFICIAL USE ONLY

- 5.2. Phase correction of wave fronts. Dynamic holography and induced scattering 285
 Optical-mechanical correction systems (285). Principles of holographic correction (288). Conditions for implementing the process of holographic "pumping" and its power effect. "Pumping" with thermal grids (292). Relationship between dynamic holography and phenomena of induced scattering. Lasers with various kinds of induced scattering (297).
- 5.3. Method for "reversing" the wavefront 301
 Idea and principal possibilities of the method (301). "Reversal" with induced backscattering (305). "Reversal" by classical optics and holography (308). "Reversal" with parametric light amplification (311).

Bibliography 314

Foreword

Papers by Nobel prize winners N. G. Basov, A. M. Prokhorov and Ch. Townes (United States) laid a path to creating coherent light beam oscillators-lasers. Operating lasers appeared in 1960. Among their amazing characteristics that attracted general attention, the beam divergence should be mentioned first -- since, in principle, the degree of directivity of a coherent light beam is limited only by diffraction at the output aperture of the laser and, as appeared to many, there were no special obstacles in the path of reaching this limiting directivity. Literature of that time was full of the most optimistic forecasts for laser applications in extremely long communications lines (including space) for transmitting energy over great distances, etc. All these forecasts were based, as a rule, on simple manipulations of the well-known formula for the diffraction limit of beam divergence $\varphi_0 = 1.2 \lambda / D$ where λ is radiation wavelength and D is diameter of the coherent light beam. Actually, the value of φ_0 for the first ruby lasers ($\lambda = 0.694$ microns) was 4×10^{-5} radians or eight angular seconds for easily attainable crystal diameters! However, the first observations of oscillations of such lasers, with six to ten mm diameters of active bodies, indicated that their angular beam divergence was considerably greater than expected (usually one or two orders of magnitude).

FOR OFFICIAL USE ONLY

It was far from simple to find the reasons for such laser behavior and to influence it in the necessary direction. This required innumerable experiments and the development of a theory of actual resonators with an active medium, which rests greatly on the theory created in 1961-1966 of ideal cavity resonators, etc. All this formed an entire direction of quantum electronics consolidating the most varied methods of influencing the spatial characteristics of laser radiation. Many of these methods are of cognitive interest; however, as far as the practical importance of the work directed toward reducing the angular beam divergence, it is truly difficult to overestimate it. Therefore, it is not surprising that a huge number of publications is devoted to the divergence problem. However, as yet, not one serious attempt has been made to present the basic concepts about the given problem as a whole. In all the books on the theory of lasers, as well as laser equipment, results, at best, are cited on the theory of ideal resonators with an optically uniform active medium (or vacant). Nor has the gap been filled by the few surveys in which individual particular problems are considered. Whether this book will be found to be useful and to what extent, only its readers will be the best judges and the author will accept all their comments with gratitude and attention.

From the theory of ideal vacant resonators, we will present only the most general information necessary to understand the following material. After that, the problem of beam divergence in resonators with small diffraction losses, primarily, in the most widely used resonator with plane mirrors will be considered. The presentation of this question also cannot claim special completeness: a laser with a plane resonator is, in essence, a most complex oscillating system with a huge number of resonance frequencies, subjected to the strong influence of the smallest perturbations. Therefore, the problem of beam divergence of a laser with plane resonators is closely associated with a more complex and general problem of their kinetics which is truly inexhaustible. This book presents only that information which is sufficient to clarify the general situation and is needed in reading special literature.

Then follow lasers with so-called unstable resonators. Their creation is a result of the direction of research whose representatives strove not so much to describe exhaustively a system with a huge number of degrees of freedom, as to limit this number. Although not everyone has yet become accustomed to lasers with unstable resonators, they are, essentially, much simpler than the traditional laser with a plane resonator. Here we do not have to deal with such an excess of modes with similar Q-factors or with sensitivity to the smallest perturbations. Therefore, at present, the theory of lasers with unstable resonators has progressed farther than the theory of oscillators of different types that appeared long ago. Its results will be presented in fairly great detail and attention is concentrated on the most important experimental work.

FOR OFFICIAL USE ONLY

FOR OFFICIAL USE ONLY

In conclusion, the problem of optical nonuniformity of active media will be considered briefly and several attempts to solve this problem will be described.

The author is deeply grateful to N. A. Svetsitskaya, V. Ye. Sherstobitov, O. A. Shorokhov, N. I. Grishmanova, V. P. Kalinin, L. V. Koval'chuk and his other coworkers for their participation in work whose results make up a considerable part of this monograph, and help in preparing the manuscript for publication. The discussion of individual problems with V. V. Lyubimov, M. S. Soskin were useful. The author is also grateful to P. V. Zarubin and Ye. M. Sukharev whose advice contributed to many editorial corrections.

The constant attention to his work and active support of the idea for writing this monograph by Rem Viktorovich Khokhlov to whose memory it is dedicated was very important to the author.

Leningrad, August 1977. Yu. Anan'yev

Introduction

Development of concepts about the optical resonator as a device for forming narrow-directional beams.

The first papers on the possibility of creating resonators in the optical range intended for oscillation of coherent beams were published by Prokhorov [1], as well as Shawlow and Townes [2] in 1958. These papers predetermined to a great extent the direction of the investigations that led to the appearance of lasers.

As is well known, the action of lasers is based on the ability of some media to amplify light beams passing through them under certain conditions. Therefore, without doubt, the role of the properties of the active medium itself and the method of its excitation is great. However, the properties of the resonant system in which this medium is placed also have a great effect on many characteristics of the oscillated beam. The angular divergence of the beam should be considered a primary characteristic. Here the resonator plays a truly decisive role -- without it the active medium by itself is, as a rule, capable with equal success of amplifying the beam passing through it in any direction that it is propagated.

Optical oscillators appeared considerably later than radio frequency and microwave ones. Therefore, in their description, concepts and terminology used widely are taken from the indicated related areas. We will also use this terminology.

FOR OFFICIAL USE ONLY

FOR OFFICIAL USE ONLY

To convert an amplifier into an oscillator, it is necessary, as they say in radio engineering, to connect the amplifier output to its input and create a feedback circuit (Fig. V.1a). The meaning of the feedback circuit is that part of the amplified radiation is fed back to the system, amplified again, etc., maintaining thereby continuous oscillations. In optical range oscillators, the light beam and not the electrical signal is amplified. In accordance with this, new demands are imposed on feedback circuits here -- the initial direction of beam propagation and its structure must be preserved after its passage. The simplest analog of the system shown in Fig. V.1a, that satisfies this requirement is an optical resonator shown in Fig. V.1b. Actually, such resonators, called ring resonators, found some application. However, the first resonator in optics was the usual Fabry-Perot interferometer consisting of two plane mirrors (Fig. V.1c). One of these mirrors allows partial passage and the exit of the beam being oscillated is implemented through it. The basic difference between this and the ring resonator is that the feedback circuit passes through the same active medium and the beam is amplified again.

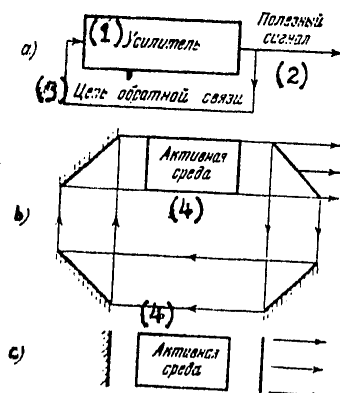


Fig. V.1. Oscillator circuits: a) oscillator in radio engineering; b) oscillator in optics; c) oscillator with plane resonator.
 1. Amplifier
 2. Useful signal
 3. Feedback circuit
 4. Active medium

FOR OFFICIAL USE ONLY

The Fabry-Perot interferometer was such a successful resonator system that until this time it is probably the most widely used type of laser resonator. Its "popularity" is due not only to extreme simplicity, but also to the possibility of obtaining high power characteristics of the output beam (we will dwell on the reasons for this in Section 1.4). However, the divergence of the beam generated in the resonator made with flat mirrors is not too good. The origination of comparatively high divergence is clarified to a great extent, by a theoretical analysis of plane resonator properties which may be made by methods developed previously as applied to resonators of the microwave range [3]. It shows, first, that in passing the feedback circuit in a plane resonator, there is a reproduction not of any beam directed along the axis and nearly parallel to it, but a beam with strictly determined distribution of amplitude and phase of the wavefront. This beam is called the basic type of oscillation (mode) of the resonator. It is more remarkable, however, that there also exist beams (modes) reproduced with somewhat greater attenuation whose radiation is propagated at not very large, but still noticeable angles to the axis of the resonator. These beams form a discrete set with a slope to the axis of adjacent modes according to classification, differing by about half of the diffraction angle.

Thus, a plane resonator in a certain sense (and, of course, within certain limits) is indifferent to the direction of the radiation propagated along it. The reasons for such "indifference" is rooted in the fact that when passing along the feedback circuit, the inclined beams, as well as the axial one, preserve the initial directions of propagation; their "overshooting" to the side is prevented by the fringe diffraction, about whose mechanism we will dwell in Section 2.2.

Types of oscillations with various slope angles to the axis have somewhat different excitation thresholds due to various attenuation; however, because of the nonlinearity of the medium, they may be present in the oscillation simultaneously (Chapter 2), which must lead to a large angular divergence of the beam. For this reason, plane resonators with large apertures cannot provide a small beam divergence even with a highly uniform medium.

This is the situation in the idealized case of an optically uniform medium. A still greater shortcoming of a plane resonator, from the standpoint of radiation directivity, is the extremely sharp dependence of the field distribution in it on small distortions of the shape (deformations) of the resonator. This can be clarified on the simplest example of a misaligned resonator. The mirrors being out of parallel is equivalent to an optical wedge being inserted in the feedback circuit, that changes the beam direction by angle δ , double the misalignment angle. If we send a parallel beam into such a resonator, then after the first passage, it will be turned by angle δ , after the second -- by angle 2δ , etc. Its shift in

FOR OFFICIAL USE ONLY

FOR OFFICIAL USE ONLY

the transverse direction will increase still faster and a considerable part of the beam will begin to come out of the system bypassing the mirrors. After some number of passages (at small δ , it may be fairly large) the shape of the beam is so distorted that it becomes impossible to consider the process of its further propagation without taking into account the diffraction effects. Therefore, a steady state field distribution is obviously not so simple; it is, essentially, the result of an equilibrium between diffraction processes and beam turning. We will stress that this equilibrium is established after a process of accumulation of aberrations occurs for a number of passages. It is also noteworthy that, as shown by analysis (Section 2.5), the number of passages in which the aberrations are accumulated increases rapidly with the increase in the dimensions of the transverse cross section of the resonator. Therefore, plane resonators with large mirrors are especially sensitive to the smallest aberrations.

A similar, but still more complicated situation occurs in the case of irregular resonator deformations. In general, the sources of such deformations are extremely varied: these include errors in manufacturing (and adjusting) mirrors, the initial optical nonuniformity of the active medium and nonuniformity induced in the process of pumping due to the nonuniform excitation and heating of the medium; dispersion of light by microinclusions; mechanical vibration of the active component and turbulence of the gas flow. This list could be continued. It is not surprising that the majority of papers published in 1965-1969 are devoted to the problem of a nonideal plane resonator. The results of the papers devoted to the most general patterns of the behavior of oscillators with nonideal resonators will be presented in Section 2.5. Carrying out all of these investigations could not, of course, eliminate the principal defects of a plane resonator, but was found to be very useful for the understanding of processes occurring in an actual resonator.

No less numerous were the attempts made at the same time to find some new solution to the problem of laser beam divergence. Two directions of searching may be noted.

In one of them an attempt was made, without discarding the plane resonator, to place in its feedback circuits so-called angular selectors -- filters that pass the beam only in a narrow range of angles. Such filters may be made by various methods: on the basis of full internal reflection, by means of additional Fabry-Perot etalons, by a combination of lenses and diaphragms. All these approaches were tested, however, later, due to their great complexity, and the number of difficulties in principle, on which we will dwell in Section 2.6, only few found particular applications.

FOR OFFICIAL USE ONLY

FOR OFFICIAL USE ONLY

In the other direction, attempts were made to solve the divergence problem (or at least that of single-mode lasing), not by complicating the resonator arrangement, but by changing the shape of its mirrors. In particular, lasers with so-called stable resonators, one or both of whose mirrors were slightly curved (which is equivalent to placing a weak positive lens in the feedback circuit) were thoroughly investigated. Obviously, in such a system, the steady state beam with an approximately uniformly distributed amplitude and nearly plane front must have such a small cross section that the focusing influence of the mirrors would be compensated by diffraction. From this follows the principal shortcoming of stable resonators -- they can provide single-mode lasing only with very small volumes of the active medium. Indeed it is in lasers with a low-volume active medium that stable resonators have been used up until now. The usual helium-neon lasers may serve as an example of this. If the medium is large in volume, broad beams with a complex structure originate in stable resonators corresponding to an angular divergence greater than for the same conditions in plane resonators (Sections 2.3, 2.4).

Several other kinds of resonators with small diffraction losses (Section 2.6) have been investigated but as before, no success has been achieved.

With this situation, it was the common opinion that the problem of beam directivity cannot be solved by improving the resonator and that the single possible way is to design multistage systems consisting of a master oscillator and amplifiers (since in the amplifiers there is the effect of multiple accumulation of aberrations as in a plane resonator). The way out of the situation was indicated by Sigman's paper [4]. In this paper Sigman considered a simplified "unstable" resonator (according to the adopted classification in Section 1.2), formed by two convex mirrors. The consideration indicated that in such a resonator, as in an ideal plane one, there exists a solution in geometrical approximation, except that not parallel but diverging beams are propagated along the resonator in both directions, while a part of the radiation bypasses the mirrors (Section 3.1).

At first, Sigman's article evoked no special response -- several investigators already dealt with unstable resonators, obtaining undesirable instead of encouraging results (see start of Section 3.1). Sigman himself soon switched his attention to the peculiarity of the fringe effects in unstable resonators and studied this problem for several years, a curious one but, as will be seen later, not at all a decisive one. From the viewpoint of beam directivity, the most interesting special features of unstable resonators were discovered only when analyzing the aberrations effect on the steady state field distribution. It is precisely, as a result of such an analysis, that it became clear that the resonator considered by Sigman was only the first of a broad class of resonators whose feedback was formed according to a completely new algorithm, having a number of advantages in principle.

FOR OFFICIAL USE ONLY

FOR OFFICIAL USE ONLY

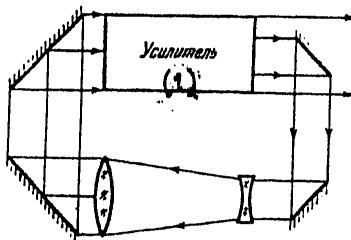


Fig. V.2. Oscillator circuit with an unstable resonator.

1. Amplifier

The essence of the new algorithm is clarified in Fig. V.2. While in a plane resonator, a part of radiation of the entire cross section of the output beam (see Fig. V.1b) was introduced into the feedback circuit, in the unstable resonator, as a rule, the entire radiation is introduced, but necessarily only from part of the cross section. For the reproductibility of the process, the feedback circuit must obviously be formed so that the beam is broadened in it. In Fig. V.2, the beam wavefront is plane and the widening is implemented by a telescopic system, but entirely different versions are possible. In particular, the cross section dimensions of the parallel beam are changed when it is reflected from the diffraction grid and when it passes obliquely through the boundaries of the interface of media with different indices of refraction. Thus, lenses and spherical mirrors are not at all compulsory accessories of an unstable resonator.

We will now examine what advantages are promised by such a seemingly insignificant change of the algorithm. We will start with the effect of intracavity sources of aberrations. Let, as in the case of a plane resonator, an optical wedge be inserted within the system, leading to the turning of the beam, and let this turning correspond to a value of wave aberrations Δ (Fig. V.3a). A part of the beam falls into the feedback circuit. In the case shown in the Figure, its cross section dimension is equal to half the size of the entire beam.

The value of wave aberrations in this part of the cross section is, naturally, equal to $1/2 \Delta$. When the beam cross section is stretched out by the above enumerated methods, the value of the wave aberrations, as is well known, is preserved. Thus the beam that goes to the input of the system has a wave aberration of $1/2 \Delta$, rather than Δ .

FOR OFFICIAL USE ONLY

FOR OFFICIAL USE ONLY

as in the case of a plane resonator. With passage through the system, Δ is added again (Fig. V.3b) and at the end of the second cycle, the value of the wave aberrations becomes equal to $3/2 \Delta$. By the end of the third cycle, it becomes $3/4 \Delta$ and at the end -- $7/4 \Delta$ (Fig. V.3c), etc. It is obvious that this value converges in the limit to 2Δ . Thus, wave aberrations in a steady state mode are only double the aberrations on one passage. The shift of the beam in the transverse direction does not play a special role here -- it only leads to a small redistribution of the parts of the beam that pass along the different sides of the output mirror, but the feedback circuit remains fully filled.

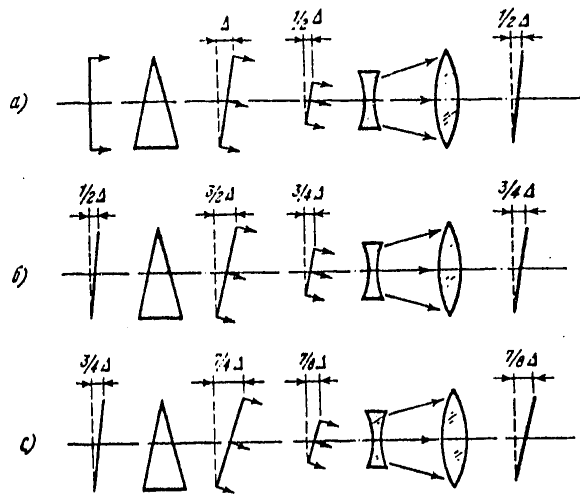


Fig. V.3. Accumulation of wave aberrations in an unstable resonator when an optical wedge is inserted.

FOR OFFICIAL USE ONLY

In the case of arbitrarily distributed aberration sources, the quantitative characteristics change, of course, but the qualitative characteristics remain as before -- the accumulation of wave aberrations occurs over the length of the counted number of passages (see Section 3.2). As the share of the beam cross section directed into the feedback circuit decreases, this number converges to one -- a value characteristic of single stage amplifiers.

From the example shown in Fig. V.3, it is also possible to conclude that in an unstable resonator there exists only one shape of the wavefront, which is preserved after the beam passes through the feedback circuit. Actually, the direction of the light beam sent into the resonator rapidly approaches a single equilibrium direction (which in the case of Fig. V.3 corresponds to steady state wave aberrations 2Δ). Thus, an unstable resonator, unlike a plane one, is rigidly selective with respect to beam direction. It seems that here the effects of multimode oscillation should not influence the value of angular divergence.

These encouraging considerations of the unstable resonator properties, obtained by means of the simplest geometrical approximation, are confirmed also by a more thorough consideration in diffraction approximation (Section 3.3). Moreover, a detailed acquaintance with the properties of unstable resonators makes it possible to formulate the following affirmation: if, in the operation of a laser in which a large volume of a comparatively uniform active medium is used, there is a strong effect of diffraction -- it means that miscalculations were permitted in its creation. This affirmation seems paradoxical at first glance: in all previously used resonators, the beam structure was determined in the final result by diffraction. However, this affirmation has a solid logical basis. In fact, the final goal is to build a laser with the smallest possible divergence of the beam. This goal is entirely attainable with a uniform medium. Beams whose wavefront is plane or spherical have a very small divergence. It is well known that the propagation of such beams for small distances is described excellently by a geometrical approximation without introducing the diffraction concept.

So much for ideology; we will now proceed to practice.

No one utilized the arrangement considered in Sigman's first paper which consisted of two convex mirrors which, due to its symmetry, remained a favorite object of investigations by theoreticians. On the other hand, many specialized arrangements came into practice that made it possible to solve a number of laser technique problems by considerably simpler means than before.

Among these problems, first to be mentioned, of course, should be the problem of building simple laser radiators highly efficient and with small angular divergence. In most practically important cases, the so-

FOR OFFICIAL USE ONLY

called telescopic resonator (Section 4.1) is suitable for solving this problem. It represents an unsymmetrical confocal system of concave and convex mirrors. The beam progress in it differs from the beam progress in Fig. V.2 only by the spatial coincidence of two oppositely directed beams, i.e., by the same way that arrangement in Fig. V.1c differs from the ring arrangement of Fig. V.1b. Of interest also is the ring version of the telescopic resonator -- in it are easily implemented such conditions as that the radiation flux, propagating along the ring to one side, without utilizing nonreciprocal devices, must exceed by many times the flux, following in the reverse direction (Section 3.5).

A number of new possibilities are related to the idea of using that special role which is played by the area near the axis in an unstable resonator. This idea is as follows. If we trace the course of the beams in an unstable resonator for several cycles, we will convince ourselves that the radiation "spreads" over the entire cross section from a small section, which adjoins the line of the resonator axis. By introducing into this section radiation with given time and spectral characteristics, it is possible, obviously, to control the radiation of the entire laser efficiently. When the "priming" radiation is taken from an external source and introduced through a hole to the mirror on the resonator axis, our device becomes simply a multipass amplifier with a very high amplification coefficient (Section 4.3). As the radiation in it is amplified, the cross section of the beam widens which eases the obtaining of the maximum possible power characteristics. The control of radiation properties based on this principle may also be implemented by creating unique lasers that have that valuable quality of having cross sections of control components (gates, spectral selectors) many times smaller than the cross sections of the output apertures.

Several particular problems may be solved successfully by varying the feedback algorithm slightly. As an example, we will take a problem on stabilizing the direction of the beam. It originates in a very great number of cases when there is an optical wedge inside the resonator, whose value changes during the pulse generation time (for example, due to mechanical vibrations of the active component). To weaken the effect of the wedge considerably, it is sufficient to design the feedback circuit so that besides widening the cross section, the beam would also be turned. If this change is introduced in the version illustrated in Fig. V.3, then by the start of the second cycle, the value of the wave aberrations will become equal to -0.5Δ and at its end -- $(-0.5)\Delta + \Delta = 0.5\Delta$; at the start of the third cycle -- $(-0.25)\Delta$ and at its end -- $(+0.75)\Delta$, etc. In the final result a front is established at the system output with aberrations 0.67Δ , i.e., one-third of the case in Fig. V.3. We will note that Fig. V.3 and the example now considered belong essentially to various types of telescopic ring resonators. In the case of systems that are not ring systems, when the beam, following

FOR OFFICIAL USE ONLY

along the feedback circuit, passes through the same wedge, it is possible to build a circuit with still greater stability of direction of the output beam (Section 3.5).

Finally, we must mention the problems that originate with the appearance of a number of new laser types. For example, in the so-called rapid flow-through lasers, the active medium passes through the resonator in the transverse direction and frequently is excited not inside it, but beforehand. This leads to entirely different, compared to previously existing lasers, patterns of the radiation field distribution. In particular, when using plane mirrors, lasing may be localized in a narrow zone near that edge of the resonator where the active medium enters. There, the radiation density of lasing naturally proves to be excessively high. An entirely similar situation also occurs in lasers with forced Raman scattering with transverse pumping. Such difficulties are easily overcome by using unstable resonators: a peculiar self-balancing mode originates and the radiation flux distributes over the cross section of the resonator more or less uniformly (Section 4.2).

All these possibilities were very rapidly implemented in actual devices (see Chapter 4). Thus, after only a few years after the publication of the first paper on the experimental observation of angular selection in an unstable resonator [5], it became entirely clear that precisely this resonator was the optimal for the most varied kinds of lasers with narrow beams.

All that was touched upon above and other aspects of the divergence problem will be strictly and sequentially considered further. Before proceeding with that, we will note one curious special feature in the history of the given question. We just spoke about to what degree the presence of considerable optical nonuniformities of the medium makes the solution of the divergence problem more difficult. As shown by results of numerous investigations at the beginning of the sixties (Section 2.3), difficulties also increased rapidly with the increase in the diameters of the generated beams: the diffraction limit of divergence is difficult to achieve only in the case where the diameter of the active component is great, while the limit itself is correspondingly small. If, however, the beam diameter is reduced (for example, by using a diaphragm in the resonator) to a value of the order of 1 mm and smaller, the beam divergence, as a rule, will be the diffraction divergence without taking any special measures.

The first gas lasers, whose typical representative is the best known helium-neon laser, operated on an active mixture enclosed in a very narrow discharge tube and generated a small diameter light beam. The mixture itself was very rarefied and negligible power (by the yardstick of modern laser technique) was spent for its excitation. Therefore, the active medium was practically ideally uniform. Due to this combination of circumstances, gas laser developers did not seriously encounter the

FOR OFFICIAL USE ONLY

FOR OFFICIAL USE ONLY

divergence problem for many years. To a superficial observer, it would seem that this problem in general was a specific problem of solid-state lasers and originated mainly due to the imperfection of solid active media. However, in later years, the rapid development of gas laser physics led to the creation of such new types of lasers as chemical, gas-dynamic, etc., whose radiation power exceeds by several orders of magnitude the power of the "customary" helium-neon lasers. The increased radiation power is achieved by increasing the working medium pressure, the dimensions of the volume it occupies and the unit power expenditures for excitation. The problem of considerable optical nonuniformities of the medium become prominent. Thus the problem of beam divergence became a problem not only of solid-state lasers but without exception, of all lasers with high radiation power. Developers of powerful gas lasers now encounter about the same difficulties as the creators of the solid-state lasers met and they use about the same measures to overcome them. Therefore, papers in the area of gas lasers added little information on the angular selection methods. The majority of the investigations whose results played a considerable role in solving the divergence problem and will be used in this book applies to solid-state lasers.

COPYRIGHT: "NAUKA" GLAVNAYA REDAKTSIYA FIZIKO-MATEMATICHESKOY LITERATURY,
1979
[8144/0027-2291]

2291
CSO: 8144/0027

FOR OFFICIAL USE ONLY

FOR OFFICIAL USE ONLY
MAGNETOHYDRODYNAMICS

UDC 533.9.07

MAGNETIC PLASMA COMPRESSOR WITH EXPLOSIVELY-DRIVEN MAGNETIC-FIELD COMPRESSION GENERATOR

Leningrad, ZHURNAL TEKHNIЧЕСКОЙ ФИЗИКИ in Russian Vol 50, No 7, 1980
pp 1521-1524 manuscript received 3 Apr 79

[Article by V. V. Vladimirov, I. I. Divnov, I. I. Zotov, A. S. Kamrukov, N. P. Kozlov, P. A. Ovchinnikov, Yu. S. Protasov and B. D. Khristoforov, Moscow Higher Technical Academy imeni N. E. Bauman]

[Text] 1. Powerful sources of electromagnetic energy are needed for making large-scale electrophysical facilities of various categories (dense non-ideal plasma generators, generators of high-intensity optical radiation and high-current electron beams, and so on). Of interest in this connection is the use of inductive energy accumulators based on explosively-driven magnetic-field compression generators [EMCG] with stored energy density several orders of magnitude greater than that of capacitive accumulators [Ref. 1].

As a result of numerical modeling of processes of energy transfer from the EMCG to a resistive-inductive load such as high-current discharge of a magnetic plasma compressor [MPC], it has been demonstrated that fairly effective matching can be realized by electrical engineering methods between the generator and the plasma load through a matching pulse transformer. The electrical energy input to the discharge is several times greater than the initial (feed) energy of the EMCG.

This paper gives the results of an experimental investigation of the possibilities of using an EMCG as the power supply for high-current discharges in a magnetic plasma compressor.

2. The experiments used an EMCG of planar configuration with nearly linear change of inductance in the process of magnetic flux compression. The design of the generator is analogous to that described in Ref. 2, 3. The working principle of the EMCG is based on converting the energy of an explosive to magnetic field energy as a closed electrical current-carrying

FOR OFFICIAL USE ONLY

FOR OFFICIAL USE ONLY

circuit is rapidly deformed by the explosion. The initial magnetic flux in the circuit, which is formed by external specially shaped copper busbars and a single-turn solenoid, was set up by discharging a capacitor bank with energy capacity of $W_0 \sim 100$ kJ charged to a voltage of $U_0 = 4$ kV. At the instant of maximum feed current $J_{0m} \sim 250$ kA ($t_0 = 240$ μ s) the explosive was detonated at the end of a copper cassette placed between the current-carrying busbars, initiating compression of the magnetic flux and displacing it into the solenoid by the plates of the cassette spreading apart under the action of the products of explosion. The energy was transferred to the load (discharge in the MPC) through an iron-free matching pulse transformer in which the primary winding was the solenoid, and the secondary was a seven-turn single-layer coil of copper band. The principal parameters of the EMCG: length 2.5 m, weight of explosive charge 5.5 kg, initial and final inductances $L_0 = 1.88$ μ H, $L_1 = 0.065$ μ H, inductance of secondary winding $L_2 = 3.21$ μ H, duration of working cycle $T_c \sim 300$ μ s.

The load of the EMCG was localized discharge in the MPC developing in a cylindrical quartz channel $d_{in} \times l = 100 \times 400$ mm at a residual gas pressure of $p \sim 10^{-2}$ mm Hg. Dimensions of the MPC electrode system: anode diameter 80 mm, cathode diameter 20 mm, plasma-forming material -- Teflon.

3. In the experiments (Fig. 1) oscillographic recordings were made of currents and voltages in the capacitor bank-EMCG and the EMCG-MPC circuits, magnetic field intensity in the center of the EMCG solenoid,

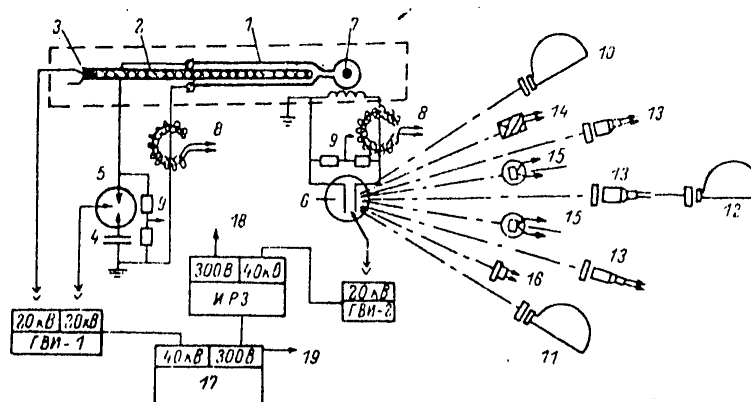


Fig. 1. Diagram of explosion experiment: 1--EMCG; 2--explosive strip; 3--electric detonator; 4--capacitor bank ($C_0 = 1.3 \cdot 10^{-2}$ F; 5--vacuum commutating discharger; 6--MPC; 7--induction probe; 8--Rogowski loop; 9--voltage divider; 10--SFR-2M camera (time loupe); 11--SFR-2M camera (recorder); 12--FR-10 slave photorecorder; 13--photocells; 14--calorimeter; 15--thermoelectric radiation receivers; 16--pyrosensors; 17--SFR command panel; 18--"1" mark; 19--oscilloscope trigger, "0" mark; ΓBH --high-voltage pulse generator; $MP3$ --controlled delay pulse relay

FOR OFFICIAL USE ONLY

FOR OFFICIAL USE ONLY

stagnation pressure of the plasma jet of the MPC on an obstacle, and the fluxes and energy of discharge radiation in the visible and the near infrared and ultraviolet regions of the spectrum, and a photographic record was made of the dynamics of discharge development in the MPC, and of the space-time distribution of brightness temperature in the discharge channel.

The circuit arrangements (Fig. 1) provided the necessary time matching of working processes in the EMCG and MPC systems as well as their synchronization with the reception and recording equipment.

The vacuum spark gap in the discharge circuit of the capacitor bank was commutated simultaneously with blasting of the electric detonator of the EMCG placed on an additional strip of explosive. The length of the strip was chosen so that the detonation reached the end of the MPC cassette at the instant of maximum discharge current of the capacitor bank. The instant of initiation of the discharge in the MPC relative to the beginning of operation of the EMCG could be varied by a controlled delay pulse relay and was usually taken as $\Delta t \sim 50 \mu s$ before the instant of maximum current in the EMCG circuit.

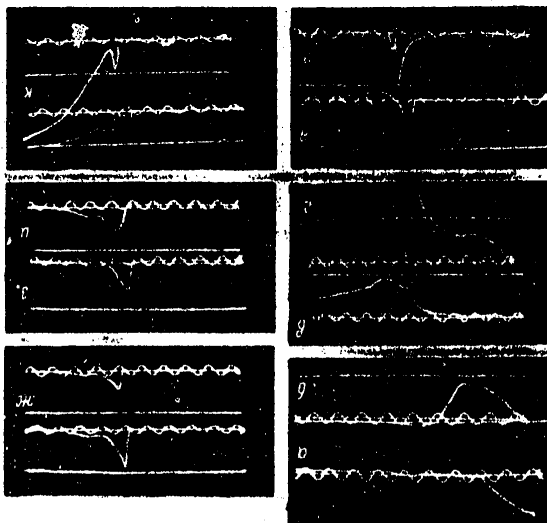


Fig. 2. Typical oscillograms of the explosive experiment. Period of the calibration sine wave $T = 100 \mu s$: a --voltage across the capacitor bank; ϕ --EMCG feed current; e , z --magnetic field intensity in the EMCG solenoid; ϕ --MPC current; e --voltage across the electrodes of the MPC; κ , 3 , u --discharge emission power in the near UV ($\Delta h\nu = 4.35-5.0$ eV)-- κ , visible ($\Delta h\nu = 2.3-3.16$ eV)-- 3 , and near IR ($\Delta h\nu = 1.36-1.95$ eV)-- u regions of the spectrum; κ --integral yield of emission in the band of transparency of quartz.

FOR OFFICIAL USE ONLY

4. Fig. 2 shows typical oscillograms of an explosive experiment illustrating the main distinguishing features of the working process of the EMCG-MPC energy complex. By the time that compression of the magnetic pulse begins ($t_0 = 240 \mu s$), about 60% of the energy stored in the capacitors ($W_1 = 60 \pm 5 \text{ kJ}$) has been transmitted from the feed bank to the EMCG circuit. Breakdown of the discharge gap of the MPC corresponds to the appearance of signals from the Rogowski loop and from the photocells, as well as to an abrupt drop in voltage across the MPC electrodes and a break on the oscillogram of magnetic field intensity. The voltage across the electrodes at the instant of breakdown ($t^* \sim 510 \mu s$) was $U_{MPC} = 20 \text{ kV}$. The maximum current in the MPC $I_{2m} = 700 \text{ kA}$ was reached at the instant of the maximum magnetic field in the solenoid of the EMCG $H_m = 64 \text{ kOe}$ ($t_m = 536 \mu s$). The maximum current and total magnetic energy generated by the EMCG as calculated from these values were $I_{1m} = 7.4 \text{ MA}$ and $W_{EMCG} \sim 500 \text{ kJ}$. The electric energy supplied to the MPC, $W_{MPC} = 90 \pm 10 \text{ kJ}$, and peak discharge power $P_{el} \sim 4.3 \text{ GW}$.

Investigation of the dynamics of development of the MPC discharge by methods of high-speed photography has shown that the main features of formation of localized discharges established in Ref. 4 for capacitive accumulators -- formation of the dense plasma focus beyond the outlet of the MPC, screening of the central zone by a peripheral layer of erosion products near the wall, the shock-wave structure of deceleration of the MPC flux -- are also retained when the MPC is fed by an EMCG.

The velocity of the plasma stream as determined from the angle of inclination of characteristic luminescence inhomogeneities on slit scans of the discharge was about 45-50 km/s, and the average velocity of the shock wave front reflected from an obstacle was 4.5-5.0 km/s. The maximum pressure of the shock-compressed plasma close to the obstacle is $p \sim 1.6 \text{ kbar}$, and p retains a value of the order of 1 kbar or more for a time Δt of the order of 100 μs or more.

The total energy output of discharge radiation in the region of transmission of quartz was about 20 kJ, approximately 50% of all radiated energy falling to the near-UV region of the spectrum ($\lambda < 400 \text{ nm}$), the discharge emission power at the maximum being about 250 MW. The densities of radiation fluxes in the visible and near-UV regions of the spectrum averaged over the lateral surfaces corresponded to a blackbody temperature $T_a = 18,000\text{-}19,000 \text{ K}$. Maximum brightness temperatures of the radiation were observed in the vicinity of MHD compression of the plasma stream (the plasma focus) -- $T_{br} \sim (50\text{-}60) \cdot 10^3 \text{ K}$, and on the reflected wave front $T_{br} \sim 40 \cdot 10^3 \text{ K}$.

Let us note that the estimates of plasma parameters in the vicinity of MHD compression and shock interaction of the stream that were made on the basis of our results show that conditions of strong nonideality [$T_e \sim 5 \text{ eV}$, N_e of the order of $3 \cdot 10^{20} \text{ cm}^{-3}$ or more, number of particles in the Debye sphere $N_D \sim 0.2$, parameter of nonideality $\gamma = e^2 N_e^{1/3} (kT)^{-1} \sim 0.2\text{-}0.3$] are realized in the zone of the plasma focus for a time Δt of the order of 100 μs or more. This means that the magnetic plasma compressor can be

FOR OFFICIAL USE ONLY

FOR OFFICIAL USE ONLY

considered an effective nonideal plasma generator at the investigated level of energy input to the discharge.

5. The realized efficiencies of energy transfer from the EMCG to the plasma load of the given type are not the limiting values, and can be considerably increased by optimizing and matching the parameters of the generator, transmission line and load. One of the ways to increase the efficiency of the system is to use polychannel discharges from several (up to ten) series-connected MPC's. The results of the first experiments done in this direction, in particular explosive experiments with two series-connected MPC discharges, have shown an increase in the energy released in the load by a factor of more than 1.5, the total light output in the discharges in the transmission region of quartz being approximately doubled to about 40 kJ.

Thus we have proposed and experimentally realized an electrical engineering technique for matching an EMCG to a plasma load typified by the discharge in a magnetic plasma compressor. The results of the experiments have shown the feasibility of using an explosively-driven magnetic-field compression generator as a fairly efficient energy source in experiments with high-current radiating discharges.

REFERENCES

1. G. Knopfel', "Sverkhsil'nyye impul'snyye magnitnyye polya" [Ultra-strong Magnetic Fields], Moscow, Mir, 1972.
2. Ye. I. Bichenkov, A. Ye. Voytenko, A. F. Demchuk, A. A. Deribas, B. I. Kulikov, Yu. Ye. Nesterikhin, O. P. Sobolev, DOKLADY AKADEMII NAUK SSSR, Vol 182, 1968, p 1289.
3. I. I. Divnov, Yu. A. Gus'kov, I. I. Zotov, O. P. Karpov, B. D. Khris-toforov, FIZIKA GORENIYA I VZRYVA, No 6, 1976, p 959.
4. A. S. Kamrukov, N. P. Kozlov, Yu. S. Protasov, DOKLADY AKADEMII NAUK SSSR, Vol 239, 1978 p 831.

COPYRIGHT: Izdatel'stvo "Nauka", "Zhurnal tekhnicheskoy fiziki", 1980 [8144/0060-6610]

6610

CSO: 8144/0060

FOR OFFICIAL USE ONLY
OPTICS AND SPECTROSCOPY

UDC 621.373.826:621.78

INTERFERENCE PHENOMENA WHEN METALS ARE HEATED BY LASER IN AN OXIDATIVE ATMOSPHERE

Moscow KVANTOVAYA ELEKTRONIKA in Russian Vol 7, No 7(97), Jul 80 pp 1548-1556
manuscript received 16 Jan 80

[Article by F. V. Bunkin, N. A. Kirichenko, V. I. Konov and B. S. Luk'yanchuk,
Physics Institute imeni P. N. Lebedev, Academy of Sciences USSR]

[Text] An investigation is made of the dynamics of laser heating of metal targets in air. It is shown that as wavelength decreases (in particular from $10.6 \mu\text{m}$ to $1.06 \mu\text{m}$ or less) the nature of the heating changes considerably. In the first place there is an increase in the number of oscillations of absorptive power of the target, and secondly the "high-frequency" oscillations are modulated by "low-frequency" oscillations. It is shown that such behavior of absorptivity is due to the formation of several oxide layers on the target surface with different oxygen contents. Based on the example of a copper target, a detailed analysis is made of the behavior of various quantities that characterize heating (thickness of oxide layers, temperature, rates of growth of oxide layers and so on). The experiments agree well with theory.

1. Introduction

The rate of laser heating of metal targets in air may be appreciably increased by the growth of oxide films on the surface of metals, as these films have considerable molecular absorption. An examination was made in Ref. 1-5 of the dynamics of heating in air by the emission of a CO_2 laser. It was shown that for a number of metals (such as Cu, Fe) the absorptivity A of targets may increase from a few percent to 50-90 percent, which is of practical interest for technological applications of CO_2 lasers.

At the same time, the effectiveness of thermochemical action of laser emission may vary considerably with wavelength λ , for example due to the frequency dependence of the optical constants of oxides. Therefore it is of interest to study the dynamics of heating of metal targets in air as a function of emission wavelength, and also to determine the optimum wavelength where energy expenditures on heating are minimized. Another important question is whether thermochemical phenomena can be sufficiently effectively utilized to increase A for those wavelengths for which the absorptivity A_0 of the metal itself is fairly high, as for example in the case of argon lasers ($\lambda = 0.515 \mu\text{m}$) or YAG lasers ($\lambda = 1.06 \mu\text{m}$).

FOR OFFICIAL USE ONLY

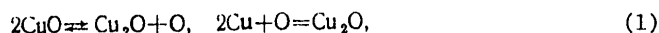
As shown in Ref. 3, 4, the absorptivity of a target with increasing temperature undergoes oscillations associated with interference phenomena in the oxide layer. These phenomena are specific to oxide films in which $\alpha\lambda \ll 1$ (α is the coefficient of absorption of radiation in the oxide). The dynamics of the behavior of interference phenomena in laser heating of targets enables determination of the optical constants of films [Ref. 6]. The period of interference oscillations corresponds to an increase in the oxide layer by a thickness of $\Delta x \sim \lambda/2n$ (n is the index of refraction of the oxide). Under typical heating conditions of, say, a copper target by CO_2 laser emission ($\lambda = 10.6 \mu\text{m}$), the absorptivity undergoes 1-3 oscillations [Ref. 3-5]. It is clear from this that with a transition to shorter-wave emission (if the index of refraction does not change too strongly), the number of oscillations should increase in proportion to the frequency of the incident emission.

However, the change in the nature of heating of the target with decreasing wavelength of radiation does not reduce to a simple increase in the number of oscillations of absorptivity: the "high-frequency" oscillations are modulated by "low-frequency" oscillations. The reason for this is that several layers of oxides with different oxygen contents [Ref. 7] are formed on the surface of the metal. For example when iron is oxidized, a three-layer oxide -- $\text{Fe}_2\text{O}_3/\text{Fe}_3\text{O}_4/\text{FeO}/\text{Fe}$ -- is formed on its surface, and when copper is oxidized a two-layer oxide -- $\text{CuO}/\text{Cu}_2\text{O}/\text{Cu}$ -- is formed. If the thickness of the layer is comparable to $\lambda/2n$, it may have a considerable effect on A.

In this paper we have made a theoretical and experimental study of the dynamics of heating of a copper target covered by a double oxide layer. Generalization of the proposed theory to other metals (including those with a large number of oxide layers) is not complicated, but in the case of a large number of layers it leads to more cumbersome calculations.

2. Kinetics of Two-Layer Oxidation

To determine the thickness of oxide layers on the surface of a copper target during heating, we use the Valensi-Wagner theory [Ref. 7]. According to this theory, The inner oxide layer of Cu_2O is formed as a result of the reactions



while the outer layer of CuO is formed by the reactions



The total consumption of oxygen q per unit of surface (in gram-atoms per square centimeter) during oxidation of the target is related to the thicknesses and specific volumes of the oxide layers $\text{CuO}(x_1, V_1)$ and $\text{Cu}_2\text{O}(x_2, V_2)$:

$$q = x_1/V_1 + x_2/V_2 = q_1 + q_2, \quad (3)$$

the expenditure of oxygen on reactions (1) and (2) being respectively

$$q_2 = x_2/V_2 + x_1/2V_1, \quad q_1 = x_1/2V_1. \quad (4)$$

The oxidation process is divided into the following stages. For fairly thick oxide layers oxygen initially diffuses through the layer of CuO , and in this case all the

FOR OFFICIAL USE ONLY

FOR OFFICIAL USE ONLY

oxygen is expended on reaction (2). The kinetics of this process is described fairly accurately by the parabolic law

$$\frac{dq}{dt} = \frac{1}{V_1} \frac{d_1(T)}{x_1}. \quad (5)$$

The next stage of the oxidation process consists in partial dissociation of the oxide CuO on the CuO/Cu₂O interface:



The oxygen formed as a result of the reaction diffuses into the oxide Cu₂O and interacts with the copper atoms in accordance with reaction (1). The kinetics of this process is described by the formula

$$\frac{dq_2}{dt} = \frac{1}{2V_2} \frac{d_2(T)}{x_2}. \quad (7)$$

The quantities $d_1(T)$ and $d_2(T)$ in (5) and (7) depend on temperature in the following way:

$$d_1(T) = d_{10} \exp(-T_1/T), \quad d_2(T) = d_{20} \exp(-T_2/T). \quad (8)$$

Substituting (3), (4) in (5), (7), we get a system of differential equations of the kinetics of two-layer oxidation

$$\begin{aligned} \frac{dx_1}{dt} &= 2 \frac{d_1(T)}{x_1} - \mu \frac{d_2(T)}{x_2}; \\ \frac{dx_2}{dt} &= \frac{d_2(T)}{x_2} - \frac{1}{\mu} \frac{d_1(T)}{x_1}, \end{aligned} \quad (9)$$

where $\mu = V_1/V_2$. Dividing one equation by the other in (9), we get a differential equation for x_1 and x_2 . If oxidation takes place under isothermal conditions, this formula yields the well known Valenci formula [Ref. 7]

$$\frac{x_1}{x_2} = \frac{1}{2} \left[\frac{1}{\mu} \frac{d_1(T)}{d_2(T)} - \mu + \sqrt{\left(\frac{1}{\mu} \frac{d_1(T)}{d_2(T)} - \mu \right)^2 + 8 \frac{d_1(T)}{d_2(T)}} \right]. \quad (10)$$

Expression (10) takes consideration of the experimental fact that the ratio x_1/x_2 is independent of thickness x_2 over a wide range [Ref. 7].

3. Heating of a Thermally Thin Film

To theoretically describe laser heating of a target with a two-layer oxide film on the surface, it is necessary to simultaneously solve system of equations (9) for oxidation kinetics, and the equation of thermal conductivity. In the simplest case where the laser beam uniformly covers the surface of the target -- a thermally thin plate -- the equation of thermal conductivity takes the form

FOR OFFICIAL USE ONLY

$$mc \frac{dT}{dt} = PA(x_1, x_2) - P_{\text{нот}}(T), \quad (11)$$

where m , c are the mass and heat capacity of the target, and P is the power of incident radiation. [The subscript NOT stands for "loss" (потеря)]. The absorptivity $A(x_1, x_2)$ of the layered system $\text{CuO}/\text{Cu}_2\text{O}/\text{Cu}$ is described by the expression [Ref. 8]

$$A(x_1, x_2) = 1 - |R(x_1, x_2)|^2, \quad (12)$$

where

$$\begin{aligned} R(x_1, x_2) &= \frac{r_{13} \exp(-2i\psi_1) + r}{\exp(-2i\psi_1) + r_{13}r}; \quad r = \frac{r_{33} \exp(-2i\psi_2) + r_{34}}{\exp(-2i\psi_2) + r_{33}r_{34}}; \\ \psi_{1,2} &= \frac{2\pi}{\lambda} x_{1,2} \sqrt{\epsilon_{1,2}}; \quad \sqrt{\epsilon_k} = n_k + i\kappa_k \quad (k=0, 1, 2); \\ r_{33} &= (r_{13} - r_{12}) / (r_{13}r_{12} - 1); \quad r_{34} = (r_{13} - r_{14}) / (r_{13}r_{14} - 1); \\ r_{12} &= (1 - \sqrt{\epsilon_1}) / (1 + \sqrt{\epsilon_1}); \quad r_{13} = (1 - \sqrt{\epsilon_2}) / (1 + \sqrt{\epsilon_2}); \\ r_{14} &= -1 + A_0(1 - i\kappa_0/n_0)/2 + A_0/2n_0; \quad A_0 = 4n_0 / [(1 + n_0)^2 + \kappa_0^2]; \end{aligned}$$

ϵ_1, ϵ_2 are the permittivities of the oxides, n_0, κ_0 are the optical constants of the metal, $A_0 \ll 1$ [Ref. 9].

The power of thermal losses in (11) is equal to

$$P_{\text{нот}}(T) = s[\eta(T - T_0) + \sigma\sigma_0(T^4 - T_0^4)], \quad (13)$$

where s is the surface of the target, T_0 is ambient temperature. The first term in (13) describes convective thermal losses, and the second term describes radiation heat losses.

Now we give an approximate expression for $A(x_1, x_2)$ that is valid if the conditions $\alpha x \ll 1$, $\alpha \lambda \ll 1$, $n \gg 1$ are satisfied for each of the oxide films:

$$A(x_1, x_2) = \frac{n_1^2 A_0 + 2\kappa_1 K [\beta_1 x_1 - (K - \sin^2(\beta_2 x_2/2)) \sin(\beta_1 x_1)/K] + C_1}{D_1^2 + D_2^2}, \quad (14)$$

where

$$\begin{aligned} K &= 1 - (1 - n_1^2/n_2^2) \sin^2(\beta_2 x_2/2); \\ C_1 &= 2\kappa_1 \left(\frac{n_1^2}{n_2^2} \right) \left[\beta_2 x_2 - \left(1 - 2 \frac{\kappa_1 n_2}{\kappa_2 n_1} \sin^2 \frac{\beta_1 x_1}{2} \right) \sin \beta_2 x_2 \right]; \\ D_1 &= \frac{n_1}{n_2} \sin \frac{\beta_2 x_2}{2} \cos \frac{\beta_1 x_1}{2} + \sin \frac{\beta_1 x_1}{2} \cos \frac{\beta_2 x_2}{2}; \\ D_2 &= n_1 \left(\cos \frac{\beta_2 x_2}{2} \cos \frac{\beta_1 x_1}{2} - \frac{n_1}{n_2} \sin \frac{\beta_2 x_2}{2} \sin \frac{\beta_1 x_1}{2} \right); \quad \beta_{1,2} = \frac{4\pi n_{1,2}}{\lambda}. \end{aligned}$$

FOR OFFICIAL USE ONLY

FOR OFFICIAL USE ONLY

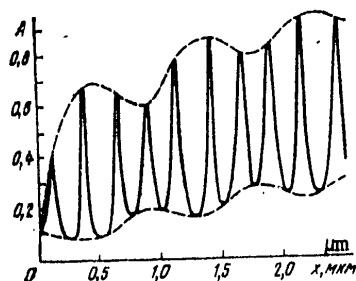


Fig. 1. Absorptivity $A(x_1, x_2)$ of a two-layer system (for isothermal oxidation $T=1100$ K) as a function of thickness x_2 of oxide Cu_2O , as plotted from formulas (10), (12) at $n_1=2.57$, $n_2=1.5$, $\kappa_1=0.05$, $\kappa_2=0.0005$, $\lambda=1.06 \mu\text{m}$, $A_0=0.12$, $x_1/x_2=0.23$

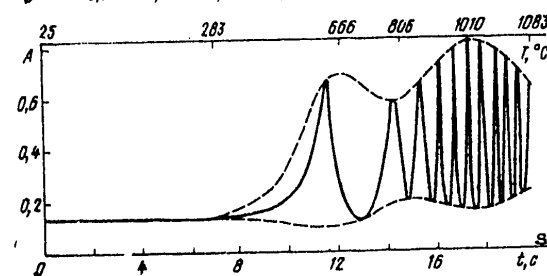


Fig. 2. Dependence $A(t)$ for a copper target in the case of heating by a YAG laser ($\lambda=1.06 \mu\text{m}$): optical constants are the same as on Fig. 1; $d_1=10^{-6} \text{ cm}^2/\text{s}$; $d_2=4 \cdot 10^{-2} \text{ cm}^2/\text{s}$; $T_1=9000 \text{ K}$; $T_2=19,000 \text{ K}$; $\mu=0.524$; $m=80 \text{ mg}$; $c=0.382 \text{ J/g} \cdot \text{deg}$; $\eta=1.5 \cdot 10^{-3} \text{ W/cm}^2 \cdot \text{deg}$; $\sigma_0=0.415$; $s=0.25 \text{ cm}$, $P=10 \text{ W}$

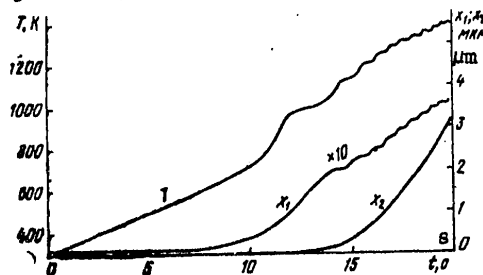


Fig. 3. Time dependences of temperature and thickness of layers of oxides when a copper target is heated by YAG laser emission (values of parameters are the same as in Fig. 2)

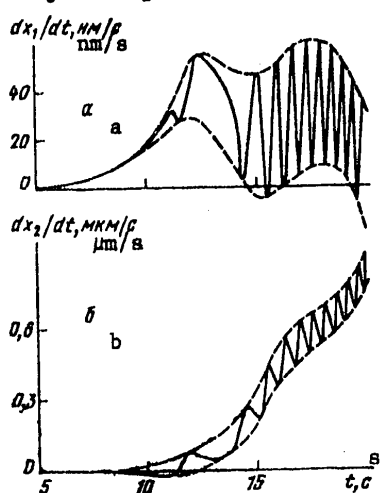


Fig. 4. Time dependences of rates of formation of oxide layers of CuO (a) and Cu_2O (b) when a copper target is heated by YAG laser emission (parameters the same as in Fig. 2)

FOR OFFICIAL USE ONLY

FOR OFFICIAL USE ONLY

Fig. 1 shows how the absorptivity $A(x_1, x_2)$ behaves with a change in thickness of one of the oxides under isothermal conditions (the thickness of the second oxide being determined by the Valenci formula (10)).

We solved system of equations (9), (11)–(13) numerically on a computer for the case of heating of a copper target by YAG laser emission. An example of calculation of relation $A(t)$ is shown in Fig. 2. It is clear that in the heating process a double interference pattern arises in the change of absorptivity -- high-frequency oscillations are modulated by low-frequency oscillations. The former are due to growth of the oxide Cu_2O , and the latter are caused by growth of CuO . The corresponding dependences of $T(t)$, $x_1(t)$ and $x_2(t)$ are shown in Fig. 3.

Besides the oscillations associated with interference phenomena, during the growth of the oxide films a modulation is imposed on the dependence $A(t)$ that is due to the nonmonotonic nature of change in x_1 and x_2 . These peculiarities in the variation of x_1 and x_2 can be seen most clearly on the time dependences of rates of oxidation $dx_{1,2}/dt$ (Fig. 4). The depth of the corresponding modulations of absorptivity depends on the kinetic constants of the problem.

Analysis has shown that the overall pattern of change in absorptivity of a copper target when heated in air by radiation with $\lambda = 1.06 \mu\text{m}$ is made up of interference oscillations complicated by nonuniformity in the growth of oxide layers. On the other hand, when the copper target is heated by CO_2 laser emission, calculation by the model given above shows that at heating rates close to those shown in Fig. 3, oxide CuO has practically no influence on heating dynamics since its maximum thickness is $x_{\text{max}} \ll \lambda/2n_1$.

It can be readily understood that the number of interference oscillations of $A(t)$ should increase (other parameters remaining unchanged) with decreasing λ , and for three-layer oxide films (for example with heating of iron), a triple interference pattern may show up.

4. Relaxation of Perturbations in the Case of Two-Layer Oxidation

It should be noted that in the laser heating process, when oxidation conditions are not isothermal, formula (10), strictly speaking, is not valid. However, it can be shown that the deviation from this law in cases of interest can be disregarded.

Actually, let relation (10) be violated at time $t=0$ at some temperature T . We denote

$$x_1(t)/x_2(t) = u(t) = u_0 + \delta(t), \quad \delta(t=0) = \delta_0 \quad (|\delta_0| \ll u_0), \quad (15)$$

where $\delta(t)$ is the deviation of $u(t)$ from $u_0 = u_0(T)$ assigned by the Valenci formula (10).

Substituting (15) in (9), and linearizing the equations with respect to δ , we get a solution that describes relaxation of the initial perturbation:

$$\delta(t) = \delta_0 \exp \left(- \frac{Rd_2(T)}{\mu\mu_0} \int_0^t \frac{dt_1}{x_2^2(t_1)} \right), \quad (16)$$

FOR OFFICIAL USE ONLY

where $R = [(\mu^2 - z)^2 + 8\mu^2 z]^{1/2}$, $z = d_1(T)/d_2(T)$. Hence the logarithmic decrement is

$$\gamma = R d_2(T) / \mu u_c x_{20}^2, \quad (17)$$

where x_{20} is the initial thickness of oxide x_2 .

Thus the Valenci formula can be used even under nonisothermal conditions if the characteristic times of temperature change Δt during heating satisfy the condition $\Delta t \gg \gamma^{-1}$. Estimates show that in typical cases of laser heating of a copper target this condition is met in the temperature range of practical interest where the oxide film that is formed has a noticeable effect on the optical properties of the target. For example Fig. 3 shows that at $T \sim 990$ K, $x_2 \sim 0.1$ μm , which gives $\gamma \sim 0.6$ s^{-1} from (17).

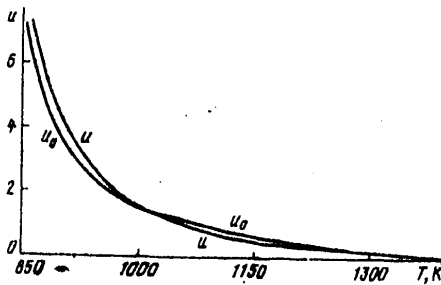


Fig. 5. Curves for $u(T) = x_1/x_2$ and $u_0(T)$: graph for $u(T)$ plotted from data of Fig. 3, and graph for $u_0(T)$ -- from formula (10) for the same thermal diffusion constants

Satisfactory fulfillment of the Valenci formula is confirmed by the graphs of $u(T)$ and $u_0(T)$ given in Fig. 5 as calculated on the basis of Fig. 3, and from formula (10). It is of interest to note that the oscillations that show up on the graphs of x_1 and x_2 (Fig. 3) are practically absent on the dependence of $u(T)$.

Under isothermal conditions in accordance with (9) the oxide layers grow parabolically, but with altered constants,

$$\begin{aligned} d_1^{\text{eff}} &= d_1(1 - (\mu u_0 - z)/z) < d_1, & x_1^2 &= 2d_1^{\text{eff}}t + x_{10}^2; \\ d_2^{\text{eff}} &= d_2(1 - z/\mu u_0) < d_2, & x_2^2 &= 2d_2^{\text{eff}}t + x_{20}^2. \end{aligned} \quad (18)$$

i. e. there is a mutual slowing of the growth of the oxide films. Growth of the overall thickness takes place with constant D^{eff} , which is determined from the relation

$$\sqrt{D^{\text{eff}}} = \sqrt{d_1^{\text{eff}}} + \sqrt{d_2^{\text{eff}}}. \quad (19)$$

We can easily see that at small T , $D^{\text{eff}} \rightarrow d_1$ and at large T , $D^{\text{eff}} \rightarrow d_2/2$ (in (8), $T_2 > T_1$). We also note that when $u_0(T) \gg 1$ (low temperatures),

$$\frac{x_1}{x_2} \approx \frac{1}{\mu} \frac{d_1(T)}{d_2(T)}, \quad (20)$$

and when $u_0(T) \ll 1$ (high temperatures)

$$\frac{x_1}{x_2} \sim \frac{2}{\mu} \frac{d_1(T)}{d_2(T)}. \quad (21)$$

FOR OFFICIAL USE ONLY

Experimental Results

Three types of cw lasers were used in the experimental study of heating of targets in air: an argon laser ("Spectra-Physics" model 271, $P \approx 4$ W, $\lambda = 0.515$ μm), a YAG laser ($P \approx 10$ W, $\lambda = 1.06$ μm) and the LG-25 CO_2 laser ($P \approx 30$ W, $\lambda = 10.6$ μm). The problem of heating of a thermally thin plate was modeled. The absorptivity of the target in air during laser heating was measured directly by a method described in Ref. 4, 5.

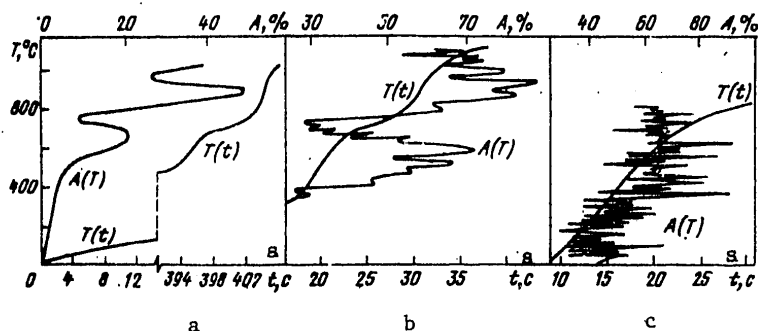


Fig. 6. Experimental curves for the change in temperature of a copper target with time, and in absorptivity with temperature as it is heated by radiation from a CO_2 laser (a; $\lambda = 10.6$ μm , $m = 116$ mg, $s = 0.4$ cm^2 , $P = 30$ W, $A_0 = 2\%$), a YAG laser (b; $\lambda = 1.06$ μm , $m = 80$ mg, $s = 0.29$ cm^2 , $P = 4.88$ W, $A_0 = 12\%$) and an argon laser (c; $\lambda = 0.515$ μm , $m = 54$ mg, $s = 0.21$ cm^2 , $P = 2.4$ W, $A_0 = 45\%$)

Fig. 6 shows graphs of $T(t)$ for copper targets and the corresponding graphs of $A(T)$ for three wavelengths. They agree well with the theory proposed above. The double interference pattern of the change in $A(T)$ is clearly visible for the YAG laser.

Certain facts must be kept in mind when making a quantitative comparison of the theoretical and experimental results. First of all, a certain "fuzziness" of the experimental interference pattern is apparently due to nonuniformity of the growth of the oxide film over the area of the target, as well as to the fact that a multimodal YAG laser was used in the experiment. Secondly, the relation between the number of high-frequency interference oscillations within the first and second low-frequency oscillations is determined by the kinetic constants of the problem, which may differ appreciably under laser heating conditions from the corresponding values for isothermal oxidation. Finally, there may be a difference between the kinetic laws themselves under isothermal conditions and in laser heating. For example the CuO oxide formed during laser heating is porous and is less strongly bound to the Cu_2O oxide than for oxidation under isothermal conditions. This may mean that a combination of parabolic and parabolic laws more adequately describes the kinetics of oxidation than system of equations (9). The experimental data available up to now are not sufficient for making a final choice.

The experimental results (see Fig. 6) show that thermochemical phenomena can be successfully used to increase the efficiency of laser action for argon and YAG lasers as well as for CO_2 lasers. This can also be readily seen by comparing the energy expended on heating in an inert atmosphere (i. e. for $A = A_0 = \text{const}$) and in

FOR OFFICIAL USE ONLY

FOR OFFICIAL USE ONLY

an oxidative atmosphere (such a comparison has been made for a CO_2 laser under conditions that are optimum with respect to emission power in Ref. 10). For example in the experiment with the YAG laser (see Fig. 6b), the time for heating the target to the melting point in air is $t_a \approx 37.5$ s. This time is less than the minimum possible time for heating the same target in an inert gas (i. e. in the absence of heat losses) $t_1 \approx mc\Delta T/PA_0 \approx 64$ s. There is a more detailed analysis of energy expenditures on heating of a target as emission wavelength changes in Ref. 11.

6. Conclusion

The study of the dynamics of heating of metal targets in an active gas medium provides certain information on the kinetics of heterogeneous reactions that take place under the action of laser emission. The coherence of laser emission enables observation of interference phenomena as absorptivity changes (hence providing data on the rate of growth of oxide layers), while the high emission power, and accordingly the high rate of heating of the target enables realization of structures that differ appreciably from those that arise under conditions of isothermal oxidative reactions. For example by increasing the emission power we can satisfy the condition $\Delta t \ll \gamma^{-1}$ (see (10) and after).

Mathematical processing of the results of the experiment using the theory given above in principle enables determination of both the optical constants of the oxide films and the kinetic constants that figure in the oxidation laws. This is fairly simple to do in the case of single-layer oxide films [Ref. 6]. However, in the multilayered oxide films the analogous information can be obtained by determining the optical and kinetic constants that minimize the quadratic form

$$\Phi = \int_0^t [A_{\text{теор}}(t) - A_{\text{эксп}}(t)]^2 dt, \quad (22)$$

where $A_{\text{теор}}(t)$ and $A_{\text{эксп}}(t)$ are the theoretical and experimental $A(t)$ respectively. In doing this, it must be kept in mind, as shown in this paper, that a multilayered structure of the oxide film shows up in the dynamics of target heating only when sufficiently short-wave radiation is used. This inevitably involves an increase in "noises" of the experiment, which are due for example to nonuniformity of the oxide film over the area of the target.

As has already been stated, the chemical reactions that occur on the surface of the target are conducive to an increase in the rate of laser heating, which is of interest for laser technology. We would like to point out one other possible practical application of laser initiation of thermochemical surface reactions. Chemical compounds of metals with oxygen, nitrogen, boron, chlorine and so on usually have semiconductor properties. Depending on the degree of saturation of the valence of the metal, there may be a change in conductivity type of the corresponding compound. For example the oxide CuO is a semiconductor of n-type, while the oxide Cu_2O is a semiconductor of p-type [Ref. 7]. As a result, the $\text{CuO}/\text{Cu}_2\text{O}$ interface is a pn-junction. A "sandwich" of semiconductor layers with required properties can be produced by laser treatment of a metal target in an atmosphere of different gases when the gas pressure and the corresponding dose of laser emission are appropriately selected. The metal faces of the "sandwich" can be produced by laser reduction of the metal in a hydrogen atmosphere. Thus in principle we have a new

FOR OFFICIAL USE ONLY

FOR OFFICIAL USE ONLY

technique for making microcircuits and some semiconductor devices. The most attainable scales of thicknesses of homogeneous semiconductor layers that can be produced by this method are $10\text{--}10^4$ nm, and their area can be varied over quite a wide range. It is noteworthy that in producing such compounds the laser acts both as a source for rapid energy input into the material, and as a diagnostic tool that enables observation of the change in absorptivity of the target during heating.

The authors thank M. I. Arzuov for assisting with the experiments.

REFERENCES

1. J. F. Asmus, F. S. Baker, "Rec. X Symp. Electron, Ion, Laser Beam Techn.," 1969, p 241.
2. V. L. Volodkina, K. I. Krylov, M. N. Libenson, FIZIKA I KHIMIYA OBRABOTKI MATERIALOV, No 5, 1973, p 145.
3. M. I. Arzuov, V. I. Konov, S. M. Metev, FIZIKA I KHIMIYA OBRABOTKI MATERIALOV, No 5, 1978, p 19.
4. M. I. Arzuov, F. V. Bunkin, N. A. Kirichenko, V. I. Konov, B. S. Luk'yanchuk, KVANTOVAYA ELEKTRONIKA, Vol 6, 1979, p 466.
5. M. I. Arzuov, A. I. Barchukov, F. V. Bunkin, N. A. Kirichenko, V. I. Konov, B. S. Luk'yanchuk, KVANTOVAYA ELEKTRONIKA, Vol 6, 1979, p 466.
6. M. I. Arzuov, F. V. Bunkin, N. A. Kirichenko, V. I. Konov, B. S. Luk'yanchuk, PIS'MA V ZHURNAL EKSPERIMENTAL'NOY I TEORETICHESKOY FIZIKI, Vol 27, 1978.
7. O. Kubashevskiy, B. Hopkins, "Okisleniye metallov i splavov" [Oxidation of Metals and Alloys], Moscow, Metallurgiya, 1965.
8. M. Born, E. Wolf, "Osnovy optiki" [Fundamentals of Optics], Moscow, Nauka, 1972.
9. A. V. Sokolov, "Opticheskiye svoystva metallov" [Optical Properties of Metals], Moscow, GIFML, 1961.
10. M. I. Arzuov, F. V. Bunkin, N. A. Kirichenko, V. I. Konov, B. S. Luk'yanchuk, KRATKIYE SOOBShCHENIYA PO FIZIKE, Lebedev Physics Institute, No 11, 1978, p 43.
11. F. V. Bunkin, N. A. Kirichenko, B. S. Luk'yanchuk, O. I. Minervina, PIS'MA V ZHURNAL TEKHNIЧЕСКОY FIZIKI, Vol 6, 1980, p 101.

COPYRIGHT: Izdatel'stvo "Sovetskoye radio", "Kvantovaya elektronika", 1980 [3-6610]

6610
CSO: 1862

FOR OFFICIAL USE ONLY

UDC 535.21

TIME FOR THE ORIGIN OF PLASMA WITH THE EFFECT OF LASER RADIATION OF VARIOUS WAVELENGTHS ON AN ALUMINUM OBSTACLE IN THE AIR

Moscow KVANTOVAYA ELEKTRONIKA in Russian Vol 7, No 8, 1980 pp 1831-1834
manuscript received 12 Mar 80

[Article by A.P. Golub' and I.V. Nemchinov, USSR Academy of Sciences
Institute of Earth Physics imeni O.Yu. Shmidt, Moscow]

[Text] A numerical solution is given to the problem of the origin of a plasma in the air above an aluminum surface exposed to the pulse of a neodymium or CO₂ laser. Agreement is noted between published experimental data and the results of calculations for a model of evaporation of the obstacle taking into account the reduction of thermal conductivity in the surface layer and the "burst" of absorption in vapors. For a radiation pulse of rectangular form, on the assumption of the existence of heat-insulated layers one micron thick, dependences are arrived at for the time for the start of evaporation and the time for the origin of the burst on the radiation flux density in the range of 0.5 to 100 MW/cm². From the calculations it follows that the difference in plasma formation thresholds with a variation in radiation wavelength from 1.06 to 10.6 microns is relatively small.

The effect of laser radiation on an obstacle results in the formation of a plasma. This phenomenon is accompanied by a "burst" of absorption in vapors of the obstacle's material [1, 2] or by low-threshold breakdown [3, 4]. In [5] a comparison was made between the burst theory and an experiment on the effect on an obstacle of radiation pulses of a neodymium laser with a pulse length of $\tau \approx 1 \mu s$. For certain materials, bismuth, for example, is observed good agreement between the calculated and experimental values and the shapes of the pressure pulse transmitted to the obstacle at the evaporation stage, as well as the time for the origin of the plasma. For other materials such as aluminum there is also agreement in terms of order of magnitude of the time for the burst, although there is observed a somewhat faster, than in the calculations, growth in the brightness temperature of the exposed surface of the specimen both at the stage when the rise in pressure resulting from evaporation has not been registered and at the stage when the pressure already noticeably exceeds

FOR OFFICIAL USE ONLY

FOR OFFICIAL USE ONLY

atmospheric. High brightness temperatures, testifying to the formation of a plasma, are recorded even before the beginning of the drop in pressure associated with the development of screening of the target by the absorbing plasma layer. In [5] this was explained by the presence on the surface of microdefects with disrupted heat transfer into the depth of the specimen in keeping with the hypothesis in [6], confirmed by an investigation of the surface under an electron microscope, as the result of which were detected defects with a characteristic dimension on the order of 0.3 to 1 micron, as well as by investigation of the radiation of the plasma formed [7], which demonstrated that the plasma is initiated in individual points of the surface. In the experiments in [5] the time for the burst practically did not depend on what kind of gas (air, nitrogen or helium) surrounds the target and what its density is (normal pressure or vacuum). This confirms the hypothesis regarding formation of the plasma in vapors of the target's material. Let us note that the calculations in [5] were performed by utilizing experimental coefficients of the reflection of the laser radiation from targets.

In [8] a comparison was made between calculated times for the origin of the burst and times for the formation of the plasma, measured with aluminum exposed in air to the radiation pulses of a CO_2 laser with $\tau \sim 0.1$ [9] and $10 \mu\text{s}$ [10]. By virtue of the lack of experimental data on the dependence of the reflection coefficient, k_r , of radiation with $\lambda = 10.6 \mu$ on the temperature, T_0 , of the exposed surface, the theoretical dependence in [11] was employed, according to which for aluminum $k_r = 0.93$ at room temperature and drops to 0.85 at the melting point, T_{mt} . The presence of heat-insulated layers with a thickness of $\ell = 1$ and 0.3μ was assumed. The best agreement with the experimental data was observed with $\ell = 0.3$ both for $\tau \sim 0.1 \mu\text{s}$ and for $\tau \sim 10 \mu\text{s}$. With $\ell = 1 \mu$ the agreement is not bad for $\tau \sim 10 \mu\text{s}$ and somewhat worse for $\tau \sim 0.1 \mu\text{s}$.

Let us now make a comparison of calculations for a burst model similar to those made in [5, 8] as applied to the conditions in [5, 9, 10] with the utilization of the entire remaining group of experimental data published in recent times on the time for the development of a plasma over an aluminum target in air of normal density. The calculations were performed by using the experimental forms of the laser pulse and the theoretical dependence of $k_r(T_0)$ in [11].

In [12] a study was made of the effect of the radiation pulse of a CO_2 laser with a total length of $5 \mu\text{s}$, a leading edge of $0.73 \mu\text{s}$ and a half-width of $0.60 \mu\text{s}$ with a spot area of 1.4 cm^2 . The target was polished before each pulse. A study of the surface under an electron microscope showed the presence of grooves about four microns deep and wide. A pulse with a maximum radiation flux density of $g_m = 22 \text{ MW/cm}^2$ proved to be the threshold for formation of the plasma. In fig 1 are shown dependences, arrived at as the result of our calculations, of the maximum temperature of electrons, T_{em} , on time, t , corresponding to $\ell = 4 \mu$. The shape of the laser pulse is also shown there. It is obvious that the critical

FOR OFFICIAL USE ONLY

FOR OFFICIAL USE ONLY

value of q_m for the origin of the burst according to the calculations also equals 22 MW/cm^2 .

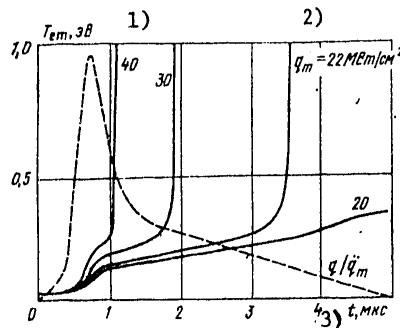


Figure 1.

Key:

1. eV
2. MW/cm²

3. μs

In [13] were studied "combustion" waves originating in irradiation of aluminum foil 25.4 microns thick by a millisecond radiation pulse with a wavelength of 10.6 microns (the times for the formation of the plasma for these experiments are given in [14]). If it is assumed that the foil possesses homogeneous physical properties, then the time for warming it up throughout its entire thickness is approximately 20 μs . Calculations with a radiation flux density of $q = 0.1 \text{ MW/cm}^2$ have demonstrated that as of moment $t = 400 \mu\text{s}$, when the formation of a plasma was recorded in the experiments, $T_0 < T_{\text{mt}}$. This slight warmup cannot make possible the origin of a plasma. Let us now assume that on the surface of the foil there are microdefects which can be modeled by heat-insulated layers with a thickness of $\lambda = 4 \mu$. Calculations for this case have demonstrated that as of moment of time $t = 320 \mu\text{s}$, after the beginning of the effect of the laser pulse (the time for the increase in radiation flux density equals 200 μs), temperature $T_0 = 0.23 \text{ eV}$, which corresponds to the pressure of saturated vapors of aluminum, $p = 1 \text{ bar}$. Steady evaporation is established relatively quickly, taking place at $p = 1.5$ to 1.6 bar and $T_0 = 0.24 \text{ eV}$. One hundred and thirty microseconds after the beginning of evaporation the slow growth in T_{em} is replaced by a rapid increase to values higher than 1 eV. Thus, the time for the burst agrees not too badly with the experimental data.

In [14] a comparison has already been made of the experimental results in [13] with a calculation for a model close to the equilibrium theory of

FOR OFFICIAL USE ONLY

FOR OFFICIAL USE ONLY

the absorption burst in [1]. Here for agreement of the calculated data with the experimental it was assumed that the coefficient of absorption of the radiation by the surface equals not seven percent, as is usually arrived at in experiments (e.g., in [12]), but 15 percent. In [15] an even stronger drop in k_r was assumed. In fig 2 the dots correspond to the dependence of the density of the energy, E_s , transmitted to the target within the limits of the exposed spot on the maximum radiation intensity, q_m , or on the total energy, E , in the laser pulse arrived at in [12]. Also presented there are the results of our calculations for $\lambda = 4 \mu$ (dotted line) and for a target with homogeneous properties (solid-line curve). As is obvious, the calculated values of E_s are somewhat higher than the experimental. This testifies to the fact that the absorption coefficient of real aluminum specimens is obviously even lower than in [11]. From this it follows that the assumption regarding the reduction of the mean thermal conductivity coefficient of the surface layer is more valid than the assumption in [14, 15] regarding an increase in the average absorption coefficient for the area of the spot. Let us note that in these calculations the increase in heat transfer to the target resulting from radiation from the plasma formed after the "burst" was not taken into account. In the experiments in [12] this effect within the limits of the effective spot was apparently not evidenced to a sufficient degree because of the relatively small size of the spot and the heavy spreading of the plasma.

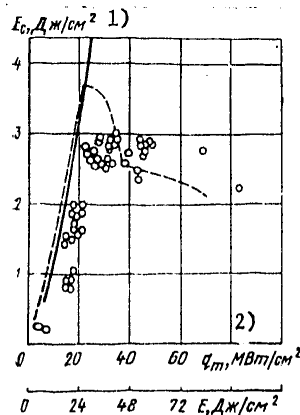


Figure 2.

Key:

1. J/cm^2 2. MW/cm^2

FOR OFFICIAL USE ONLY

FOR OFFICIAL USE ONLY

In fig 3 are given calculated dependences of the time, t_v , for the start of evaporation (dotted line) and of the time, t^* , for the origin of the burst on q with $\lambda = 10.6$ and 1.06μ for a rectangular shape of the laser pulse with the assumption of the presence on the surface of the target of a heat-insulated layer with $\ell = 1 \mu$ (the dots represent the experimental data in [16] for $\lambda = 1.06 \mu$ and $\tau \approx 10 \mu s$). Agreement between the calculated and experimental data is again not too bad.

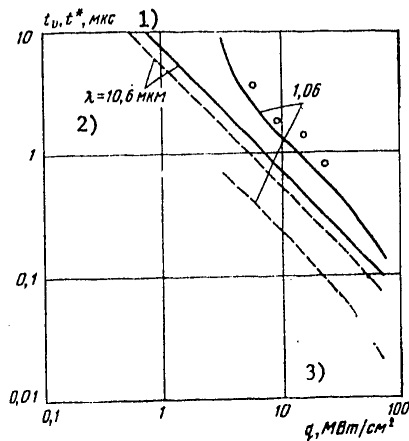


Figure 3.

Key:

- 1. μs
- 2. μ

3. MW/cm^2

From comparison of the data on the time for the burst for $\lambda = 1$ and 10μ it follows that the thresholds for the origin of the plasma over a wide range of variation of q differ only by a factor of 1.5 to 2. This is associated with the fact that the reduction in k_t equaling 93 percent for a CO_2 laser and 85 percent for a neodymium laser at room temperature results in a reduction in t_v , but the time from the beginning of evaporation to the development of the plasma with $\lambda = 10 \mu$ is much shorter than with $\lambda = 1 \mu$, by virtue of the substantially higher absorption coefficients of slightly ionized vapors.

Since, as follows from the foregoing, the threshold for the origin of the plasma depends on the state of the surface, in particular, on the method of treating it, it is of interest to verify our theoretical predictions of the rules for the change in the burst threshold with λ and τ in identical specimens. This probably occurred in one group of experiments [10, 16], whose data for $\lambda = 1.06 \mu$ and 10.6μ with

FOR OFFICIAL USE ONLY

FOR OFFICIAL USE ONLY

$\tau \approx 10 \mu s$ agree with the calculated with identical thickness of the heat-insulated layer (or, possibly, of a layer with reduced thermal conductivity). It is also desirable to extend the range of materials for which plasma formation thresholds have been determined, for the purpose of more extensive verification of the adequacy of the burst model (taking into account the reduction in heat transfer in the surface layer for several of these materials) by means of the actual condition for the development of evaporation and for formation of the plasma under the effect of laser irradiation of various wavelengths.

Bibliography

1. Vilenskaya, G.G. and Nemchinov, I.V. DAN SSSR, 186, 1048 (1969); PMTF, No 6, 3 (1969).
2. Bergel'son, V.I., Golub', A.P., Nemchinov, I.V. and Popov, S.P. KVANTOVAYA ELEKTRONIKA, No 4 (16), 20 (1973).
3. Barchukov, A.I., Bunkin, F.V., Konov, V.I. and Prokhorov, A.M. PIS'MA V ZHETF, 17, 413 (1973).
4. Barchukov, A.I., Bunkin, F.V., Konov, V.I. and Lyubin, A.A. ZHETF, 66, 965 (1974).
5. Golub', A.P., Markovich, I.E., Nemchinov, I.V., Petrukhin, A.I., Rybakov, V.A. and Pleshanov, Yu.Ye., DEP. VINITI, No 3300-79, 1979.
6. Walters, C.T., Barnes, R.H. and Beverly, R.E., III. J. APPL. PHYS., 48, 2937 (1978).
7. Bessarab, A.V., Zhidkov, N.V., Kormer, S.B., Pavlov, D.V. and Funtikov, A.I. KVANTOVAYA ELEKTRONIKA, 5, 325 (1978).
8. Golub', A.P. and Nemchinov, I.V. KVANTOVAYA ELEKTRONIKA, 7, 209 (1980).
9. Boyko, V.A., Danilychev, V.A., Duvanov, B.N., Zvorykin, V.D. and Kholin, I.V. KVANTOVAYA ELEKTRONIKA, 6, 1323 (1979).
10. Bessarab, A.V., Romanov, V.M., Samylin, V.A. and Funtikov, A.I. ZHETF, 48, 1751 (1978).
11. Ujihara, K. IEEE J, QE-8, 567 (1972); J. APPL. PHYS., 43, 2376 (1972).
12. McKay, J.A., Bleach, R.D., Nagel, D.J., Schriempf, J.T., Hall, R.B., Pond, C.R. and Manlief, S.K. J. APPL. PHYS., 50, 3231 (1979).
13. Klosterman, E.L. and Byron, S.R. J. APPL. PHYS., 45, 4751 (1974).

FOR OFFICIAL USE ONLY

FOR OFFICIAL USE ONLY

14. Pirri, A.N. AIAA J., 13, 1279 (1975).
15. McMordie, J.A. and Roberts, P.D. J. APPS, D: APPL. PHYS., 8, 768 (1975).
16. Bessarab, A.V., Dolgaleva, G.V., Zhidkov, N.V., Kaynov, V.Yu., Kormer, S.B., Pavlov, D.V., Urlin, V.D., Funtikov, A.I. and Yakutov, B.P. FIZIKA PLAZMY, 5, 558 (1979).

COPYRIGHT: Izdatel'stvo 'Sovetskoye Radio', 'KVANTOVAYA ELEKTRONIKA', 1980
[4-8831]

8831

CSO: 1862

FOR OFFICIAL USE ONLY

FOR OFFICIAL USE ONLY
OPTOELECTRONICS

UDC 621.378.325

INFLUENCE THAT PUMPING FLUCTUATIONS HAVE ON THE SENSITIVITY OF AN INFRARED RECEIVER WITH PARAMETRIC FREQUENCY CONVERSION

Moscow KVANTOVAYA ELEKTRONIKA in Russian Vol 7, No 7(97), Jul 80 pp 1592-1594
manuscript received 8 Jan 80

[Article by N. A. Iskanderov, V. A. Kudryashov and I. N. Matveyev]

[A numerical estimate is made of the sensitivity of receivers in the near and intermediate IR ranges with parametric signal frequency conversion on crystals in the case of fluctuating single-mode pumping with gaussian amplitude fluctuations. It is shown that an increase in pumping fluctuations up to 10% leads to deterioration of the threshold sensitivity by a factor of approximately 2 as compared with non-fluctuating pumping.]

In an experimental study of the sensitivity of a receiver with parametric frequency conversion it has been established pumping fluctuations of the parametric frequency converter influence the sensitivity of such a receiver [Ref. 1]. It would be of interest to find a numerical estimate of the sensitivity of a receiver with parametric frequency converter for the case of fluctuating single-mode pumping with gaussian amplitude fluctuations.

The probability distribution function of photoreadings $P(n, T)$ at the input of the photodetector in the case of semigaussian description of the registration process can be obtained as a combination of laws of distribution of the number of signal photons $P(n_c)$, background photons $P(n_\phi)$, thermal $P(n_T)$ and spontaneous $P(n_m)$ noises at the input of the parametric frequency converter, and also the conversion coefficients of the converter for signal photons $P(\eta_1)$ and photons of spontaneous noise $P(\eta_2)$ and the distribution of the number of photons equivalent to photodetector noises $P(n_d)$:

$$P(n, T) = \int_0^\infty \int_0^\infty \int_0^\infty \int_0^\infty \{ [\eta_{\phi K} \eta_1 (n_c + n_\phi + n_T) + n_d + \eta_{\phi K} \eta_2 n_m] \} \times \\ \times \exp \{ - [\eta_{\phi K} \eta_1 (n_c + n_\phi + n_T) + n_d + \eta_{\phi K} \eta_2 n_m] \} P(n_c) P(n_\phi) \times \\ \times P(n_T) P(n_m) P(\eta_1) P(\eta_2) dn_c dn_\phi dn_T dn_m d\eta_1 d\eta_2, \quad (1)$$

where $\eta_1 = \gamma_1/T$; $\eta_2 = \gamma_2/2T$; $\gamma_{1,2}$ are constants that characterize the parameters of the nonlinear element; I is pumping intensity; T is measurement time; $\eta_{\phi K}$ is the quantum efficiency of the photocathode.

FOR OFFICIAL USE ONLY

In the case of non-fluctuating pumping, $P(\eta_1) = \delta(\eta_1 - \bar{\eta}_1)$, $P(n_c, \phi, \tau, \omega) = \delta(n_c, \phi, \tau, \omega - \bar{n}_c, \phi, \tau, \omega)$ and expression (1) coincides with the expression for the law of distribution of the number of photons at the input of the photodetector given in Ref. 2.

If the pumping is single-mode radiation that is the sum of a monochromatic field of fixed intensity I_C and a random phase that is uniformly distributed in the interval $0, 2\pi$, plus a narrow-band gaussian noise field with zero average and inversion I_N , then the moments of the distribution functions of the conversion coefficients of the parametric frequency converter by analogy with Ref. 3 can be represented as follows:

for signal, background and thermal photons

$$\langle n!/(n-m)! \rangle = (\eta_1' n_{c, \phi, \tau})^m m! L_m(-1/x), \quad (2)$$

for photons of spontaneous noise of the converter

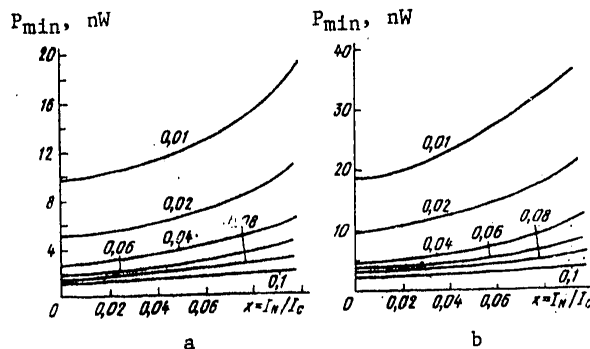
$$\langle n!/(n-m)! \rangle = (\eta_2' n_w)^m (2m)! L_{2m}(-1/x). \quad (3)$$

Here $L_m(-1/x)$ are the associated Laguerre polynomials of order m ; $x = I_N/I_C$;

$\eta_1 = \eta_{\phi\kappa\gamma_1}/N T$; $\eta_2 = \eta_{\phi\kappa\gamma_2}/N T$. At $P(n_c, \phi, \tau, \omega) = \delta(n_c, \phi, \tau, \omega - \bar{n}_c, \phi, \tau, \omega)$ with consideration of (2) and (3) we get the following expression for sensitivity of a receiver with parametric frequency converter in the given model of fluctuating pumping

$$P_{min} = \frac{h\nu b}{\tau_c (eb^2 - a)} (1 + \sqrt{1 + 4\sigma^2 (eb^2 - a)/b^2}), \quad (4)$$

where $a = \eta_1'^2 [2L_2(-1/x) - L_1^2(-1/x)]$; $b = \eta_1' L_1(-1/x)$ is the efficiency of the parametric frequency converter for the given pumping model; $\sigma^2 = (n_\phi^2 + n_\tau^2)a + (n_\phi + n_\tau)b + \eta_2'^2 n_w^2 [4L_4(-1/x) - 4L_2^2(-1/x)] + 2\eta_2' n_w L_4(-1/x) + n_w$; $1/e$ is the signal-to-noise ratio at the photodetector input; τ_c is the duration of the signal pulse; ν is the average signal frequency.



Near-IR (a) and middle-IR (b) sensitivity of receiver as a function of the ratio of variance of a narrow-band gaussian noise field to monochromatic field intensity at values of $\gamma_1(I_C + I_N)$ indicated on the curves.

FOR OFFICIAL USE ONLY

Specific calculations of the sensitivity of a receiver with parametric frequency conversion by formula (4) as a function of the ratio of variance of a narrow-band gaussian noise field I_N to monochromatic field intensity I_C for different values of the average pumping intensity $I = I_C + I_N$ were done for the following parameters: signal-to-noise ratio of 3; signal pulse duration of 30 ns; measurement time $T = 30$ ns; $\gamma_2 = \gamma_1'$; values of $\eta_{\Phi K}$, η_{Φ} , η_T , η_{II} , η_{II} taken from Ref. 4. The results of the calculation for a receiver that has parametric frequency conversion of a signal from the near infrared ($\lambda_C = 1.06 \mu\text{m}$) on a crystal of LiIO_3 and from the middle infrared ($\lambda_C = 10.6 \mu\text{m}$) on a crystal of Ag_3AsS_3 are shown on the figure.

We can draw the following conclusions from the results.

1. An increase in pumping fluctuations up to 10% causes a deterioration of threshold sensitivity of a receiver with parametric frequency converter by a factor of 2 as compared with non-fluctuating pumping.
2. Suppression of amplitude fluctuations of pumping of a parametric frequency converter that is an element of the circuit for predetector processing of the optical signal is necessary only in the case where it leads to a reduction of converter power by no more than 6% per 1% of the fluctuations for the given range of converter efficiencies.

REFERENCES

1. V. S. Dugin, I. N. Matveyev, S. M. Pshenichnikov, N. P. Sopina, A. F. Umnov, KVANTOVAYA ELEKTRONIKA Vol 2, 1975, p 2101.
2. V. A. Kudryashov, I. N. Matveyev, S. M. Pshenichnikov, KVANTOVAYA ELEKTRONIKA, No 5, 1971, p 140.
3. M. C. Teich, P. Diamant, J. APPL. PHYS., Vol 40, 1969, p 625.
4. S. M. Pshenichnikov, I. N. Matveyev, V. A. Kudryashov, RADIOTEKHNIKA I ELEKTRONIKA, Vol 19, 1974, p 1985.

COPYRIGHT: Izdatel'stvo "Sovetskoye radio", "Kvantovaya elektronika", 1980
[3-5610]

6610
CSO: 1862

- END -

FOR OFFICIAL USE ONLY